A PRELIMINARY INVESTIGATION OF
THE "THERMAL AND ELECTRICAL BEHAVIOUR
OF THIN METAL FILMS"

by

DENIS CLYDE BEATTY, B.A., B.Eng.Sc.

PART A: MCMASTER (OFF-CAMPUS) PROJECT*

A Report Submitted to the School of Graduate Studies
in Partial Fulfilment of the Requirements
for the Degree
Master of Engineering

Department of Engineering Physics
McMaster University
Hamilton, Ontario, Canada.
April 1974

---

* One of two project reports: The other part is designated PART B: ON-CAMPUS PROJECT.

MASTER OF ENGINEERING (1974)
Department of Engineering Physics

MCMASTER UNIVERSITY
Hamilton, Ontario.

TITLE: A Preliminary Investigation of the Thermal and Electrical Behaviour of Thin Metal Films

AUTHOR: Denis Clyde Beatty, B.A. (S.G.W.), B.Eng.Sc. (Western)

SUPERVISOR: Dr. J.P. Marton

NUMBER OF PAGES: iv, 46

TABLE OF CONTENTS

ACKNOWLEDGEMENTS

The author is extremely grateful to Dr. J.P. Marton and to Welwyn Company of Canada Limited for sponsoring my Industrial Internship Project.

A very special thanks goes to Dr. S.T. Pai for, being my teacher, supplying the necessary guidance and encouragement during this project.

ABSTRACT

The preliminary investigation of the thermal and electrical behaviour of thin metal films gives evidence, Part I, that several mechanisms are responsible for the change of resistance as the temperature increases from room temperature to 500°C. Firstly, there appears grain growth giving a characteristic decrease in resistance. Secondly, the formation of agglomerates upon the continued growth of grains; especially for the thinner Al and Cr films. This effect tends to increase the resistance and a mathematical model is proposed to explain the results qualitatively. Thirdly, the occurrence of what appeared to be an electromigration effect. This latter point provided the incentive for a study on the effects of electromigration in thin aluminum film, Part II. The results of this study are comparable to those obtained by other workers, except that the interpretation for the direction of electromigration in Al is reversed. One possible explanation for the difference in the direction of migration could be due to the interpretation of marker motion. A mathematical model is also proposed for electromigration, in which both the effects due to the applied electric field and the electrons collision with the ions have been taken into consideration. It was found that the effect due to electrons collision with the ions upon the migration of ions could be expressed in terms of an exponential function of the square of the electron to ion collision relaxation time.

LIST OF FIGURES

LIST OF TABLES

PART I

Annealing Effects on the Resistances of Al, Cr, Ni, Co, and Fe Thin Films

Introduction

Extremely thin metal films in the order of a few angstroms and less do not exhibit normal metallic properties of resistivity. For such thicknesses, the size or mean - free path effect imposes a geometrical boundary restriction on the electron - mobility, and the resistivity for thin films are normally much higher than that of the same bulk material. Such films exhibit negative TCR (temperature coefficient of resistance) and deviate quite widely from Ohm's Law(1). These properties are related in part to the occurrence of discreet metallic grains or agglomerates separated by finite gaps that act as barriers to current flow.

Relatively thicker films, such as the ones used in the present work where size effect is not of primary concern, can have their characteristics treated approximately as that of bulk material. A recent paper(2) proposes a model of Ni-P film based on Matthiessen's rule which takes into consideration the effects on resistivity of grain growth (ρ_1), compositional changes such as the formation of Ni_3P crystallites (ρ_2) and oxidation (ρ_3). Therefore, according to Matthiessen's rule:

$$\rho \text{ total} = \rho_1 + \rho_2 + \rho_3. \tag{1}$$

The following set of experiments were an attempt to examine the above proposed model for applicability to five elements, Al, Cr, Co, Ni, and Fe. Only the first term of the model associated with grain growth, however, was being experimentally studied. The other terms associated with impurities and oxidizing mechanisms were controlled for by first, ensuring the five elements were at least 99.995% pure and secondly, performing the experiment in a vacuum annealing furnace at a pressure of about 10^{-7} torr.

Experiment and Results

The preparation of samples for the experiment consisted of vacuum depositing the five metals onto borosilicate glass rods using standard procedures. These rods were rotated at a constant rate during the deposition in order to ensure a uniform covering. The thicknesses for the five metals were set to give resistance values at decade intervals.

Vacuum annealing of all samples was carried out in the following manner: two freshly deposited resistors were connected to two separate terminals in order that resistance changes could be monitored. The samples were then placed inside a stainless steel tube which was kept evacuated to about 10^{-7} torr pressure. Prior to annealing the tube was flushed several times with helium that had been cooled to liquid nitrogen temperatures, and then reevacuated. The samples were heated from room temperature to 500°C at a constant rate of 5°C/min. with changes to both temperature and resistance being continually monitored.

From the five graphs, plots of resistance versus temperature, as shown in Figures 1 to 5, it appears that for films within the specified thickness and temperature ranges Ni, Co and Fe exhibit a general decreasing resistance. Whereas, in the case of Al and Cr, the increase in resistance is quite pronounced.

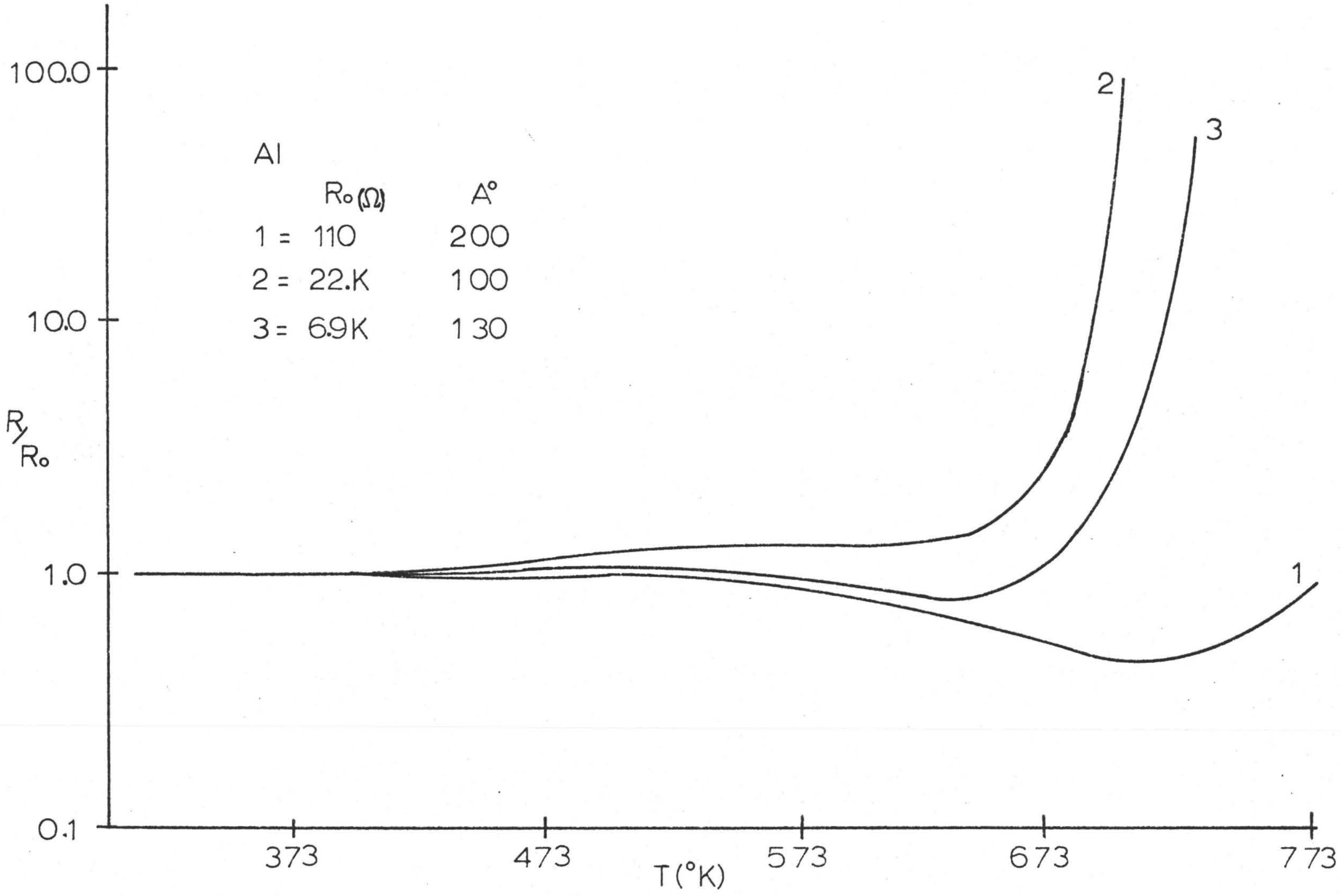

FIGURE 1: Resistance-temperature curves of Al-film during annealing in vacuum.

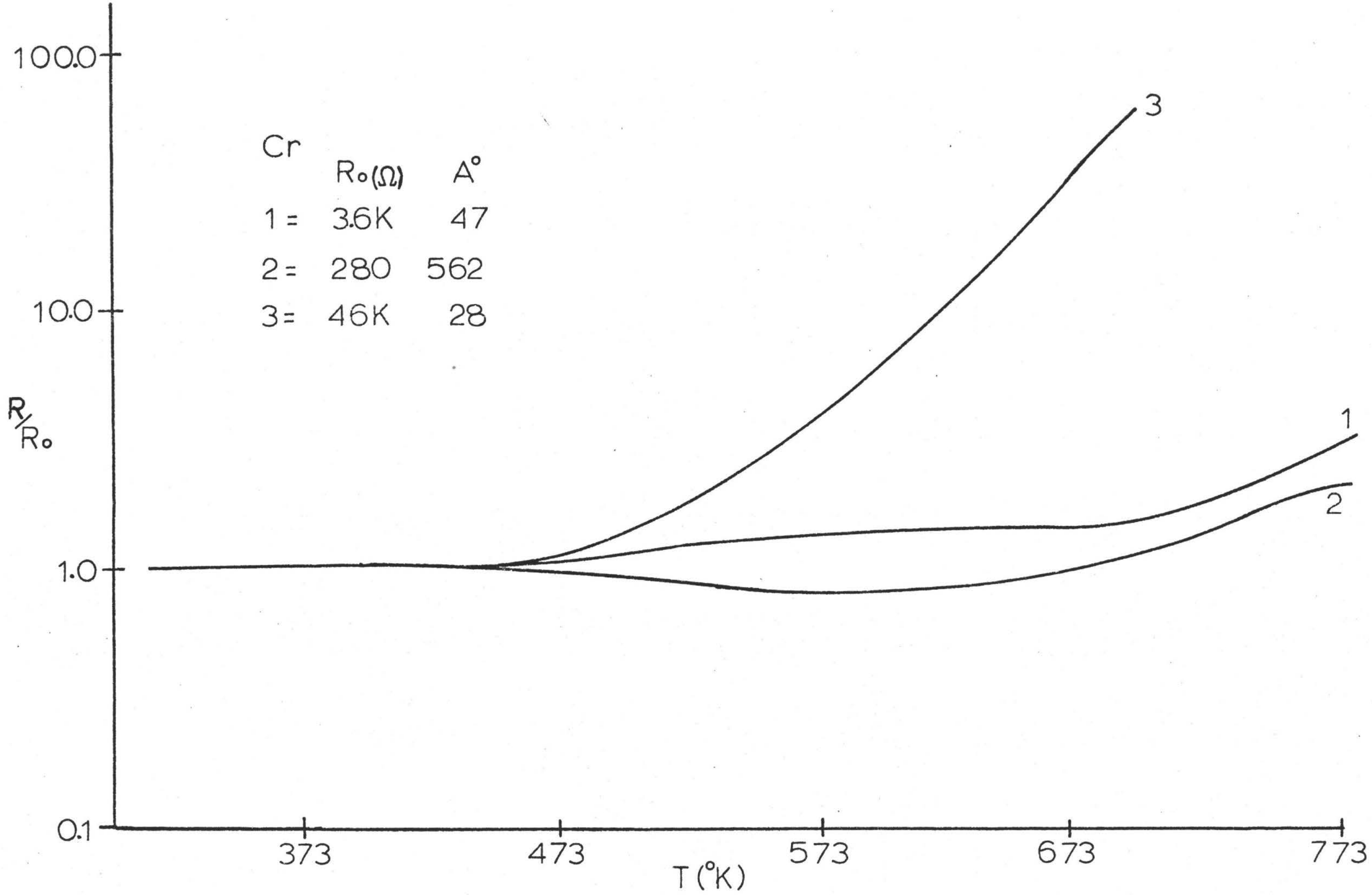

FIGURE 2: Resistance-temperature curves of Cr-film during annealing in vacuum.

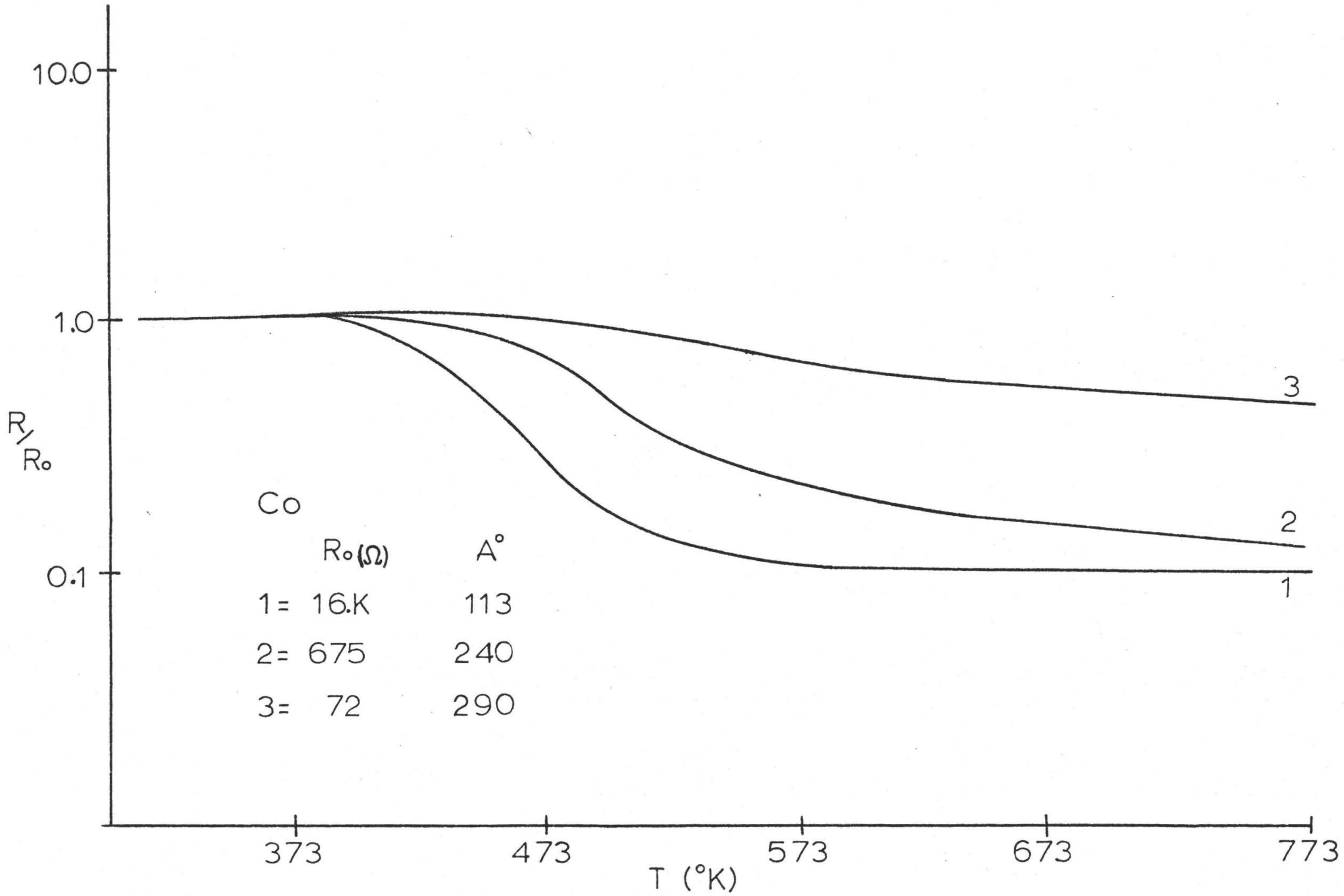

FIGURE 3: Resistance-temperature curves of Co-film during annealing in vacuum.

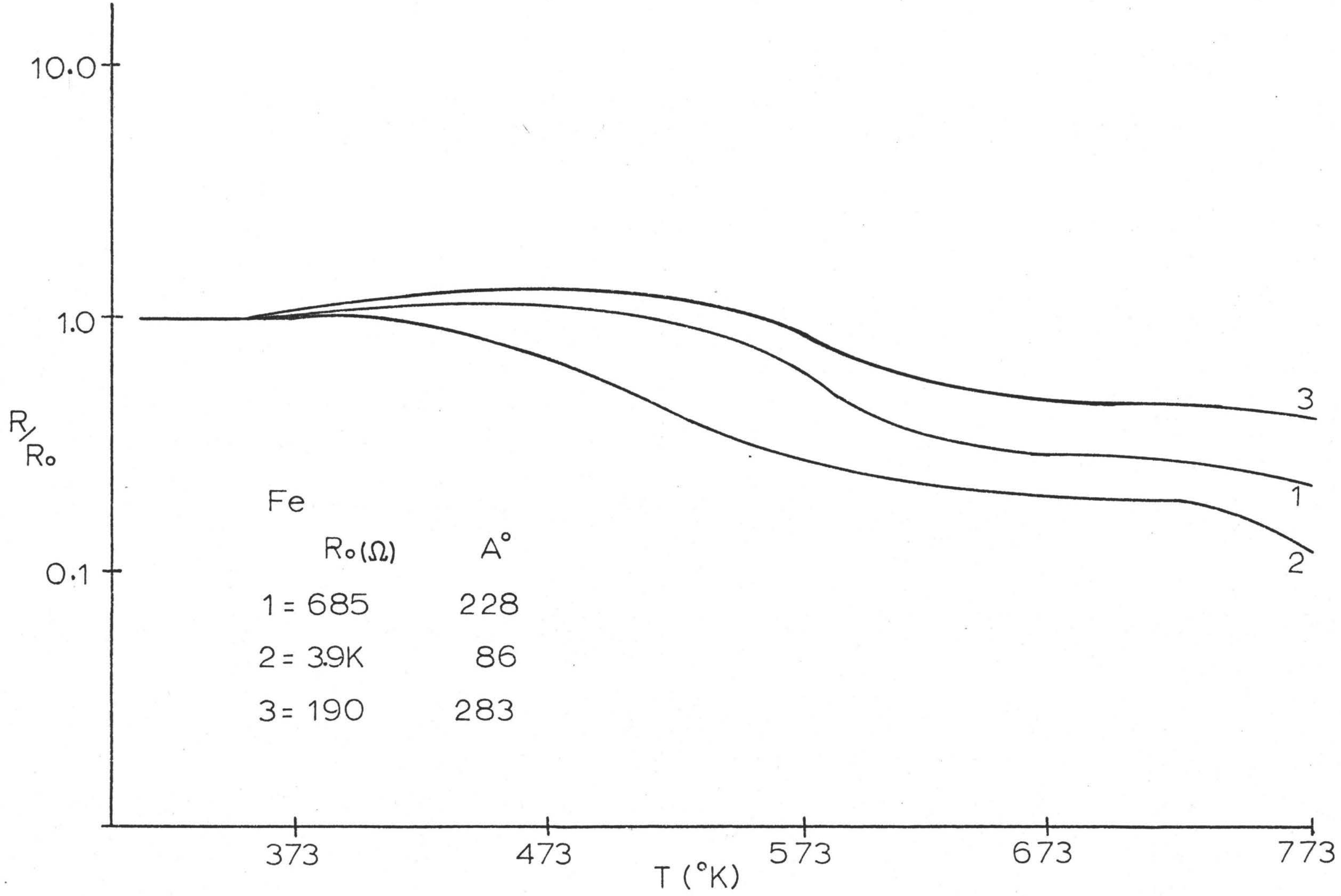

<u>FIGURE 4</u>: Resistance-temperature curves of Fe-film during annealing in vacuum.

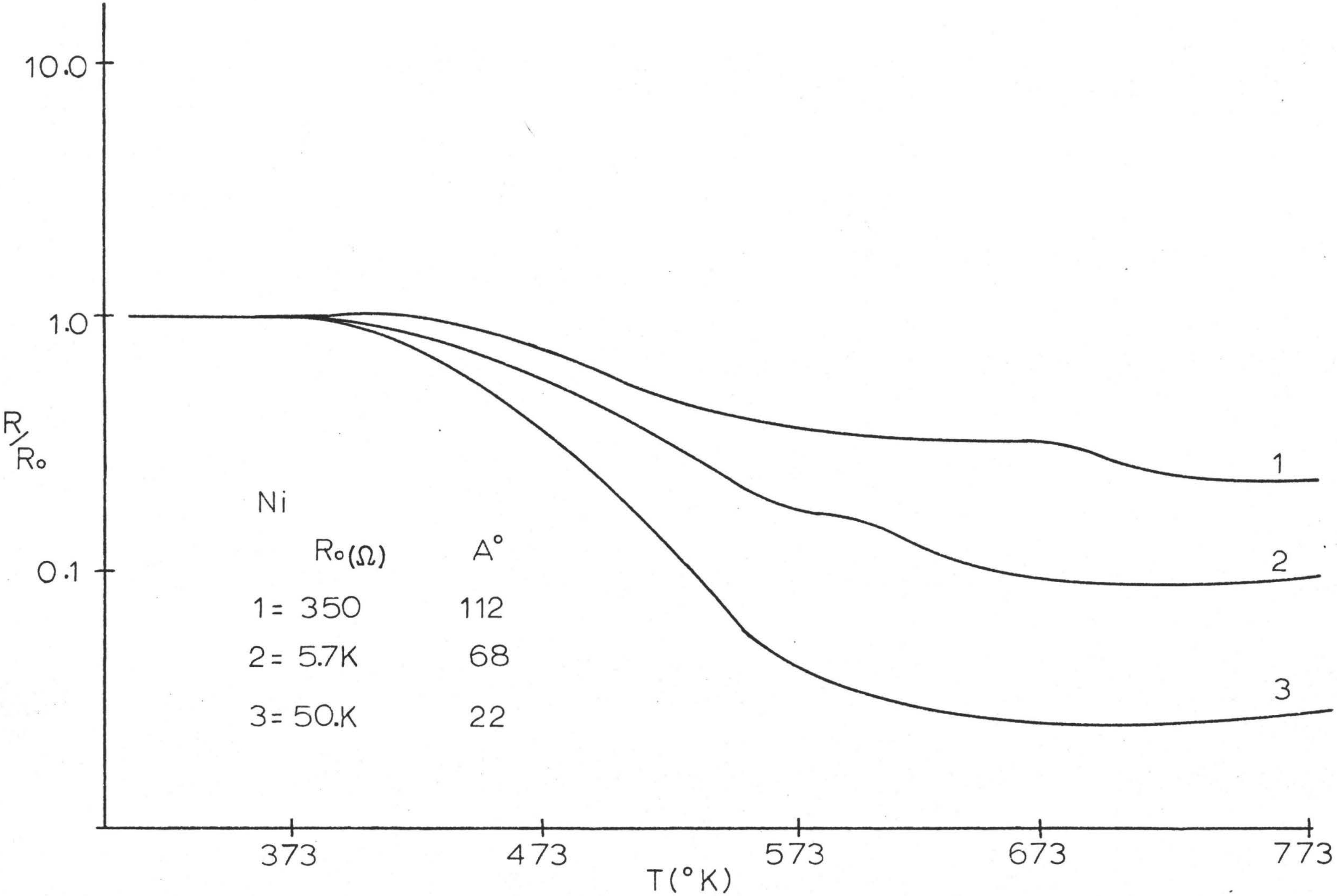

FIGURE 5: Resistance-temperature curves of Ni-film during annealing in vacuum.

Interpretation

Electron diffraction patterns as given in Figures 6 to 8, using the reflectance mode of a TEM (reference voltage 80KV), displayed increased sharpness of rings for the annealed samples. These results seem to indicate that grain growth has taken place upon annealing. In the cases of Al and Cr, the diffraction patterns were less sharp or fewer in number after annealing. Later studies showed that Al and Cr tended to form agglomerates if annealing was prolonged for any length of time at 500°C. Such a structural change would explain the increased resistance; structural changes for thinner films being more pronounced at even lower temperatures, as shown in the graphs.

It appears that, upon annealing these five metal films, the initial film thickness is a predominate factor in dictating the final resistance. The overall reaction will either tend towards grain growth or the formation of agglomerates. For Al and Cr the graphs show that for thicker films the initial trend is towards a decreased resistance. As the temperature continues to increase, the grain growth mechanism gives way to film thinning and eventually to the formation of agglomerates. In order to account for the effect on resistance due to this later process, a mathematical model is proposed (for a detailed derivation, see Appendix-Part I).

The model depicts the metal film as growing semispherical globs or islands. As the temperature increases further from room temperature, these metal globs become more pronounced with less and less material making the interconnections, as shown in Figure D of Appendix-Part I. Based on this model, the total resistance of the film can be expressed as

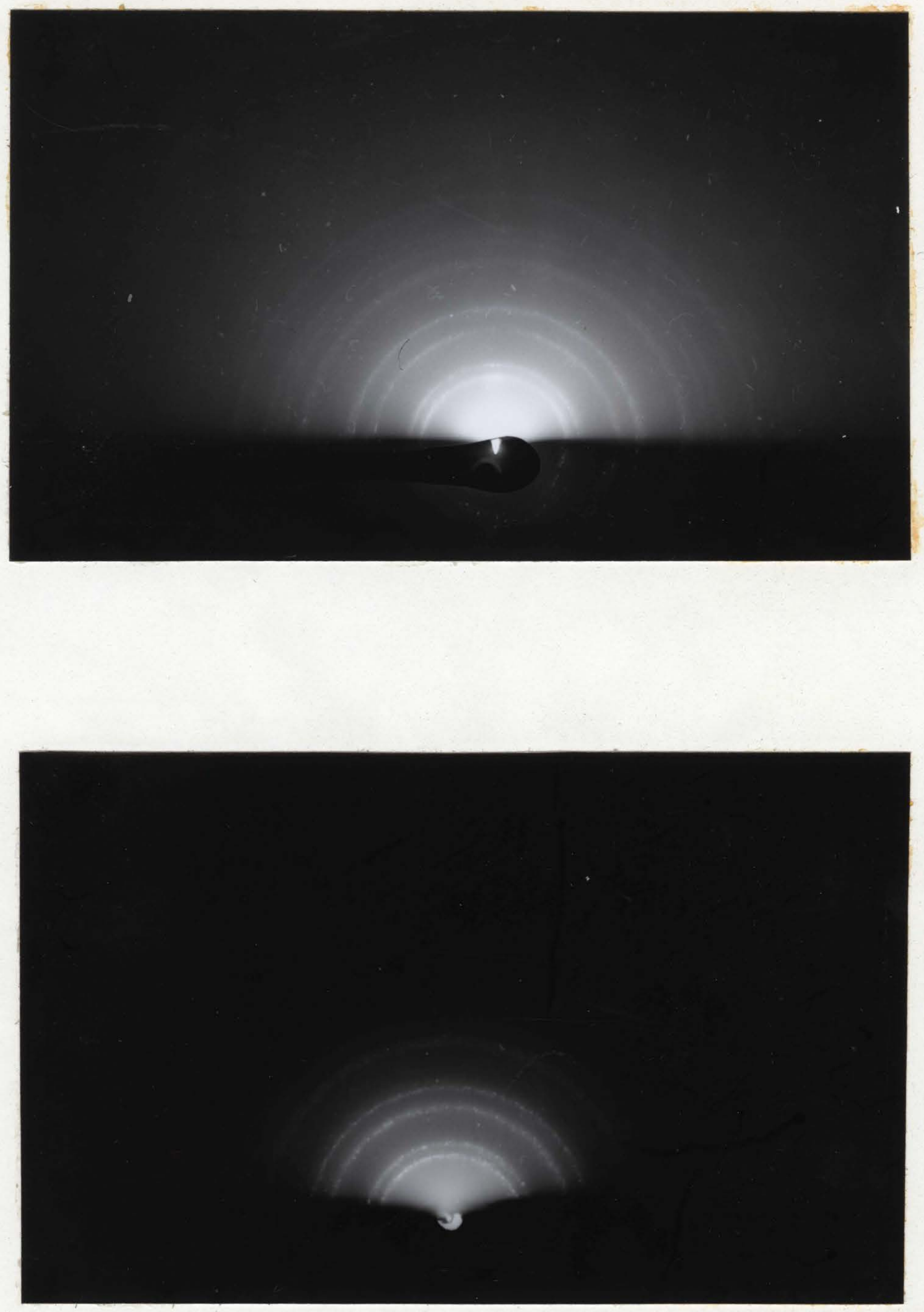

Fresh

Annealed

FIGURE 6: Diffraction patterns of Aluminum.

Fresh

Annealed

FIGURE 7: Diffraction patterns of Nickel.

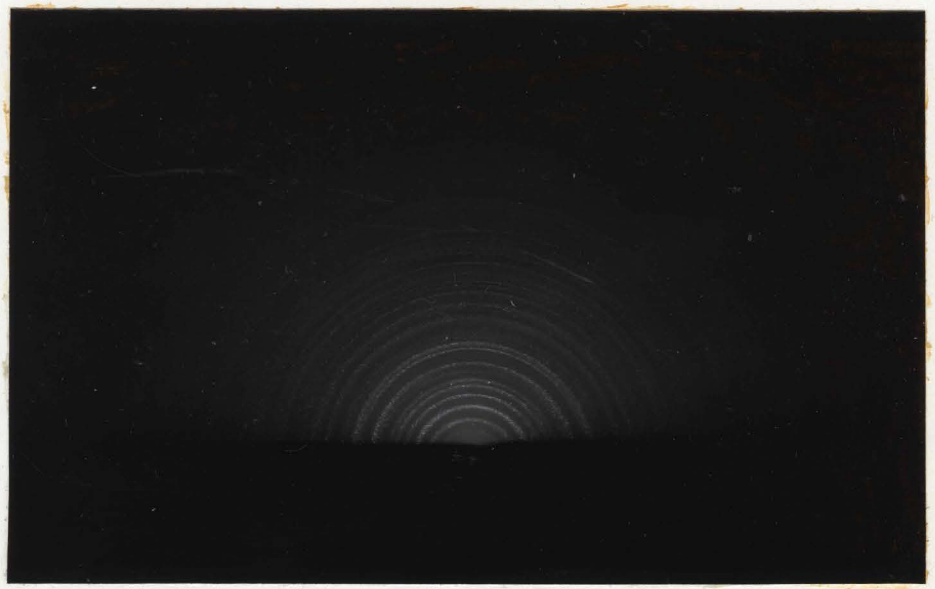

Iron

Cobalt

FIGURE 8(a): Diffraction patterns of Iron and Cobalt annealed at 500°C.

FIGURE 8(b): Diffraction patterns of Chromium annealed at 500°C.

$$R = \frac{C2\rho}{\pi a} \ln\left(\frac{2a - \Delta X}{\Delta X}\right) \qquad (2)$$

where R is the final overall resistance of the film, ρ is the resistivity of the metal, a is the radial distance of the agglomerate, ΔX is a temperature dependent variable, and C is a proportionality constant for a given film.

A plot of equation (2) is given in Figure 9. Comparisons between Figure 9 and 2 show a noticeable similarity between these curves indicating that the physical model is indeed reasonable.

This concept of semispherical formation is probably a reasonable beginning towards a model. Since the spherical configuration is of minimum free energy, it seems quite natural to assume that the formation of semispherical globs in the film as the temperature increases.

Further studies lead to a finding of what appeared to be an electromigration effect. At the instant when agglomeration appears to predominate, it was observed that the increasing resistance could either be enhanced by continually monitoring the resistance change or inhibited by intermittent monitoring. The resistance recording device used in all experiments was a Radiometer constant current, battery operated electrometer Type GVM 30a. Being a constant current device, the current density through the sample could increase at the grain boundaries. This in turn could accelerate the thinning processes of agglomeration through the effects of electromigration, which could explain the accelerated increased resistance. The appearance of electromigration initiated the research for Part II of this report.

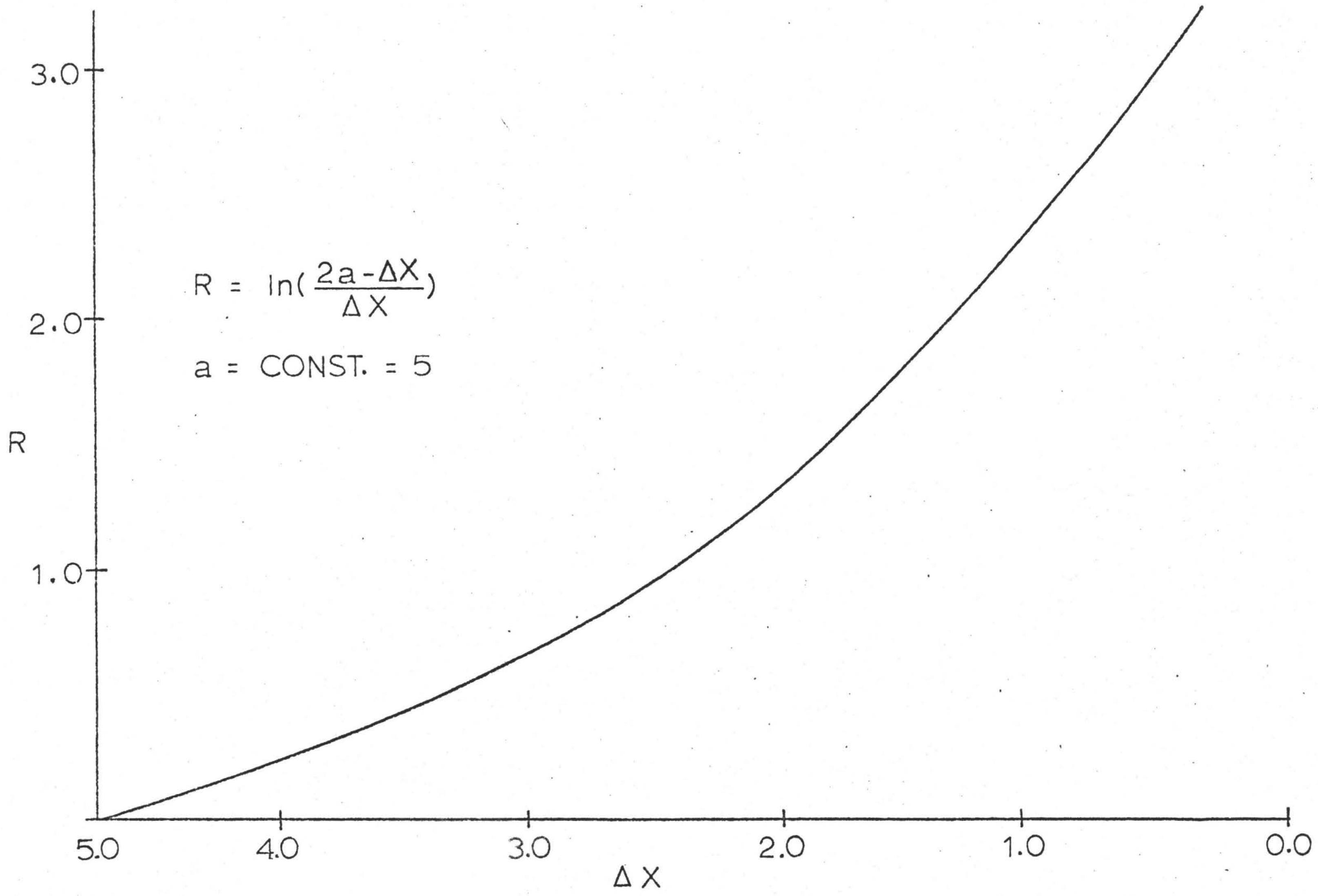

FIGURE 9: A plot of Equation (7) by using arbitrary numerical constants.

Conclusion

The results and corresponding interpretation of this portion on thermal and electrical properties of the five metals are only preliminary. From the results and associated graphs, it appears that the changing values of resistance can be associated with three predominate mechanisms that go on within the film as the temperature increases from room temperature to 500°C.

The first of these mechanisms is grain growth, providing a decrease in resistance. This decrease is quite pronounced for the films of Ni, Co, and Fe, and much less for the films of Al and Cr within the specified range of thicknesses. Secondly, there appears to be the formation of agglomerates which a proposed mathematical model attempts to illustrate as the predominate factor attributing to the increased film resistance of the Al and Cr samples. It is expected that similar results would have occurred for the metals of Ni, Co, and Fe if much thinner films had been tested. A third mechanism which can contribute to increased resistance is that of electromigration. It was suspected that this was the mechanism occurring within the latter stages of increased temperature for the Al and Cr films. Further studies are needed in order to get a better understanding of these mechanisms which contribute to increased film resistance as a function of increased temperature.

PART II

Electromigration of Aluminum in Thin Aluminum Film

Introduction

Electromigration is the phenomenon of mass transport of material resulting from the passage of a dc current. It has been identified as the cause of failures in thin film aluminum conductors, as used in planar silicon devices.

The effect of electromigration is quite similar to diffusion mechanisms. One such mechanism is the Soret effect, which can be observed simultaneously with electromigration. In this case, mass transport occurs between two regions of a sample which are maintained at different temperatures. Soret effect is therefore known as thermal migration. It can readily be distinguished from electromigration by conducting simultaneous studies with ac and dc currents, yet maintaining the same current densities.

For thin films, electromigration phenomenon is apparently not significantly different from the phenomenon which have been observed to occur in the bulk samples. Over the range of temperatures which are of interest for electromigration in films, mass transport does not occur through lattice diffusion but proceeds along the grain boundaries. This is more likely to happen in thin films where grain size is small and the boundaries are abundant. Of course lattice and grain boundary diffusion always occur simultaneously in polycrystalline materials. However, as a rule it is the most rapid mechanism which contributes most to the transport phenomenon.

The above theory on electromigration in aluminum thin films has been the object of numerous publications(3-30). The values of activation energy which have been determined, at temperatures up to 350°C, are of the order of 0.5 to 0.6 eV(10,13,16,22,25). These magnitudes of the activation energy support the theory that transport would occur through grain boundary diffusion since lattice diffusion would give a much higher value about 1.4 eV. This latter point was confirmed by an experiment(21) which shows that single crystal aluminum thin film conductors are practically uneffected by conditions of current density and temperature which usually cause rapid failure in polycrystalline films.

For all preceding work involving aluminum film, the direction of migration has always been interpreted as moving towards the anode(18,31,32). The present researchers have observed just the opposite effect, that migration appears to proceed towards the cathode.

An extensive review on electromigration in bulk metallic samples was published in 1963(33). Other works since 1963 are given in References 34 to 49. In these works the total force in the metal upon the moving atoms is conceived as the resultant of two forces which are often of opposite signs. The first force, F_C, is thought of as resulting from the exchange of momentum between scattered charge carriers and atoms(34). It is therefore the force which has the same direction as the motion of charge carriers and, for this reason, is sometimes referred to as the electron wind force. Theoretical treatment indicates the F_C is inversely proportional to the resistivity of the metal and, therefore, it decreases with increased temperature. The second force, F_E, is due to the interaction between the ionic core of the atoms and the applied field; it is assumed proportional to the product of the field strength (E) and the valence (Z) of the metal. Now all previous derivations give this force upon the ion, as being directed towards the negative electrode, and primarily independent of temperature. However, in the work by Wever(33), page 338 notes that the migration in copper reverses direction from anode to cathode when the temperature is between 900°C and 1000°C. With respect to these results by Wever and our present findings, it is proposed that $F_{E'}$ is also temperature dependent, in which $F_{E'}$ is the effective force experienced by the ions. The probability of an ion jump in the direction $F_{E'}$ is given as

$$F_E = \beta' \exp(-\Sigma m - \frac{ZeE'a}{2} + \frac{Z\alpha\omega\Sigma}{2})/kT \qquad (3)$$

where Σm is the height of the potential barrier, β' is a constant and is related to the ratio of vacancies to ions and the vibrational frequency, Z is the valence, e is the electron charge, E' is the effective field as seen by the metal ions, "a" is the lattice spacing, $\alpha\omega\Sigma$ is the energy acquired by the ion resulting from collision with electrons, k is Boltzman's constant and T is the absolute temperature. In the F_C direction, the probability of an ion jump is given as

$$F_C = \beta' \exp(- m + \frac{ZeE'a}{2} - \frac{Z\alpha\omega\Sigma}{2})/kT \qquad (4)$$

When the last term is much smaller than the second last term in the bracket, which is apparent in our case, then the drift velocity of ion migration can be written as

$$\bar{V} = (F_E - F_C)a = \beta' \frac{ZeE'a^2}{kT} \exp(- \frac{Q}{kT}) \qquad (5)$$

where Q is the activation energy. Refer to the Appendix-Part II for a more complete derivation.

Another query of former studies, which the present researchers have difficulty in interpreting, is marker mobility. Based upon Huntington's works et al(34) and a subsequent article(41), the marker on the metal surface is assumed to be similar in nature as voids within the metal. Therfore, explanation as to the direction of metal mobility is based solely upon that assumption; if the marker is a void and it moves to the cathode then presumably metal has been displaced towards the anode. These same conditions for marker studies were attempted with the present experimental set-up. However, any similarity of interpretation to the other researchers' findings was not very explicit. Either the markers, upon annealing, were absorbed and vanished, exhibiting no trend of mobility towards either electrode, or else they appeared to be displaced with the metal. Further elaboration on marker studies is outlined in the conclusion.

Experiment and Results

The aluminum used in these experiments was given as 99.995% pure. A 5.0 mm wide X 15.0 mm long strip of the metal was vacuum evaporated onto a quartz substrate using standard preparative techniques. The metal strip was then clamped between two electrodes. An identical procedure to that described in Part I was used to mount the quartz substrate in the vacuum furnace. Temperature to the furnace was preset to a desired temperature and automatically maintained at that temperature to within ±5°C limits.

D.C. current to the sample was supplied by a 12 volt car battery. The current was preset before the circuit was completed. Values of current, initial and final resistance at the preset temperature, and the time to rupture were the parameters recorded.

Tables I and II give the observed data of the calculated values of velocity $\bar{V}$ and the parameter β' for the two different currents and thicknesses. The value of S, distance, was interpreted as being one-half the distance over which the migration effect can be observed (see Figure 12). Note that for all samples and over all temperature ranges used in these experiments, migrations takes place from the anode towards the cathode (see Figures 10 to 12). The effect is more readily observed by using the transmission mode of the optic microscope (see Figure 14). Here the surface of migrating metal is opaque when compared to the surrounding matrix of metal and voids.

Repeating the experiment, but this time testing for the Soret effect by reversing the potential to the electrodes, gave identical results. Here, at least was an indication that thermal migration was not the predominant factor giving rise to the characteristic patterns.

TABLE I

Electromigration of 1000Å Aluminum Film at Constant Temperatures
With an Initial Current of 3.0 Amperes

	Temp °K	S(mm)	t(sec)	$\bar{V}$(m/sec)	R_f-Ω-T°K	β'(10^{15}sec)
1	773	2.45	3.0	9.8×10^{-4}	3.0	2.076
2	723	2.25	4.5	5.0×10^{-4}	3.1	1.854
3	673	2.10	11.5	1.9×10^{-4}	2.0	1.795
4	623	2.00	14.2	1.4×10^{-4}	2.4	2.808
5	573	2.05	28.0	0.73×10^{-4}	2.4	3.586
6	523	1.80	52.4	0.35×10^{-4}	2.4	4.935
7	473	1.65	61.8	0.27×10^{-4}	2.2	14.047
8	423	1.75	80.6	0.21×10^{-4}	2.4	58.064
9	373	1.80	355.0	0.05×10^{-4}	2.2	107.466

TABLE II

Electromigration of 2500Å Aluminum Film at Constant Temperatures
With an Initial Current of 5.5 Amperes

	Temp°K	S(mm)	t(sec)	$\bar{V}$(m/sec)	R_f-Ω-T°K	β'(10^{15}sec)
1	773	3.90	2.8	13.9×10^{-4}	1.4	4.484
2	673	2.25	3.7	6.0×10^{-4}	1.2	6.574
3	573	1.80	8.2	2.2×10^{-4}	1.1	12.544
4	473	2.05	22.8	0.9×10^{-4}	1.0	54.544
5	373	1.85	53.0	0.3×10^{-4}	0.8	958.40

Cathode

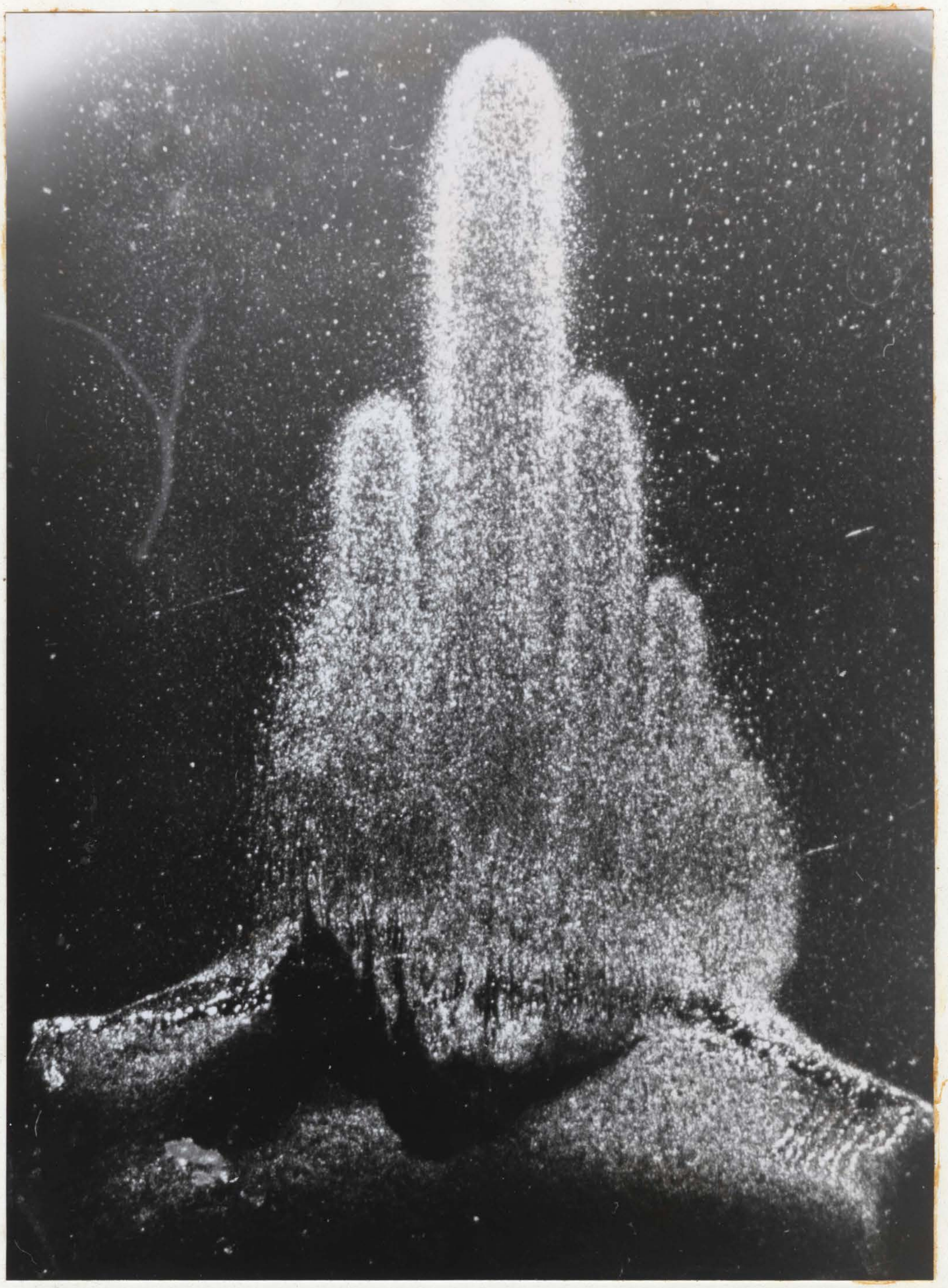

Anode

FIGURE 10: Electromigration of Al-film (reflection). The result was obtained by increasing the sample temperature linearly from room temperature to 450°C.

Cathode

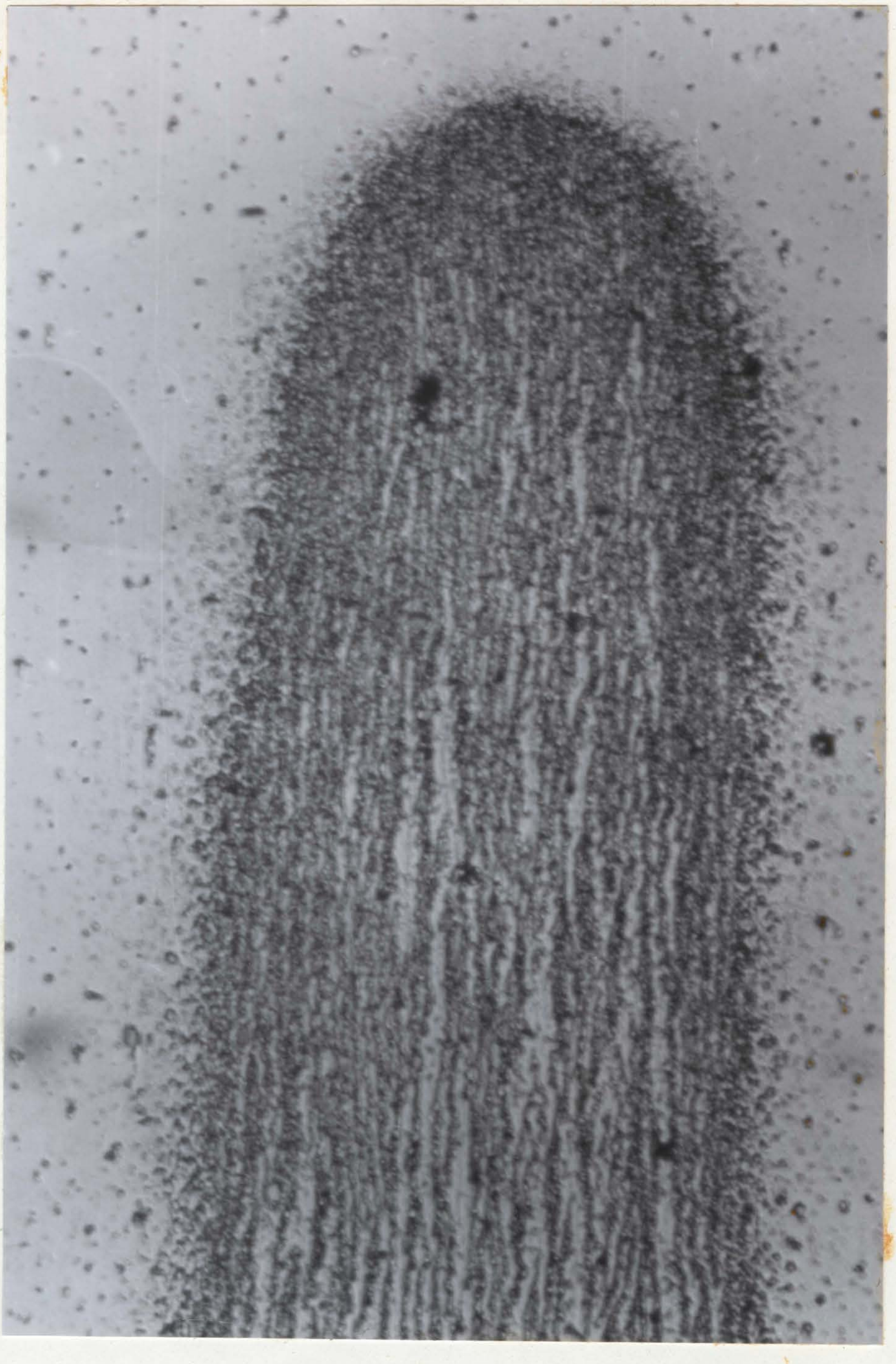

Anode

FIGURE 11: Top of Figure 10 magnified 225 times.

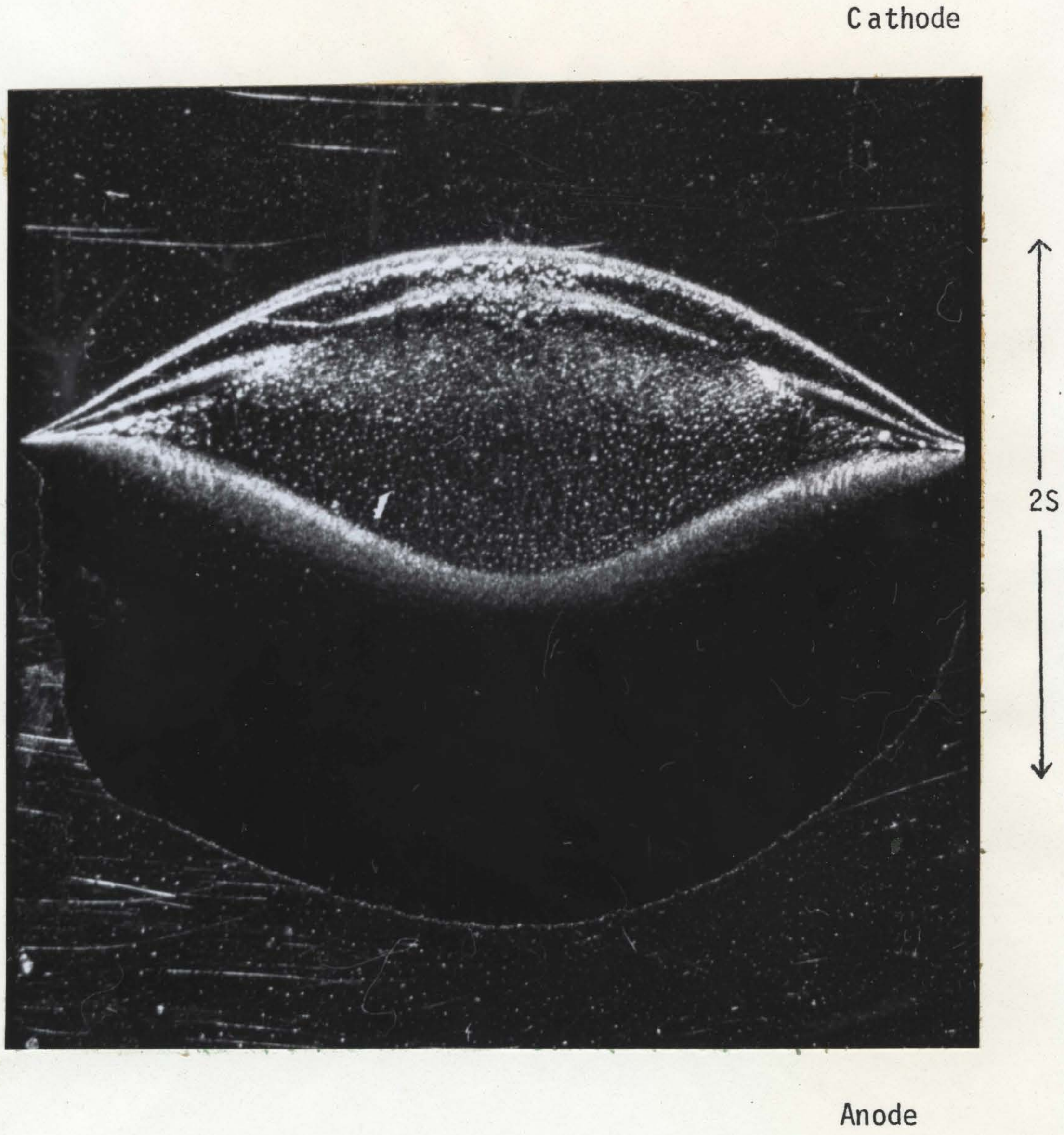

FIGURE 12: Electromigration of Al-film (reflection). The result was obtained by keeping the sample at a constant temperature of 450°C.

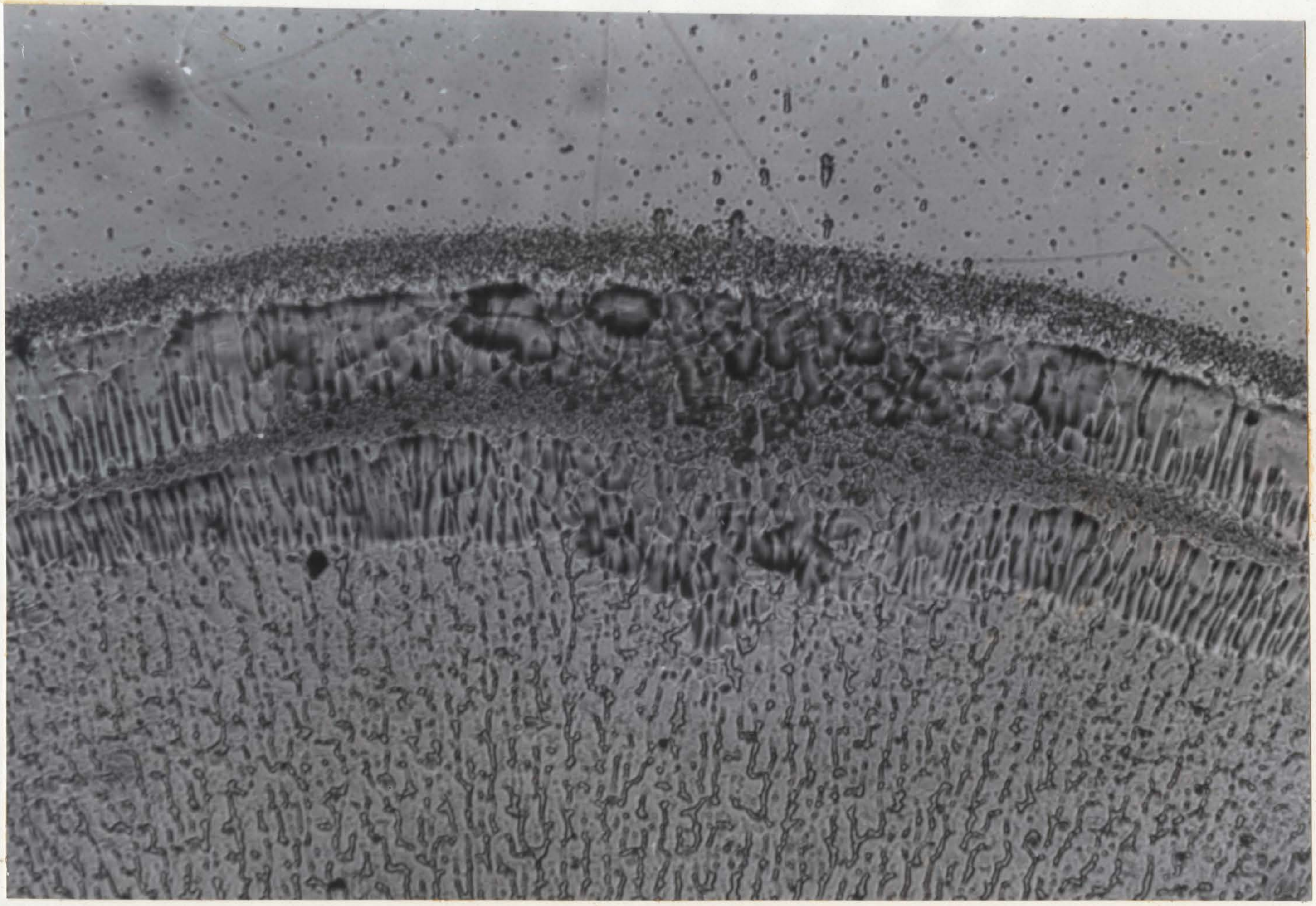

FIGURE 13:   Top part of Figure 12 (reflection) magnified 500 times.

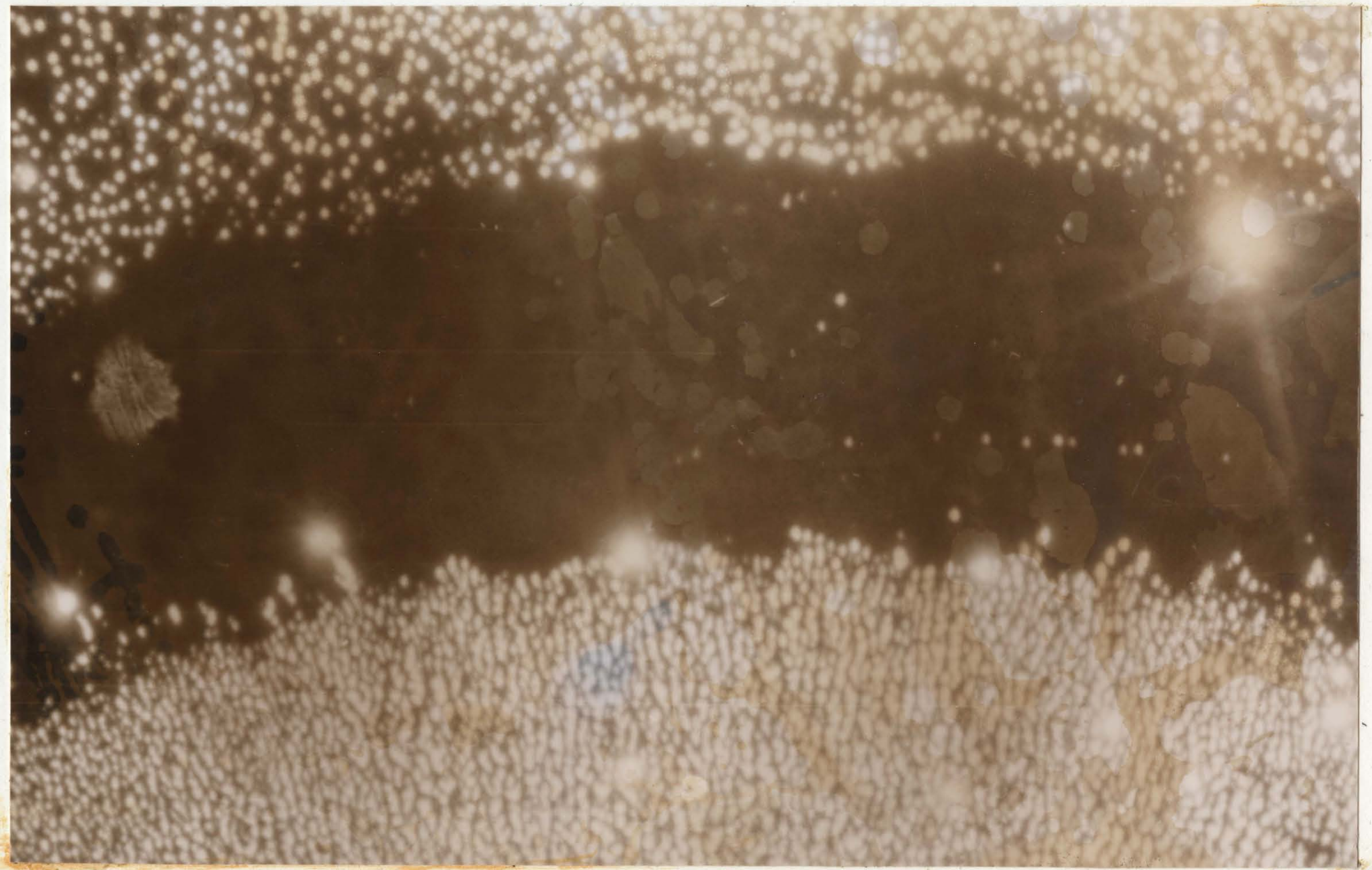

FIGURE 14: Top part of Figure 12 (transmission) magnified 500 times.

Comparative studies were again tried using alternating currents (Figures 15 and 16). The results presented show a very symmetrical design about the point of rupture without any preferential buildup of material towards either extreme. Another interesting find from this experiment was that the RMS current density needed for rupture seems to be higher than that required for dc currents.

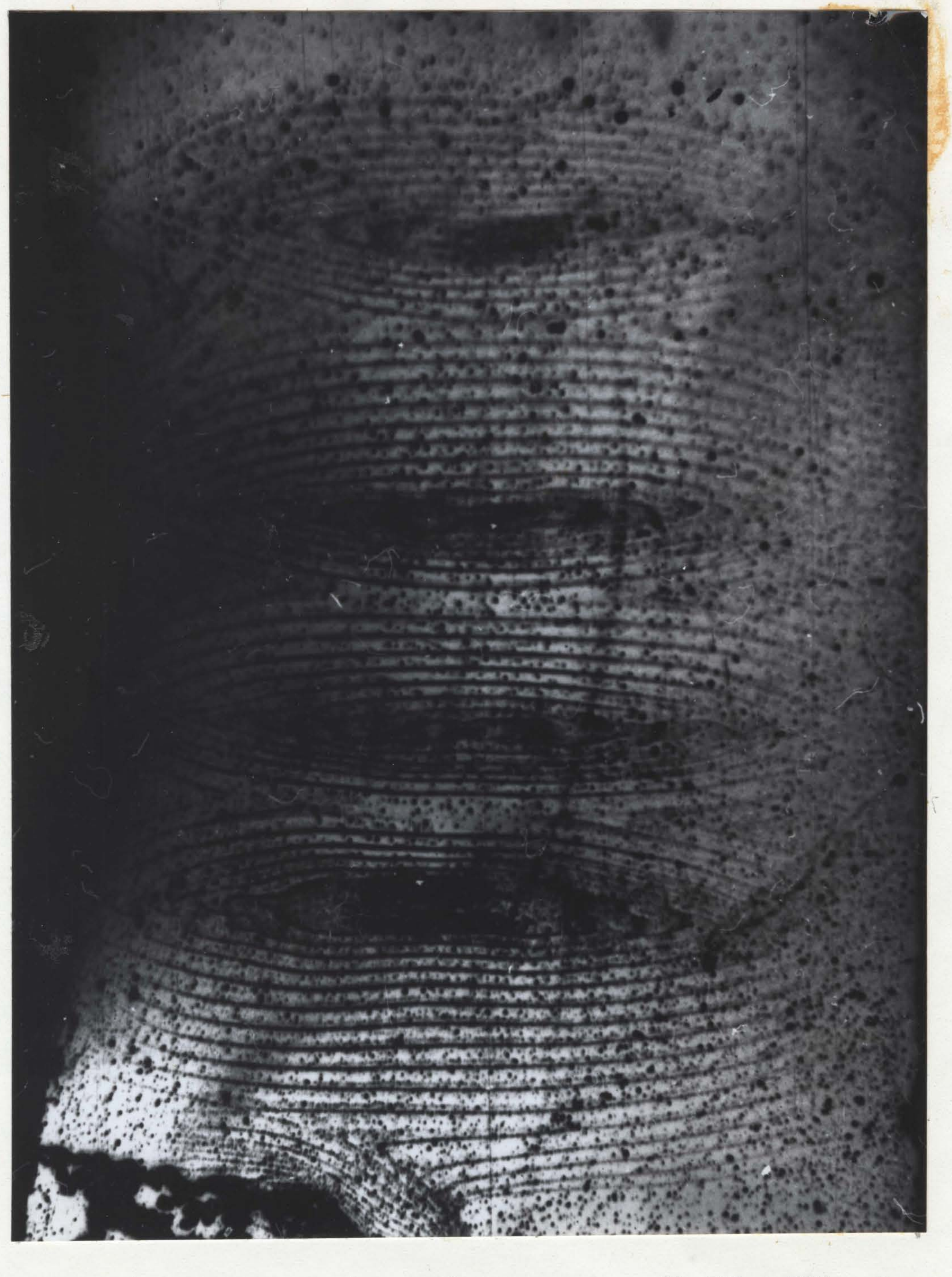

FIGURE 15: Effects of alternating current on Al-film, 75X using transmitted light.

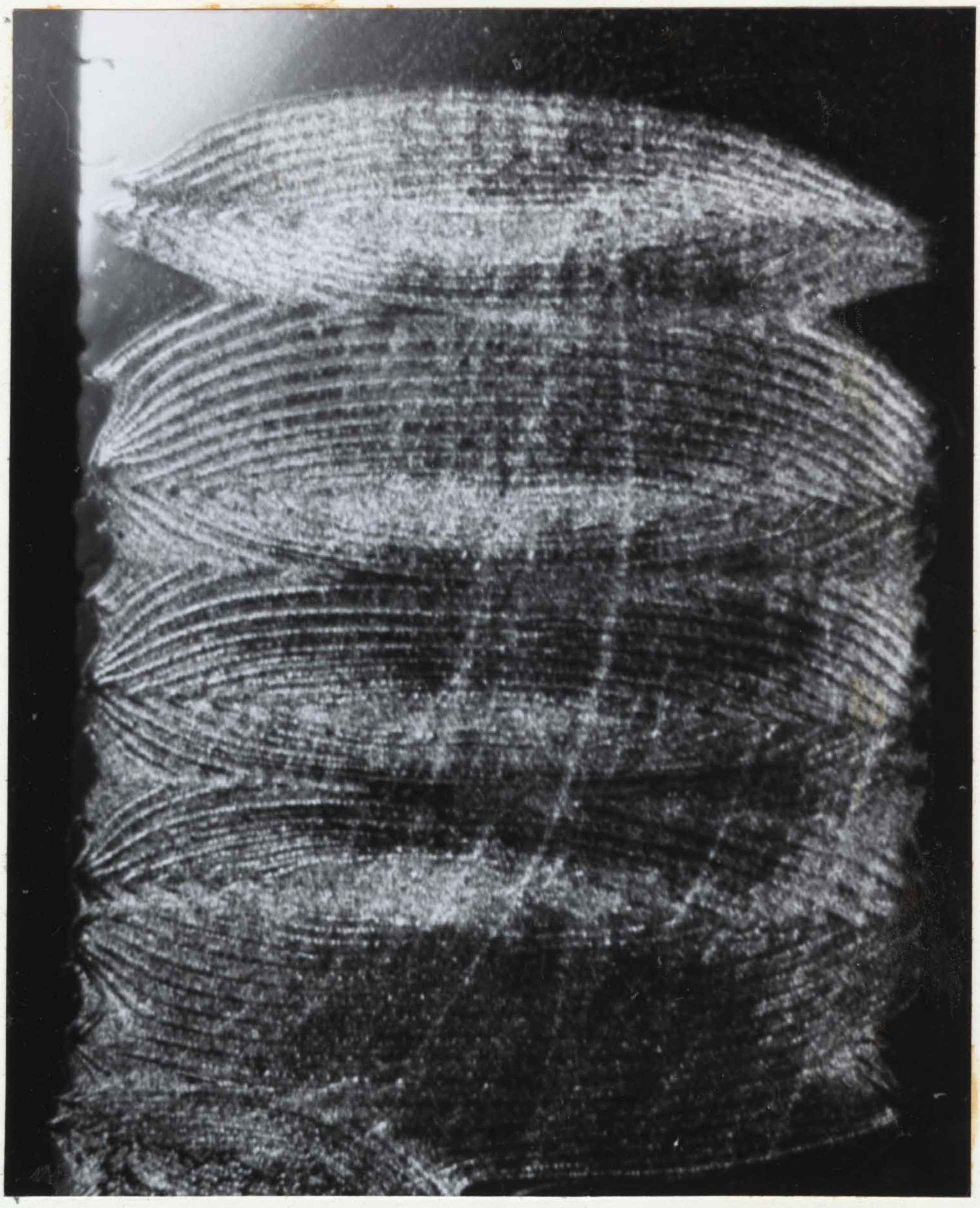

FIGURE 16: Effects of alternating current on Al-film, 75X using reflected light.

Interpretation

The graphs in Figure 17 are similar to an Arrhenius plot of diffusion coefficients for both lattice (single crystal) and for grain boundary diffusion(50). Such a plot consists of the diffusion coefficients plotted logarithmically against the reciprocal of the absolute temperature. The concept being that as the grains become larger, the polycrystalline curves should approach asymtotically the curve of the single crystal at a much lower temperature.

The difference in the intercepts which these two curves make with the velocity axis is due in part to the difference in current densities. For higher current densities, it could be expected that the velocity would increase more rapidly as the higher temperatures are approached. Some evidence of this effective mechanism is provided in Figure 18. β' at the lower temperatures increases rapidly, having a very steep curve, whereas at higher temperatures it approaches more nearly a single value. The actual value of β, referring to the appendix, is the ratio of vacancy to lattice frequencies. It may therefore be at lower temperatures where there is an abundance of vacancies in the freshly deposited film and which, in surrounding the metal ions, influences the vibrational frequncy of the ions. However, as the temperature is increased, the number of vacancies is reduced through the effects of annealing. The metal ions are less affected by the remaining vacancies and their vibrational frequency approaches more closely that of the perfect lattice. Hence, β' becomes closer to the single value of the vibrational frequency for an ion situated in a perfect lattice.

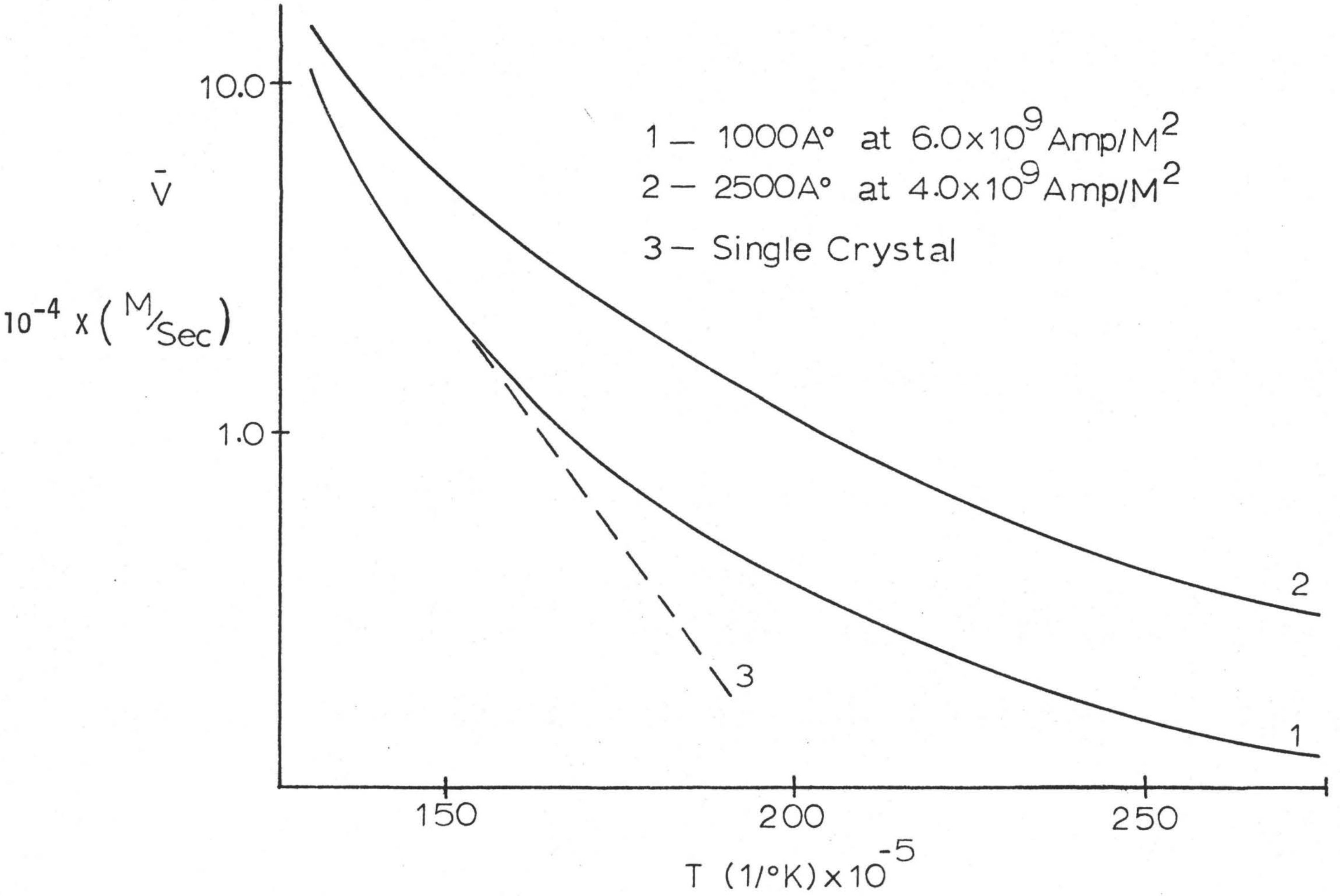

FIGURE 17: Typical plot of the observed results of electromigration in Al-film.

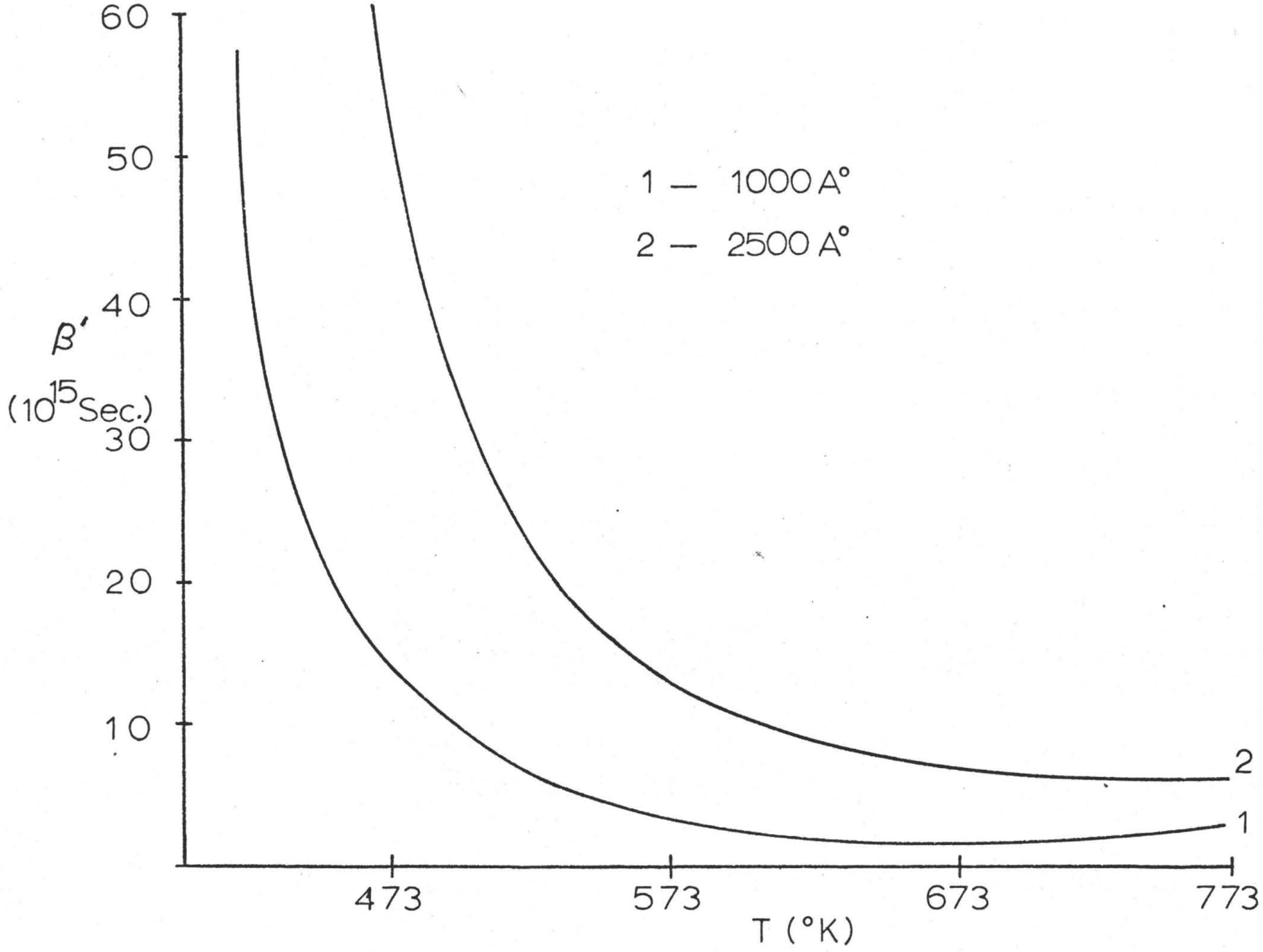

FIGURE 18: A plot of the parameter β' appearing in Equation (5) against sample-temperature T.

As to the phenomenon of reversing migration when temperature changes, such as in the case of Cu(33), it is proposed that the effect is primarily due to two reasons:

(1) Since the electron-wind effect is inversely proportional to the square of resistivity (see equation (14) of Appendix-Part II) as temperature increases this effect decreases.

(2) As temperature increases, the screening effect on the ions decreases(54), hence, increasing the effective field strength as seen by the metal ions.

Then, when the last two terms in the brackets of equation (14) become comparable, then migration could switch directions. Consequently, migration to either $\left(\begin{matrix}\text{cathode}\\ \text{anode}\end{matrix}\ \text{to}\ \begin{matrix}\text{anode}\\ \text{cathode}\end{matrix}\right)$ is possible and depends upon the magnitude of these last two terms in the proposed mathematical model.

Conclusion

Our results, except for the direction of migration, are quite compatable and with the same order of magnitude as those of other workers. It is the direction of migration which remains the point in question. It is apparent from the results displayed in Figure 14 that the metal has indeed become thicker in the direction of the cathode. That the area near the anode becomes transparent with an abrupt crest shape configuration separating substrate and metal film.

From graphical recordings of the applied current we know that the electric current is not constant throughout the experiment. There appears to be an initial slow exponential decay before a sudden breakdown. However, the applied electric field E was assumed to be constant even though the current decreased. This assumption was justified on the basis that as J, the current, decreases also the film becomes thinner due to the migration of metal and therefore, ρ, the resistivity increased.

Perhaps the greatest single difference between this piece of research, compared to others associated with aluminum thin film is in the presentation of samples within a temperature controlled environment. For this research the samples are placed in a controlled environment with a uniform ±5°C temperature gradient extending beyond the sample area. In a review article(51), the technique used extensively by Huntington and coworkers was to use the same electrical current in the study of migration to heat the specimen. This results in a temperature gradient where the temperature is at a maximum in the middle of the specimen and much lower at one end, which is apparently water cooled. Though this technique has the advantage of providing the marker velocity at many temperatures from just one sample, it will also produce marker velocity through the Soret effect. The Soret effect will produce a positive marker velocity on one side of the plane of maximum temperature and a negative marker velocity on the other side.

Marker techniques, as reported, suffer from a number of experimental difficulties in addition to the Soret effect. There are other effects which come into play as specimen creep due to surface tensions, sagging or shrinking of the specimen, specimen length change and local overheating due to void formation, surface diffusion, evaporation and condensation, and changes in the specimen's dimension in the transverse direction can produce apparent marker shift.

A much better technique to overcome most difficulties with the marker studies has been used by Gilder and Lazarus(52). The technique uses two radioactive isotopes, one of the element whose motion is to be studied, and the other of a material which behaves as an inert marker in the matrix. After a current has been passed through the sample for a given time, then the relative distance "S" between consentrations of the trace element to that of the marker gives a direct measurement of the velocity "V", independent of dimensional changes. Further experiments on electromigration, as presented here, could use the radioactive tracer technique towards a better understanding of the mechanics involved in the mobility and the parameters used to define the proposed mathematical model.

APPENDIX - PART I

The model used to formulate the mathematical expression relating increased film resistance to the formation of agglomerates is diagramatically outlined in the set of Figures A to D. When the metal film is freshly deposited, it is pictured as a continuous layer, Figure A. As the temperature increases from room temperature on up, in this case 500°C, the film begins to shrink and nucleate into grains at preferred sights. These sights develop, growing apart from neighbouring sights to form islands, Figures B to D.

Figure E shows one island and the mathematical parameters used to describe the dimensional growth of the agglomerates. Looking down onto the film, Figure F, it can be pictured as rows of spherical islands whose centres are situated an equipotential distance apart. The increasing film resistance is seen to occur at those points of intersect between spheres in the direction of current flow. An equivalent series-parallel resistance network relates this discrete intersect resistance, r, to the total circuit or thin film resistance R.

SIDE VIEWS OF THE THIN METAL FILM

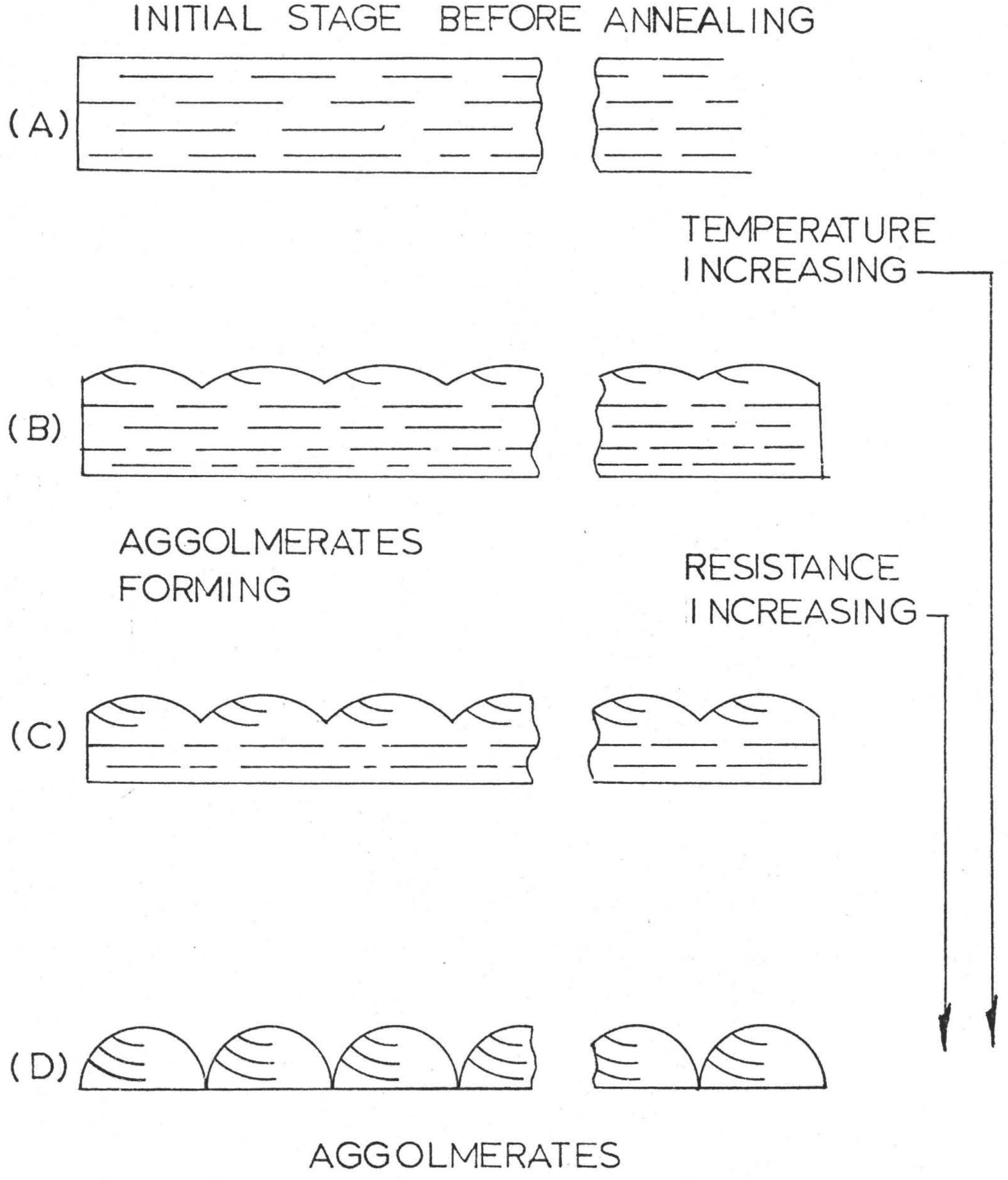

SIDE VIEW OF AN AGGLOMERATE

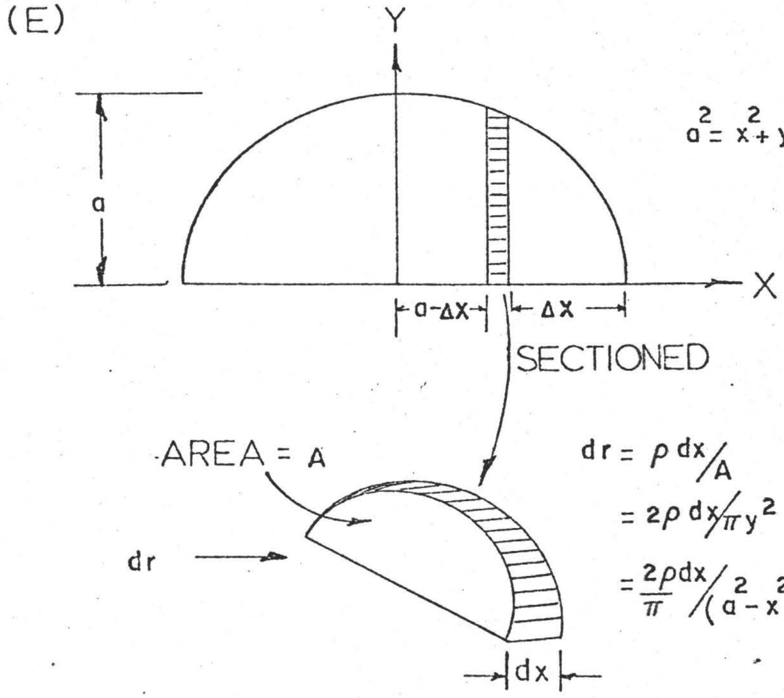

$$a^2 = x^2 + y^2 \qquad (1)$$

$$dr = \rho\, dx/A$$
$$= 2\rho\, dx/\pi y^2 \qquad (2)$$
$$= \frac{2\rho dx}{\pi} \Big/ (a^2 - x^2)$$

LOOKING DOWN ONTO THE FILM

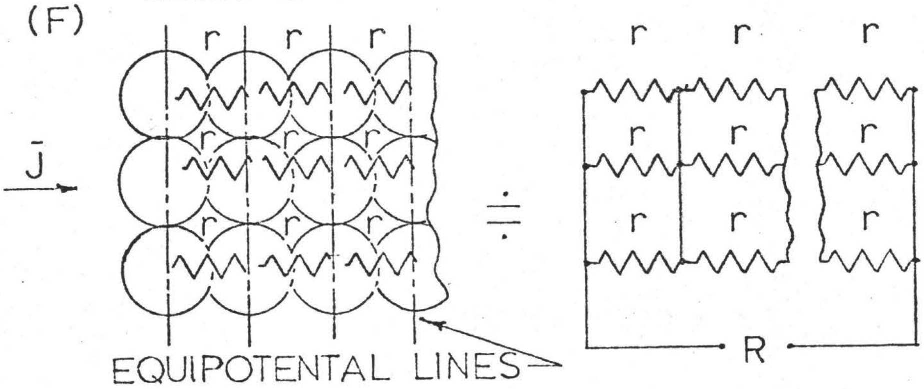

$$R = C\,\frac{4\rho}{\pi}\int_0^{a-\Delta x} \frac{dx}{a^2 - x^2} \qquad (3)$$

$$= C\,\frac{2\rho}{\pi a} \ln\left[\frac{2a - \Delta x}{\Delta x}\right] \qquad (4)$$

APPENDIX - PART II

For an electron of charge e in an electric field E, the drift velocity v can be written as

$$v = \frac{eE\tau}{m} \tag{1}$$

and the corresponding energy can be given as

$$\varepsilon = \frac{1}{2}mv^2$$

then, (2)

$$\varepsilon = \frac{e^2E^2\tau^2}{2m}$$

where m is the mass of the electron and τ is the relaxation time of collisions between electron and the positive ions.

During one collision, the electron will transfer a fraction of its energy $\alpha\varepsilon$ to the ion, where $\alpha \leqslant 1$. If there are $Z\omega$ collisions between the electron and the ion during the time interval in which the ion makes one jump over the lattice potential barrier, then the total energy transferred to a given ion resulting from the collisions can be expressed as

$$Z\alpha\omega\varepsilon \tag{3}$$

Now the jumping probability of an ion, which has acquired the energy $Z\alpha\omega\varepsilon$ in a current carrying metal moving against the applied field E, is given as;

$$f_c = \frac{n}{n'}\nu'\exp(-\varepsilon m + \frac{ZE'a}{2} - \frac{Z\alpha\omega\varepsilon}{2})/kT \tag{4}$$

In the direction of the field the jumping probability is given as;

$$f_E = \frac{n}{n'} \nu' \exp(-\varepsilon m - \frac{ZeE'a}{2} + \frac{Z\alpha\omega\varepsilon}{2})/kT \tag{5}$$

where n and n' are the densities of vacancies and positive ions where $n + n'$ = constant for the system in question, ν' is the vibrational frequency of ions under consideration, εm is the lattice potential barrier height, Z is the valence of the positive ion, E' is the effective field as seen by the ion as a result of electron screening, a is the lattice constant, k is Boltzman's constant, and T is the absolute temperature. Then the net jumping probability is

$$f = f_c - f_E$$

$$f = \frac{n}{n'} \nu' \exp(\frac{-\varepsilon m}{kT}) \{\exp(\frac{ZeE'a}{2} - \frac{Z\alpha\omega\varepsilon}{2})/kT - \exp(\frac{Z\alpha\omega\varepsilon}{2} - \frac{ZeE'a}{2})/kT\} \tag{6}$$

For the case where

$$Z\alpha\omega\varepsilon << ZeE'a \tag{7}$$

$$f = \frac{n}{n'} \nu' \frac{ZeE'a}{kT} \exp(\frac{-\varepsilon m}{kT}) \tag{8}$$

From Reference (53)

$$\frac{n}{n'} = (\frac{\nu}{\nu'})^{3x} \exp(\frac{-\varepsilon v}{kT}) \tag{9}$$

where εv is the activation energy required to form a vacancy, x is the number of nearest neighbours, and ν is the vibration frequency for an ion situated in a perfect lattice.

Combining equations (8) and (9)

$$f = \left(\frac{\nu}{\nu'}\right)^{3x-1} \nu \, \frac{ZeE'a}{kT} \exp\left(\frac{-2\varepsilon m + \varepsilon\nu}{2kT}\right) = \beta\nu \, \frac{ZeE'a}{kT} \exp\left(\frac{-Q}{kT}\right) \qquad (10)$$

where $\beta = \left(\frac{\nu}{\nu'}\right)^{3x-1} > 1$ for an imperfect crystal; $x = 12$ for the fcc structure, reference (53); and $Q = \varepsilon m + \frac{\varepsilon\nu}{2}$ is the activation energy. The drift velocity of an ion's migration is

$$\bar{v} = fa = \beta' \, \frac{ZeE'a^2}{kT} \exp\left(\frac{-Q}{kT}\right) \qquad (11)$$

where $\beta' = \beta\nu$.

For the case where ZeE'a is in the same order of magnitude as $Z\alpha\omega\varepsilon$, then

$$\bar{v} = \frac{\beta'}{kT} \exp\left(\frac{-Q}{kT}\right) \{ZeE'a^2 - Za\alpha\omega\varepsilon\} \qquad (12)$$

Now

$$\varepsilon = \frac{e^2E^2\tau^2}{2m} = \frac{E^2m}{2N^2\rho^2e^2} \qquad (13)$$

where N is the electron density and ρ is the resistivity of the metal. Substituting equation (13) into equation (12), the final form for the velocity of migration is given as

$$\bar{v} = \frac{\beta'}{kT} \exp\left(\frac{-Q}{kT}\right) \left\{ZeE'a^2 - \frac{Za\alpha\omega E^2m}{2N^2\rho^2e^2}\right\} \qquad (14)$$

where the ZeE'a term depicts migration towards the cathode due to the applied electric field and the $\frac{Za\alpha\omega E^2m}{2N^2\rho^2e^2}$ depicts migration towards the anode due to the electron wind effect.

REFERENCES

1. C.A. Neugebaur and M.B. Webb, J. Appl. Phys., 33, 74 (1962).
2. S.T. Pai, J.P. Marton and J.D. Brown, J. Appl. Phys., 43, 282 (1972).
3. I.A. Blech and H. Sello, "The failure of thin aluminum current-carrying strips on oxidized silicon", Phys. Failure Electron., T. Shilliday and J. Vaccaro, Eds., vol. 5, Rome Air Develop. Ctr., Griffiss AFB, Rome, N.Y., pp. 496-505.
4. W. Mutter, "Electromigration in metal film conductors", Abstracts (Electrochemical Soc. Spring Meet., Dallas, Tex., May 1967) pp. 96-98.
5. R.G. Shepheard and R.P. Sopher, "Effects of current density and temperature on lifetime of aluminum thin film conductors", Abstracts (Electrochemical Soc. Spring Meet., Dallas, Tex., May 1967).
6. P.B. Ghate, Appl. Phys. Lett., 11, 14 (1967).
7. J.K. Howard and R.F. Ross, Appl. Phys. Lett., 11, 85 (1967).
8. I.A. Blech and E.S. Meieran, Appl. Phys. Lett., 11, 263 (1967).
9. J.R. Black, "Mass transport of aluminum by momentum exchange with conducting electrons", presented at IEEE 6th Annual Reliability Phys. Symp., Los Angeles, Calif., 1967.
10. R. Rosenberg and L. Berenbaum, Appl. Phys. Lett., 12, 201 (1968).
11. M.J. Attardo et al., "Aluminum electromigration in long stripes", presentation Abstracts 7th Ann. Reliability Phys. Symp. (Washington, D.C., Dec. 1968) pp.7-8.
12. J.R. Black, "Aluminum conductor failure by mass transport" in Proc. 3rd Int. Cong. on Microelectronics (Munich, Germany, 1968).

13. ————, IEEE Trans. Electron Devices, ED-16, 338 (1969).

14. J.R. Devaney, "Investigation of current induced mass transport in thin metal conducting stripes" in Proc. 3rd Annual Scanning Electron Microscope Symp., O. Johari, Ed. (Chicago, Apr. 1970), pp. 417-424.

15. S.M. Spitzer and S. Schwartz, IEEE Trans. Electron Devices, ED-16, 348 (1969).

16. I.A. Blech and E.S. Meieran, J. Appl. Phys., 40, 485 (1969).

17. H. Sello, "Ohmic contacts and integrated circuits" in Ohmic Contacts to Semiconductors, R. Schwartz, Ed., New York, Electrochemical Society, 1969, pp. 277-298.

18. C.B. Oliver, "Degradation of evaporated aluminum-contacts on silicon planar transistors", presented at IEEE 6th Annual Reliability Phys. Symp., Los Angeles, Calif., 1967.

19. J.R. Black, "Etch pit formation in silicon at aluminum-silicon contacts because of transport of silicon in aluminum by momentum exchange with conducting electrons", in Ohmic Contacts to Semiconductors, R. Schwartz, Ed., New York, Electrochemical Society, 1969, pp. 211-323.

20. R. Rosenberg, Appl. Phys. Lett., 16, 27 (1970).

21. E d'Heurle and I. Ames, Appl. Phys. Lett., 16, 80 (1970).

22. M.J. Attardo and R. Rosenberg, J. Appl. Phys., 41, 2381 (1970).

23. J.K. Howard and R.F. Ross, "The effect of preferred orientation on the rate of electromigration and its implication to the cracked stripe failure mode", IBM Tech. Rep., 22, 601, March 1968.

24. B. Agrawala, M.J. Attardo and A.P. Ingraham, J. Appl. Phys., 41, 3954 (1970).

25. M.C. Shine and E. d'Heurle, "Activation energy for electromigration in aluminum films alloyed with copper", IBM J. Res. Develop., Sept. 1971.

26. P.M. Austin and A.F. Mayadas, "Correlation between resistance ratios and electromigration failure in aluminum films", submitted to J. Vac. Sci. Technol.

27. T.E. Hartman and J.C. Blair, IEEE Trans. Electron Devices, ED-16, 407 (1969).

28. L. Berenbaum and R. Rosenberg, Thin Solid Films, 4, 187 (1969).

29. E. d'Heurle, L. Berenbaum and R. Rosenberg, Trans. Met. Soc. AIME, 242, 502 (1968).

30. E.M. d'Heurle, Met. Trans., 2, 681 (1971).

31. P.P. Kuz'menko and E.I. Khar'kov, Ukrain Fiz. Zhur., 4, 401 (1959).

32. P.P. Kuz'menko and L.F. Ostrovsky, Ukrain. Fiz. Zhur., 6, 525 (1961).

33. J. Verhoeven, Metallurgical Reviews, 8, 311 (1963).

34. H.B. Huntington and A.R. Grone, J. Phys. Chem. Solids, 20, 76 (1961).

35. C. Bosvieux and J. Friedel, J. Phys. Chem. Solids, 23, 123 (1962).

36. A.R. Grone, J. Phys. Chem. Solids, 20, 88 (1961).

37. G.A. Sullivan, J. Phys. Chem. Solids, 28, 347 (1962).

38. S.M. Klotsman, A.N. Timofeev and I. Sh. Trakhtenberg, Sov. Phys. - Solid State, 8, 2386.

39. ———, Phys. Metals Metallogr (USSR), 16, No. 4 (1964).

40. H.B. Huntington and S.C. Ho, J. Phys. Soc. Japan, 18, suppl. 11, 202 (1963).

41. R.B. Penney, J. Phys. Chem. Solids, 25, 335 (1964).

42. J. Verhoeven, J. Metals, 18, 26 (1966).

43. P.S. Ho, J. Phys. Chem. Solids, 27, 1331 (1966).

44. S.C. Ho and H.B. Huntington, J. Phys. Chem. Solids, 27, 1319 (1966).

45. T. Hehenkamp, Acta Met., *14*, 887 (1966).

46. H.M. Gilder and D. Lazarus, Phys. Rev., *145*, 507 (1966).

47. S.M. Klostman, A.N. Timofeev and I. Sh. Trakhtenberg, Phys. Status Solidi, *18*, 847 (1966).

48. G.M. Newmann and W. Hirschwald, Z. Naturforsch. A., *22*, 388 (1967).

49. H.J. Stepper and H. Wever, J. Phys. Chem. Solids, *28*, 1103 (1967).

50. F.M. d'Heurle, Proceedings of the IEEE, *59*, No. 10, 1409 (1971).

51. N.L. Peterson, *Solid State Physics*, vol. 22, Academic Press, New York and London (1968).

52. H.M. Gilder and D. Lazarus, Physics Rev., *145*, 507 (1966).

53. A.J. Dekker, Solid State Physics (1959).

54. J.M. Ziman, *Principles of the Theory of Solids*, Cambridge University Press, second edition (1972).

DESIGN AND CONSTRUCTION OF THE
150 kV ION IMPLANTATION ACCELERATOR SYSTEM
WITH A CRYOGENIC EXPERIMENTAL CHAMBER"

by

DENIS CLYDE BEATTY, B.A., B.Eng.Sc.

"PART B:" MCMASTER (ON-CAMPUS) PROJECT*

A Report Submitted to the School of Graduate Studies
in Partial Fulfilment of the Requirements
for the Degree
Master of Engineering

Department of Engineering Physics
McMaster University
Hamilton, Ontario, Canada.
August 1974

---

* One of two project reports: The other part is designated PART A: OFF-CAMPUS PROJECT.

MASTER OF ENGINEERING (1974)
Department of Engineering Physics

MCMASTER UNIVERSITY
Hamilton, Ontario.

TITLE: Design and Construction of the 150 kV Ion Implantation Accelerator with a Cryogenic Experimental Chamber

AUTHOR: Denis Clyde Beatty, B.A. (S.G.W.), B.Eng.Sc. (Western)

SUPERVISOR: Dr. D.A. Thompson

NUMBER OF PAGES: iv, 79

TABLE OF CONTENTS

ACKNOWLEDGEMENTS

My sincere thanks go to Dr. D.A. Thompson for letting me work on this project towards my M.Eng. Degree and for keeping a watchful eye on the project as it progressed.

Thanks are also due to Dr. A.B. Campbell for his valuable assistance and numerous discussions concerning the system's design, construction, and the running of experiments.

I also wish to extend my sincere thanks to the Director of the Accelerator Lab., Mr. Phil Ashbough, and to all his staff who lent a helping hand in this project.

LIST OF FIGURES

LIST OF TABLES

INTRODUCTION

Currently the most important and widely used application utilizing ion beams, especially from an industrial point of view, is the doping of semiconductors. This process involves the injection of selected ions to a desired depth and concentration into the semiconductor crystal. Such as, the forming of well defined complementary substrates with controlled resistivity (C-MOS devices). The fact that dopant characteristics of a substrate can be well defined compared to diffusion techniques reduces the possibility of gate overlap. The reduction of gate overlap reduces the capacitance between the drain and the source, which in turn improves the switching speed and reduces cross-talk and switching noise. Another application which utilizes the doping accuracy are linear resistors. These resistors are used in resistor-ratios for digital to analogue converters; also as load devices for linear and digital circuits. Other applications, just in the mentioning, are the uses of ion implantation for radiation hardening, formation of high voltage and microwave devices, and for application to controlled field inversion. Using low-energy ion implantations, controlled, ordered and disordered reactions of a lattice can be undertaken. With the introduction of interstitial foreign atoms into the crystalline matrix the chemical reaction rates at surfaces can be significantly altered. Ions when deposited on or just beneath a surface can passivate the surface, reducing its susceptibility to chemical reactions. As an example, SiO_2 and Si_3N_4 passivation layers have been grown by the bombardment of silicon surfaces with intense beams of low-energy oxygen and nitrogen ions.

In the following report, a description is given of an ion-source and accelerating system mounted in line with a 3 MeV Van der Graaf (KN) accelerator. Using MeV, He^+ and H^+ particles, channeling-effect measurements can then be performed in situ. on the freshly implanted substrate. Such a set-up, where the sample remains in one location throughout the entirity of a channeling experiment should permit a more accurate quantitative measure on the amount of disorder created by the implanted ions.

These are but a few applications of an ion beam. The ion source being the most important single element in an ion-beam system. The characteristics of the source determines to a great extent the performance of the remaining systems. For this reason a considerable amount of developmental effort has been expended over the past thirty or more years to evolve improved types and embodiments of ion sources.

The first part of this report will describe the basic mechanisms underlying the "Danfysik" hot cathode type ion source giving advantages and disadvantages of this source. The second part describes those parameters necessary in getting a uniform (stigmatic) beam down to its target area. Lastly, the third section describes a cryogenic experimental chamber that permits the implantation of samples at temperatures varying from 40 to 700 degrees Kelvin.

PART I

ELECTRON IMPACT IONIZATION PHENOMENA

Positive ions can be produced in four possible ionization processes, namely,

Electron impact ionization,

Surface ionization process,

Ion impact ionization (sputtering),

Charge exchange.

The Danfysik ion source, which is the primary concern of this report, uses the first of these ionization processes.

The electron impact ionization process is probably the most usual and commonly applied technique in ion sources. This is simply the transfer of sufficient potential energy to an atom on impact by a moving electron so that the atom is ionized. The technique is used in several ways, defining the type of ion source as, in an arc discharge, in a confined electron cloud (Danfysik), in an rf discharge, and in a spark. The electron cloud ion source configuration is the arc, which will be described in most detail later in this report.

The efficiency of ionization(1), or the actual number of ionizing collisions suffered by an electron in passing through a gas per unit path length per unit pressures is called the differential ionization coefficient S_e. This coefficient depends upon the electron energy $K_o = m_e V_e^2/2$ for various elements (Figure 1); where m_e is the mass of the

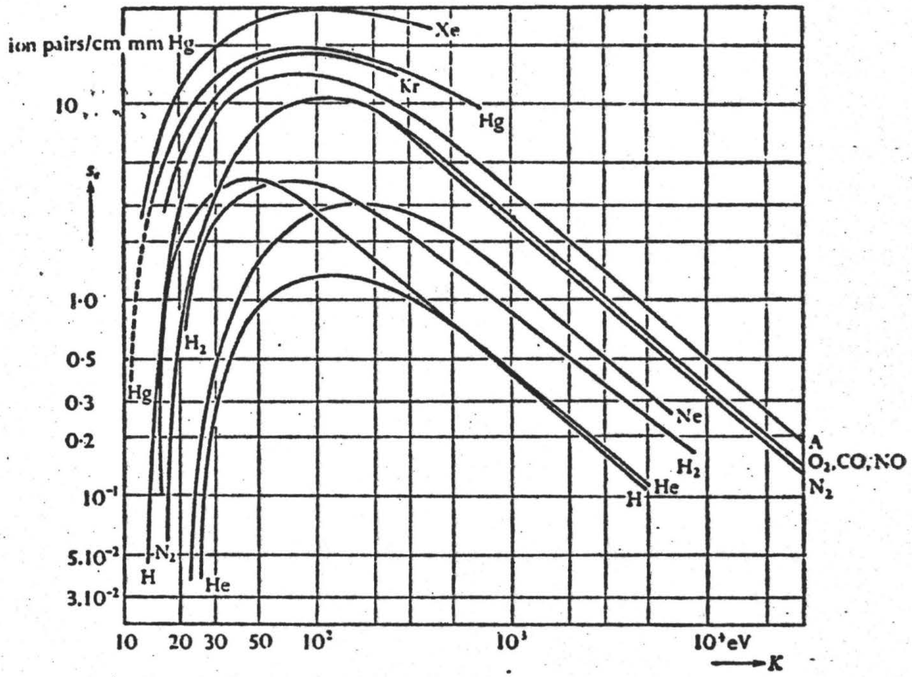

Figure 1: Ionization efficiency Se as a function of the electron energy K for various gases$^{(1)}$.

electron and V_e is the velocity of the electron after impact with an atom. Now for ionization to occur $K_o \geqslant eV_i$ where V_i is the internal potential energy of the atom. For example, the energy required to detach the electron from a hydrogen atom, which has one positive nuclear charge (Z = 1) is given by the sum of the potential and kinetic energy,

$$eV_i = \frac{Ze^2}{r} + \frac{mv^2}{2} . \qquad (1)$$

Consequently, the initial kinetic energy of an incident electron can be converted into potential energy of an atom in a single inelastic collision, and an electron can be released from an atom when the kinetic energy of the hitting electron exceeds the ionization energy of the atom. Hence an electron with a smaller energy cannot ionize the atom and so the probability of ionization is zero for $V < V_i$, V being the potential energy of the electron after conclusion. On the basis of Bohr's theory, the ionization energy is a sharply defined quantity, and therefore it would be expected that the ionization probability curve would rise sharply from zero at $V = V_i$. Figure 1 of ionization efficiency is essentially a measure of the Bohr probability. Usually this is defined for positive ions; where one incident electron produces per cm of path time at 1 mm Hg and 0°C, one electron and a singularly charged positive ion . The value of ionization efficiency is also numerically equal to the ionization cross section.

From the curves of Figure 1 it can be seen that the electrons with energies much less than or much greater than the atomic and molecular ionization energies do not ionize those particles very effectively.

Se lies for the majority of gases, so far investigated between about 80 and 120 eV. The exception being the alkali vapours whose maximum is between about 15 and 30 eV. Consequently, electron energies a few times the ionization energies are optimum for electron impact ionizations.

When the energized electron loses energy from ionizing and scattering collisions, its ionizing effectiveness varies. Energetic electrons can easily cause efficient ionization if they can be maintained in the ionizing volume for a time long enough for them to lose essentially all their energy by collisions. External restrictions can be induced by confining the electrons to gas interaction by either volumetric restrictions or from a magnetic field, or both. These techniques contribute to larger path lengths and electron lifetimes for optimizing the ionization efficiency. Consequently, referring to Figure 1, if the initial energy of the electron is $K_0 \leqslant z$ eV then von Engel's "Differential ionization coefficient Se" can be approximated as

$$Se \approx a(eV - eV_i) . \tag{2}$$

Therefore, as the primary or "knock-on" electron loses energies, the ionization efficiency or cross section of the atom increases to the optimum value "Se" and then its energies fall off until the electron no longer causes ionization. For higher states of ionization, Bleakney$^{(2)}$ showed the the electron energy required increased quite significantly. That is, using mercury, the multiple ionization energies were reported to be:

TABLE I

Ion Species	Energy Range (eV) K_0
Hg^+	10-16
Hg^{++}	29-50
Hg^{+++}	71-150
Hg^{++++}	143-200

Electron impact ionization is conceptually a very simple technique for creating ions as well as being the most effective and flexible of methods. The description of how Von Engel's theories are made applicable to the design of ion sources is given in the work by Cobine(3).

The Danfysik hot cathode or thermionic emitter type source, being the one currently employed, can be subdivided down into its various integral parts as:

1) Thermionic emitter,
2) Ion gun assembly,
3) Ion extraction assembly.

Using these as subtitles, a design analysis can be reconstructed on paper of the present system bringing to light methods for optimizing the source efficiency and improvements upon the present engineering.

Hot (Thermionic) Emitting Systems

This is the system which can use externally heated cathode in contrast to ion bombardment or cold cathode assemblies. Figure 2 illustrates diagramatically the potential and electric field versus distance in an arc with electrons furnished by a hot emitter.

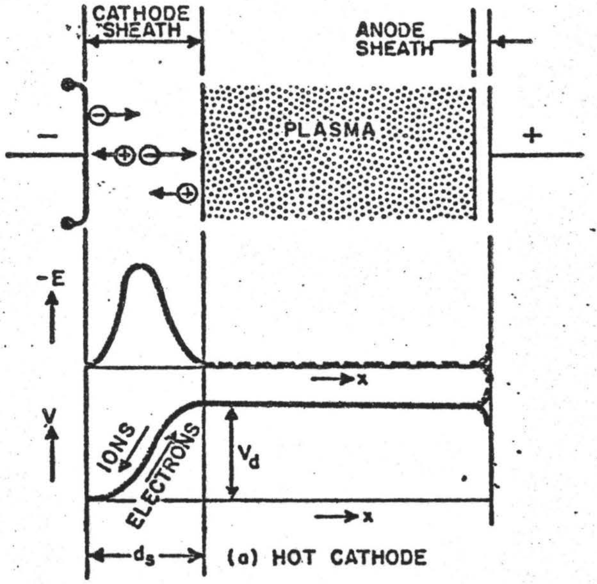

Figure 2: Potential and electric field versus distance in an arc with electrons furnished by a hot (thermionic) emitter(4).

The electric field E in the sheath region shows the typical space-charge-limited emission characteristics, that is, curving into zero field at both the cathode and sheath sides. This occurs because both surfaces are space-charge-limited emitters. The potential (V) rises rapidly near the cathode surface and remains constant (V_d) the length of the plasma. There is a slight increase in both the field and potential near the anode which reflects the existence of a thin sheath (anode) at this boundary surface. The normal value for a potential drop across the sheath is in the order of 10 to 20 V. Plasma ion density values are typically in the range of 10^{12} - 10^{14} ions/cm^3 for neutral atom densities, which corresponds to a pressure in the range of 10^{-5} to 10^{-3} torr.

Now the voltage applied between cathode and anode creates a region of space-charge-limited potential forming the cathode sheath. As illustrated in Figure 2, electrons are accelerated through this space-charge-region and in turn, ionize the gas in the interaction (plasma) region, where they form ions and secondary electrons. If the gas pressure is not too high, the electrons will flow from the cathode to the plasma as if it were the anode in a space-charge-limited diode. The corresponding electron current density(3) is given by the Child-Langmuir equation

$$J_- = \sqrt{\frac{Z_e}{m_e}}\,\frac{V_d^{3/2}}{9\pi d_s^2} \quad , \tag{3}$$

where V_d and d_s represent the potential drop and thickness of the sheath which is assumed to be geometrically planar. The ions will flow in the reverse direction as if the plasma were an ion source under the influence of a space-charge-limited emission condition. This ion current density is given by:

$$J_+ = \sqrt{\frac{z_e}{m_i}} \frac{V_d^{3/2}}{9\pi d_s^2} , \qquad (4)$$

where m_i is the atomic mass associated with the ion.

Now the ratio between these current densities is given by

$$\frac{J_-}{J_+} = \sqrt{\frac{m_i}{m_e}} , \qquad (5)$$

such that the electron current density is about roughly 200 times that of the ions. The sheath in its itself is not a neutral region since the electric field accelerating the electrons and ions, such that the potential of that region near the plasma, is determined by an ion space charge whereas the rest of the sheath is influenced predominantly by an electron space. The glow which can be observed around the discharge region is due to the small amount of recombination of the slower ions and electrons corresponding to the low energy portion of the von Engel curve (Figure 1) called a glow discharge.

If the neutral gas supply is less than a limiting value to maintain the critical pressure associated with the plasma, the rate of ion density formation in the plasma column will not be sufficient to supply the necessary ion current to maintain the discharge. Should this happen, the arc becomes a glow discharge or is extinguished.

Positive ion density can be further increased by applying a uniform magnetic field which causes a charge particle, moving perpendicular to the magnetic, to follow a circular path. Cobine(3) gives a detached description of the charge particle motion about a circular path with the radius of the circle given as

$$r = mV/qB \ , \tag{6}$$

where V and B are the velocities of the particle in the applied magnetic field strength. This resulting helical path causes the electrons to remain in the discharge region for long periods of time, which increases the probability of ion formation per charged particle, and thus increasing the ionization efficiency of the source.

Ion Gun Assembly

Most Hot Cathode Electron impact mass assemblies consist of a cylindrical ionization chamber with the gas introduced from the end or sides, an electron source and extraction electrode.

Figure 3 shows the Danfysik system with the gas or vapour internal input port located towards the anode end, cathode and filament centrally located, and a first extraction port located at the other end. The central hole arrangement through the Boron nitride (BN) keeps the discharge within a confined area, and along the magnetic field. This optimizes the exchange interaction between the electrons and vapours.

The advantage of the Danfysik system is that it does ensure

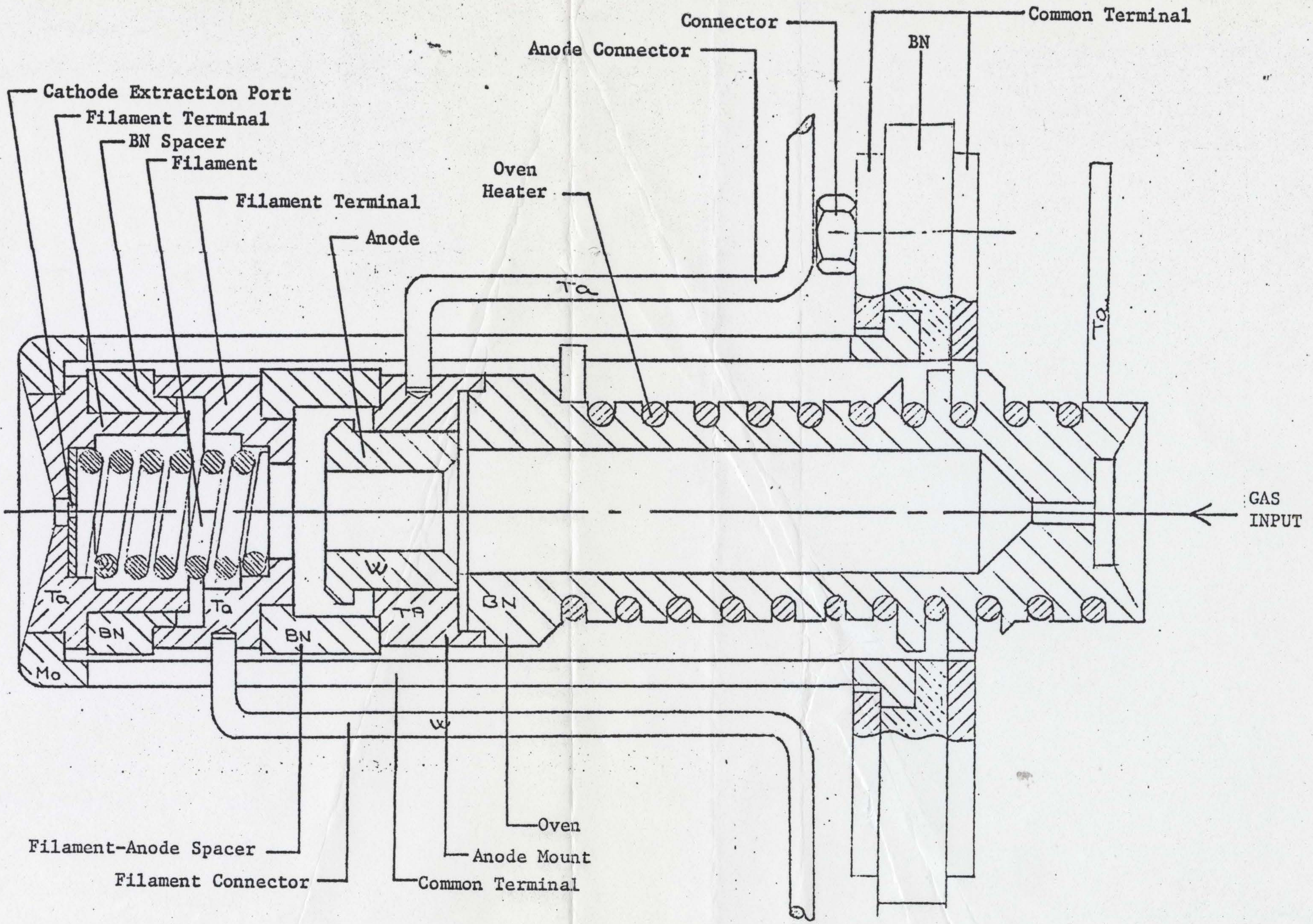

Figure 3: ION GUN ASSEMBLY.

an immediate interaction between electrons and vapours. However a very noticeable disadvantage is that if the gas flow is too great, more neutrals can be pumped down the column before the vapours have a chance to ionize. Therefore, the number of positive ions decrease and the arc will eventually extinguish. The controllability of the gas feed system becomes a very major factor in maintaining the operations of this ion source.

From within the ion source the ions leave the gun assembly through the cathode extraction port, which is maintained at a negative potential. The configuration of the plasma or meniscus at this point is dependent upon the size of port as well as the potential at the extraction electrode.

Ion Extraction Assembly

In a space in which a considerable number of ions are produced, the resulting potential well would immediately cause the attraction of the slow electrons for space charge neutralization. However some form of a plasma is always formed in the ionization chamber, whether it be the glow discharge or the production of ions. As illustrated in Figure 4, the field about the cathode port and the extraction electrode will be screened from the plasma by the formation of a space-charge sheath. As mentioned previously, at the boundary between the space-charge sheath and the plasma, the electric field is very small (equal to the penetrating field) and positive ions drift through the sheath. The total ion current at the plasma boundary is defined by the area and the current

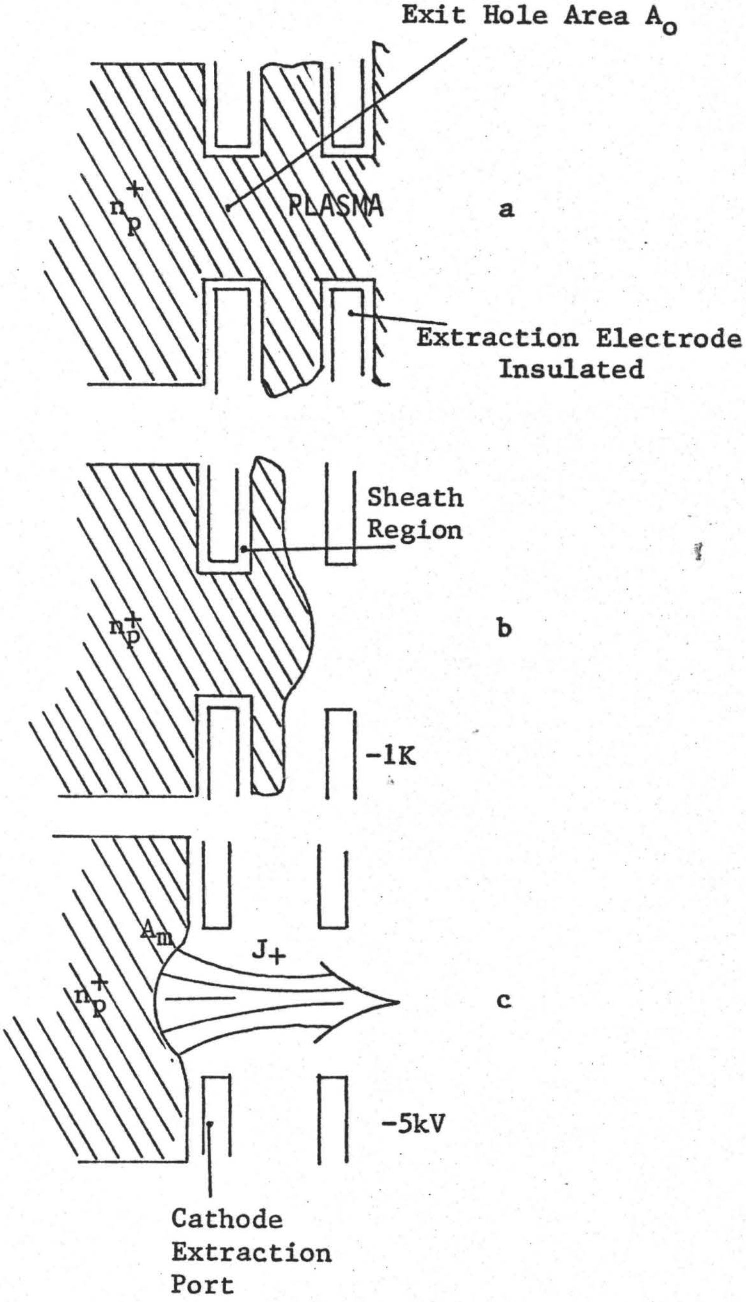

Figure 4: Mechanism of ion extraction from arc plasma.

density. Figure 4 illustrates how the increase in extraction potential re-shapes the plasma into the initial cylindrical beam of ions.

Let us first assume that the extraction electrode is electrically neutral, then the plasma will extend by diffusion out of the cathode extraction port into the space between the ion gun and the extraction electrode, Figure 4(a). However within this space, the density of positive particles will be much smaller than within the plasma region of the gun. About the extraction electrode, a space charge sheath will be formed whose characteristics are given in accordance with Langmuir's theory for space-charge-limited currents(3).

Now if a negative voltage is applied to the extraction electrode, the plasma will be pushed towards the extraction aperture while the plasma boundary takes on the shape of a so-called meniscus with area (Am). As the extraction voltage increases, the meniscus will tend to bulge more towards the plasma. Providing the meniscus does not extend too far into the plasma, the current I_+ of the beam towards the extraction electrode will remain constant; it being equal to the ion-diffusion current J_+ through the aperture area, Am.

Variations to the extraction voltage will influence the beam shape for two reasons: firstly, by changing the meniscus configurations; and secondly, by deforming the boundaries of the plasma within the space-charge region. Consequently, this portion of the ion source is uttermost in defining the geometry of the beam before it proceeds any further down the column.

PART II

BEAM TRANSPORT SYSTEM

The present system, illustrated in Figure 5, consists of an ion source, einzel lens, accelerating column, an analyzing magnet, and a series of apertures and deflection plates. The electronic system for the deflection plates has not as yet been constructed. However, when the deflection system becomes operative it will be used to sweep the ion beam uniformly across the sample surface. A thorough study of the beam transport system permits the mathematical presentation of those parameters crucial for obtaining a well-focussed beam (stigmatic beam). Any changes that will inevitably have to be made to these parameters, as future researchers dictate, can then be predetermined. This, in turn, can save the researcher invaluable time as he or she will then be able to utilize the equipment about the needs of the experiment instead of visa versa.

A study of the beam transport should begin at the point where the ions exit from the cathode extraction port. However, if the distance between the gun assembly and the extraction electrode is fixed and, providing the ion beam can move freely through the extraction ports without any angular obtrusions, then the object size of the beam can be approximated as the size of the extraction electrode port, Figure 6(a). From this point, down and through the analyzing magnet can be treated graphically.

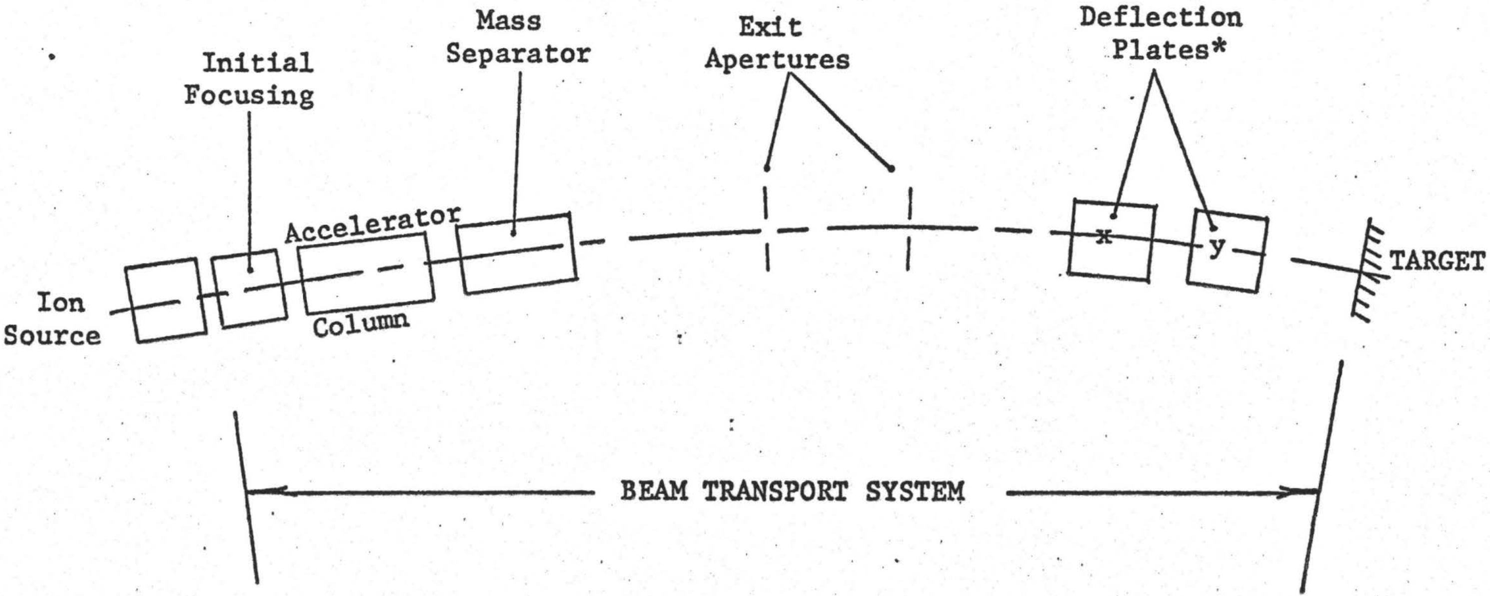

* Not necessarily required - can improve beam characteristics

Figure 5: Schematic of the Beam Transport System.

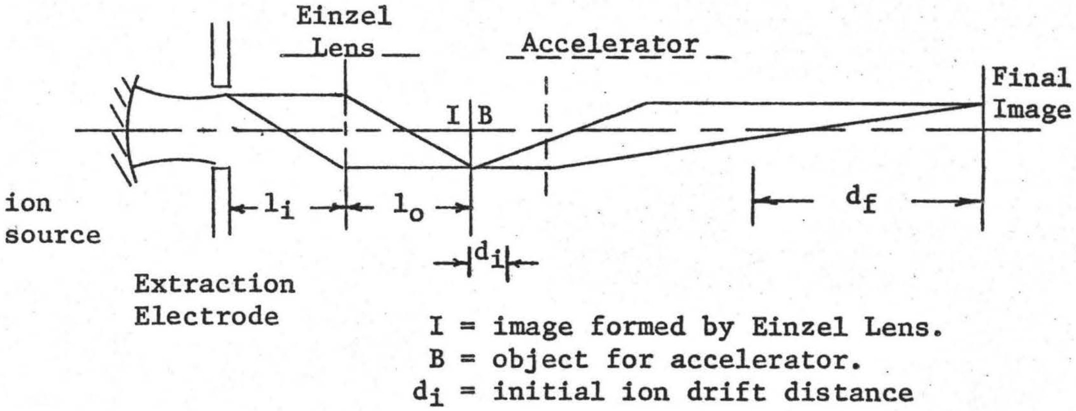

I = image formed by Einzel Lens.
B = object for accelerator.
d_i = initial ion drift distance

Figure 6(a): Ray trace illustrating the use of an Einzel Lens to form a stigmatic image.

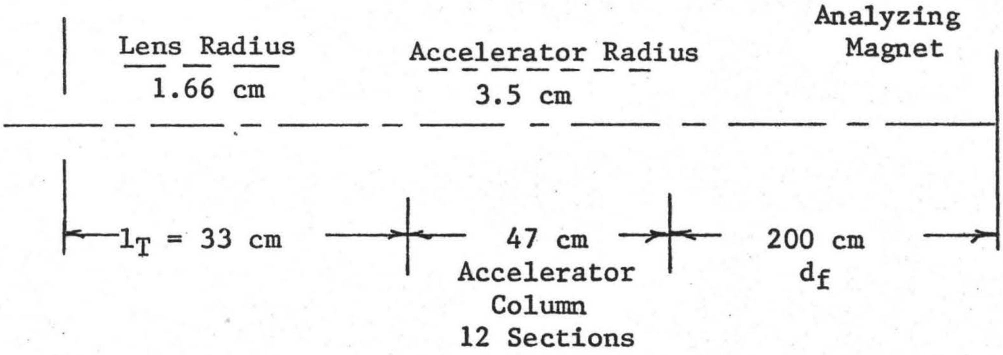

Figure 6(b): Dimensional schematic of the 150 kV ion source.

Focusing and Accelerating the Ion Beam

Focusing of the emerging ion beam is performed by the einzel lens (Figures 6(a) and 6(b)). The einzel lens is treated as a compounded Double-Aperture lens of the type described by Zworykin(5) for which the mathematical derivation is given in Appendix I. Figure 7 is a plot of the lens focal length (cm) against the voltage ratio (Q) between the lens plate. From Figure 6(b), Figure 7 and Table III, it can be appreciated that the optimum operating conditions for the lens are with the voltage ratio between 2.5 and 3.5. This permits the focal point to be within the portion of the lens column such that the image is a well-defined area of about 2 mm in diameter before accelerating any further down the line. Decreasing Q weakens the electric field about the accelerating plates of the lenses and thereby increasing the focal length towards the accelerating column. This, in turn, increases the area of the image being presented to the accelerating column which spreads the same current density over a greater target area.

Galejs and Rose(6) treat the accelerator column as a Double-Aperture lens as described by Equation (A1-12) in Appendix I. Even though the topic in itself is more complex mathematically than this, the technique proved to be quite adequate providing certain reasonable assumptions were made. It was assumed that the potential distributions for the entrance and exits to the column were mirror images and, that the middle of the column was represented by a uniform field with a potential distribution V_0 along the total length of the column.

Using the above technique, trajectories for the 150 kV were

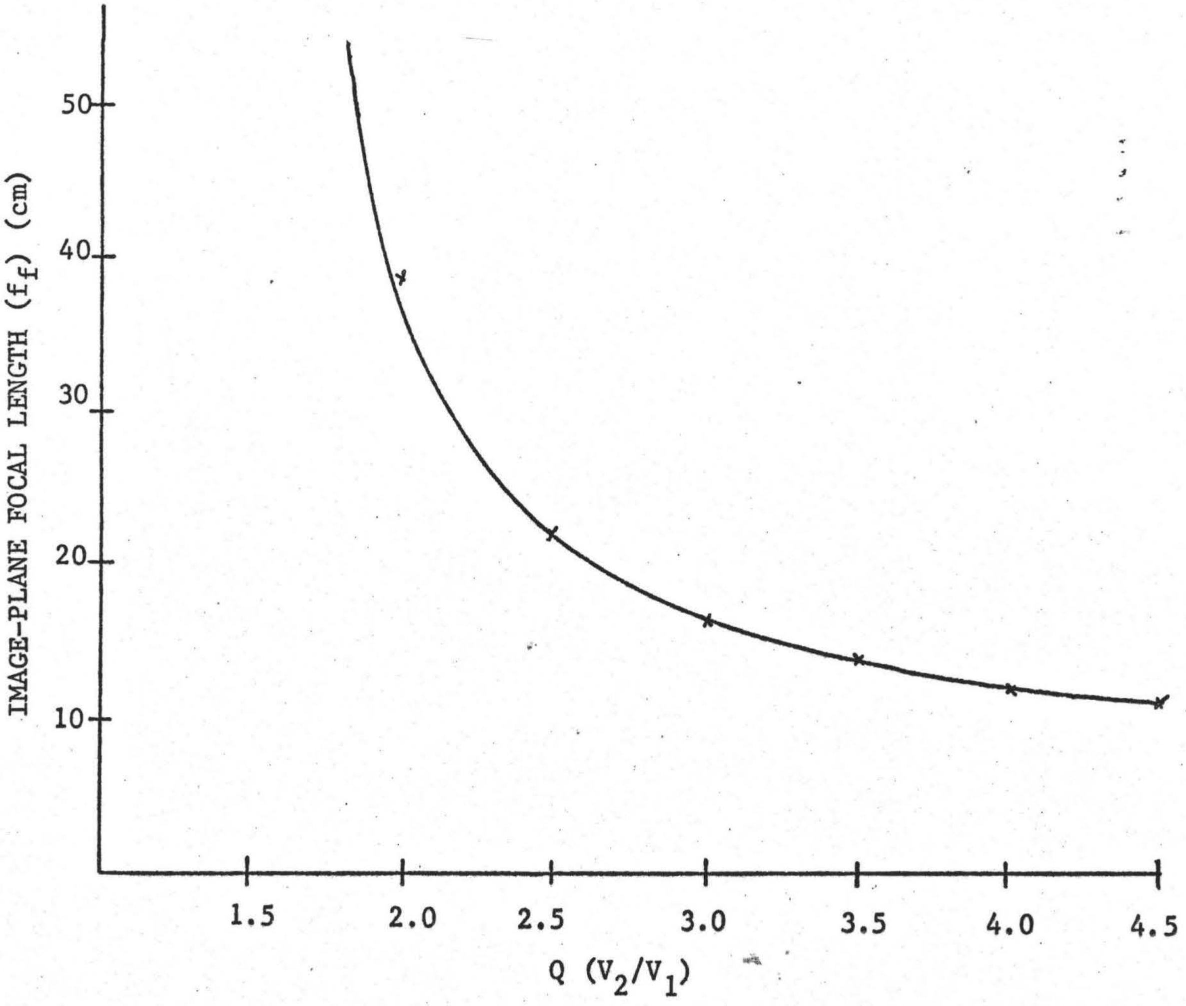

Figure 7: Einzel Lens 5 kV Extraction (V_1); d = 7 cm.

TABLE II: EINZEL LENS SETTING (V_2)

d = 7 cm Lens 5 kV Extraction (V_1)

Q	V_2(kV)	a_{21}	f_f(cm)	a_{11}	l_o(cm)	l_i(cm)	$\lvert l_o\rvert + \lvert l_i\rvert$(cm)
1.5	7.5	0.64	109.03	0.911	9.70	-10.64	20.34
2.0	10.0	1.80	38.80	0.785	8.34	-10.62	18.96
2.5	12.5	3.10	22.60	0.677	7.30	-10.78	18.08
3.0	15.0	4.23	16.54	0.532	7.74	-14.55	22.29
3.5	17.5	4.94	14.18	0.393	8.61	-21.90	30.51
4.0	20.0	5.62	12.45	0.250	9.34	-37.35	46.69
4.5	22.5	6.06	11.55	0.108	10.30	-45.39	105.69

TABLE III: ACCELERATOR SETTING (V_f)

d = 47 cm 5 kV Extraction (V_1)

Q	V_f(kV)	a_{21}	f_f(cm)
2.0	10.0	0.1652	605.16
2.5	12.5	0.3162	354.00
3.0	15.0	0.4769	256.81
4.0	20.0	0.8462	167.11
5.0	25.0	1.2477	126.74
10.0	50.0	3.4719	64.40
15.0	75.0	5.8591	46.74
20.0	100.0	8.3225	37.99
25.0	125.0	10.8322	32.63
30.0	150.0	13.3741	28.959

calculated in the composite accelerating field for the ratio of output to input beam energies (Q) from $5 \leqslant Q \leqslant 30$, Table IV.

Referring to Figures 7 and 8 as well as Figure 6(b), the question can now be answered as to the best possible position for locating the einzel lens. The position which will accomodate movement of the required object position for the greatest range of accelerating potentials. Figure 8 fixes the centre of the lens at approximately 15 cm from the extraction port. This will allow the distance (l_0) to vary over a 10 cm range for a change in focal length (f_f) between 22.6 to 14 cm (Table III) and still maintain a 2 mm object for acceleration. This calculated location for the einzel lens agrees with the "new position" recommended by the manufacturer of the ion source.

The new location of the lens should not only improve focusing but will help to eliminate flashovers between V_2 to V_1 (Appendix I, Figure A1-6). This occurs due to the glow discharge, which was previously mentioned, existing in the vicinity of the extraction electrode. Another alternative to limiting the flashover is to increase the path-length between the electrodes by increasing the outer diameter of the insulator spacers between the lens plates. This can be readily performed without changing the value of "d", the distance between the plates.

Figure 9 shows the relation between Q and the expected focal lengths for the present accelerating column. Once the einzel lens is operating properly, Figure 9 can be used to determine the best possible location for a beam current indicator (beam stop). The proper location

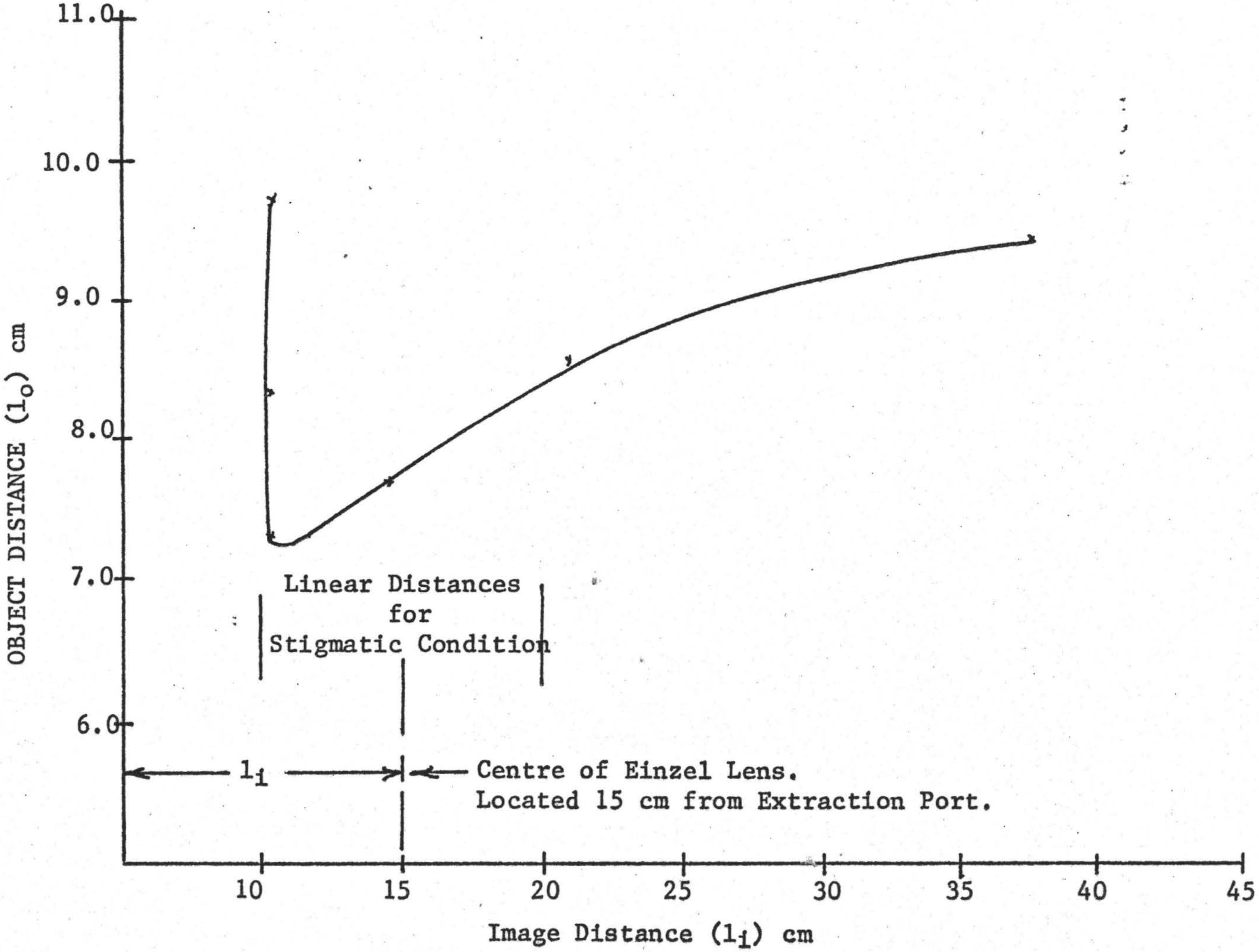

Figure 8: Location Distance for a 7 cm Einzel Lens.

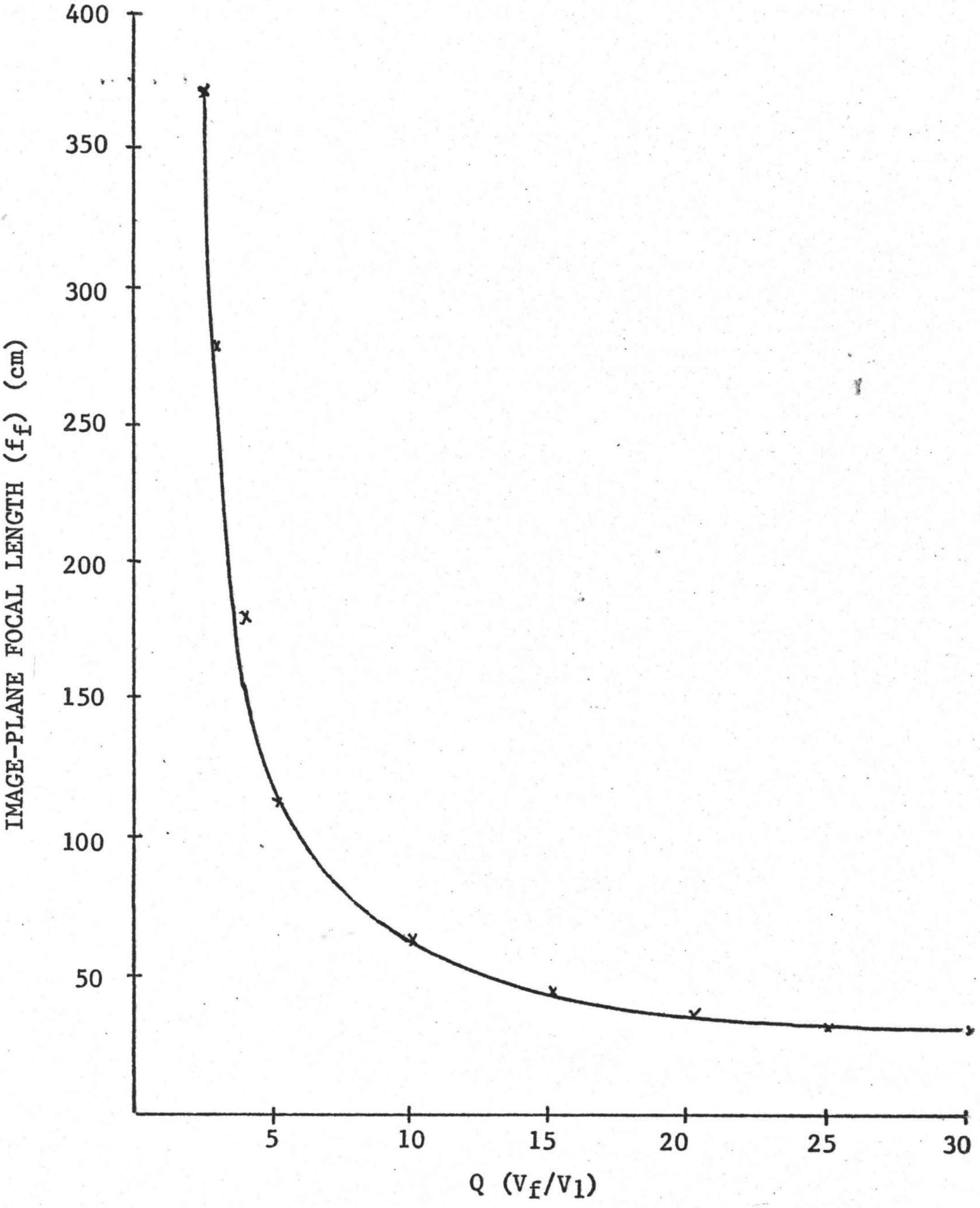

Figure 9: Accelerator Column Focal Length 5 kV Extraction; d = 47 cm.

for the beam stop is important for start-up so that the ion source parameters can be peaked for the optimum operating efficiency (Appendix III).

Mass Separator

Mass separation for the present system is performed by an analyzer magnet, Figure 10. The centre of an ion beam of momentum (p_o) can be made to follow a circular radius (ρ) and angle (ψ) through the influence of a magnetic flux (B), related by the equations:

$$\frac{1}{\rho} = \frac{eB_o}{p_o} = \frac{0.69B\ \text{(gauss)}}{\sqrt{M}\ \sqrt{V}\ \text{(volts)}}\ (\text{meters}^{-1})$$

$$\psi = \ell/\rho \ , \tag{7}$$

where ℓ is the length of the ion path in the magnetic field. Figure 11 is a plot of B versus M for an accelerator potential of 80 kV using the existing magnetic separator in conjunction with the 150 kV Danfysik ion source.

Beam transport through the magnet can also be treated using a transfer matrix. In addition to its bending action on a charged particle, which in effect provides the desired mass dispersion, the analyzing magnet can cause a focusing action on those particles in the plane of trajectory. For a more extensive analysis of an analyzing magnet and its focusing action on particles, should the problem become apparent, an excellent review on the subject can be found in either Enge(7) or Staffen(8). From Enge(7), the focal lengths about the magnet (Figure 10(b)) for the object (L_1) and the image (L_2) are given by Barber's

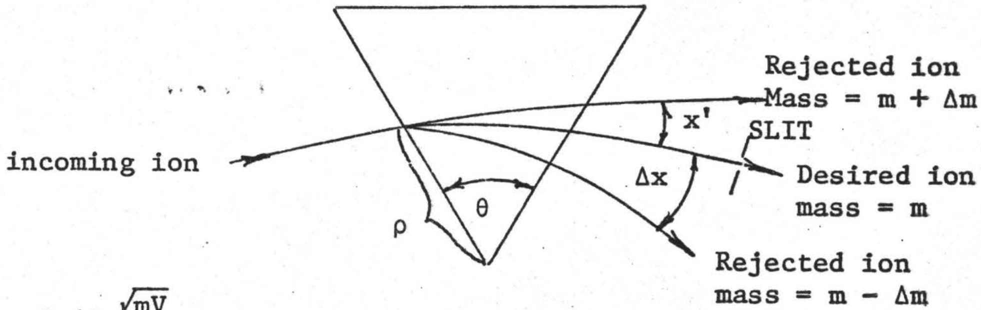

$$\rho = 0.69\,\frac{\sqrt{mV}}{B}$$

$$x' = \frac{1}{2}\,\frac{\Delta m}{m_o}\,\sin\Theta$$

$\ell = \rho\theta$ (path length through magnetic field).

Figure 10(a): Mass Separation by Analyzing Magnet.

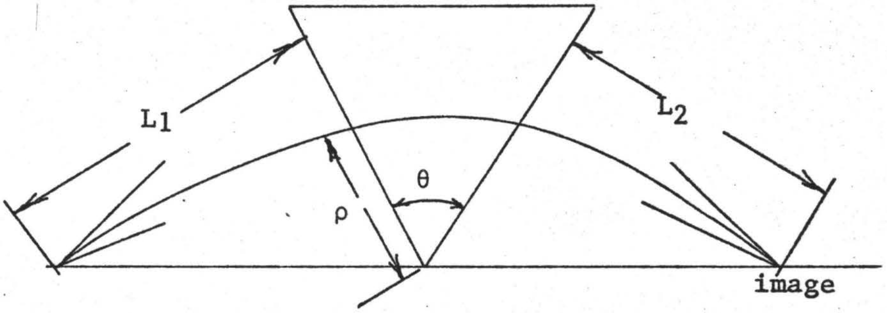

Figure 10(b): Illustrating focusing from an analyzing magnet (Barber's rule: object and image are on a line through the centre of curvature).

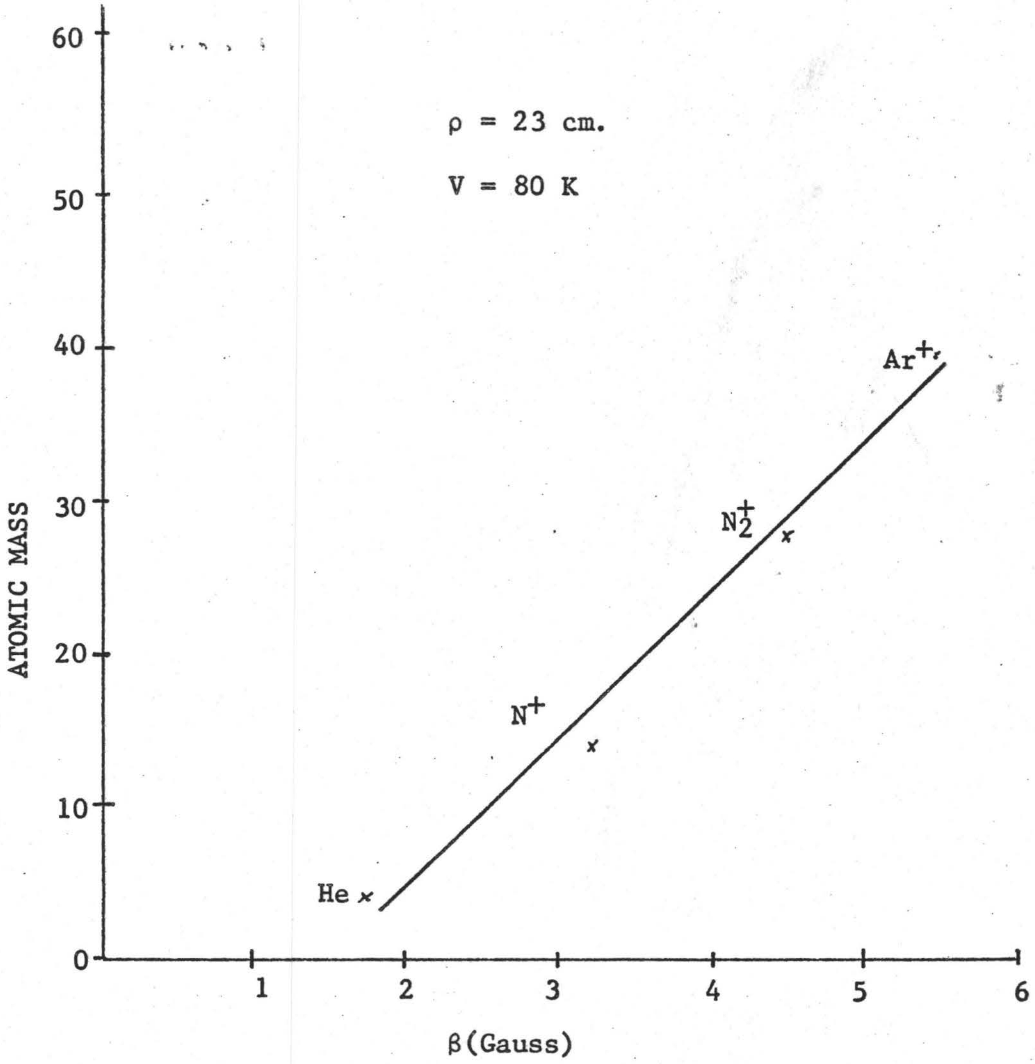

Figure 11: Analyzer Magnet settings for masses He, N^+, N_2^+ and Ar^+ using the 150 kV accelerator system.

rule and are related by,

$$L_2 = L_1\left[\frac{1 + (\rho/L_1)\tan\phi}{(L_1/\rho)\tan\phi - 1}\right] . \tag{8}$$

PART III

CRYOGENIC EXPERIMENTAL CHAMBER

The cryogenic experimental chamber (Figure 12) was designed for low-temperature and clean-environment channeling studies. The equipment consists of a cryomite refrigerator (A) coupled to the target chamber (B) by the standard dependex vacuum seal. Attached to the cryomite cold head, inside the vacuum chamber, is a long cylindrical copper block (C). The block is electrically isolated from the rest of the refrigeration system and from ground potential by a saphire crystal (D).

A liquid nitrogen cryoshield (E) is used to reduce radiation heating from the target chamber, from affecting the cooling efficiency to the cylindrical copper block, the target holder (F), and the hemispherical cryoshield (G). The copper hemisphere is attached at (H) to the cylindrical copper block. Its main purpose is to act as a cryoshield for the sample surface. There are sections where the sample surface faces areas of higher temperature. These are through the openings directed towards the solid state counter (I) and the beam line. The solid state counter is a press fit mount onto the liquid nitrogen shield.

The target holder is thermally connected to the cylindrical copper block by a 10 cm length of copper braid (J). The braid is approximately 0.6 cm in diameter, consisting of either numbers 32 to 40 gauge wires wrapped tightly together. The braid was then wrapped in teflon tape to ensure the strands stayed together and to prevent

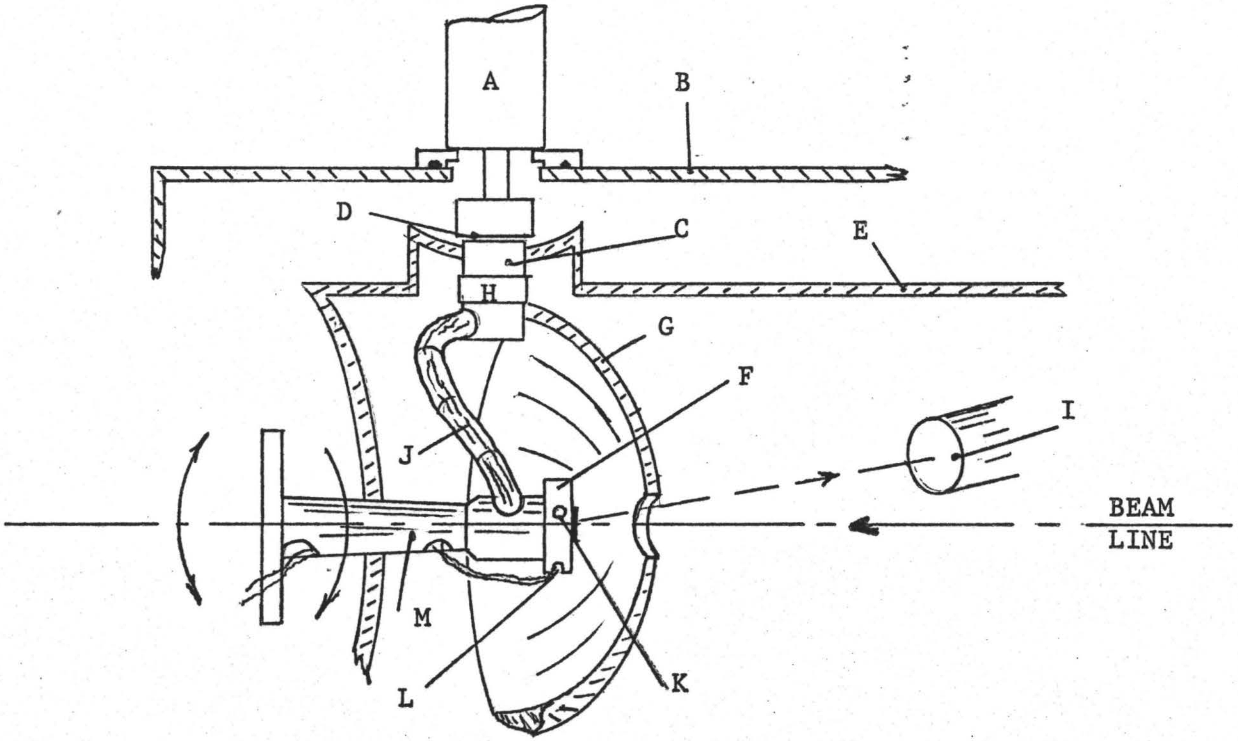

Figure 12: Cryogenic Experimental Chamber (see Table IV for parts listing).

TABLE IV

A	cryomite
B	target chamber (experimental chamber)
C	cylindrical copper block
D	saphire crystal (insulator)
E	liquid nitrogen shield
F	target holder
G	hemispherical cryoshield
H	attachment of hemispherical cryoshield to cylindrical copper block
I	solid state counter (detector)
J	copper braid
K	15 watt heater
L	thermocouple (chromal-gold (2% iron))
M	stainless steel tubing, target holder support.

unravelling during rotation of the target hold. Rotation to the target holder is performed by a standard 2-axis goniometer assembly.

A 15 watt heater (K) for the target holder is supplied by two diodes wired in series. Supplemental heating can be supplied through the control system for the cryomite. Using these two heating systems, singularly or in tandem, will provide a controllable temperature ranging between 40-300°K. Temperature recording is done with a thermocouple made of chromal and gold (2% iron). The thermocouple (L) is attached to the target holder in close proximity to both the heater supply and where the sample is fastened. To minimize thermal gradients affecting the thermocouple measurements, the leads for the thermocouple were brought down from the copper target holder and passed through the centre of the stainless steel target holder support tubing (M).

A 36 cm long piece of coaxial cable was used to make the connection between the solid state counter and the preamplifier located on the outside of the experimental chamber. This was found to reduce the occurrance of microphonic pick-up when the cryomite was turned on. The grounding shield of the coaxial cable was attached to ground at the vacuum feed-through end and was left floating at the solid state counter connection.

Start-Up

Before closing the vacuum chamber to atmosphere, several precautions should be taken in order to eliminate damaging the equipment. Firstly, all connections should be checked for continuity or possible short circuits. No interconnections should exist between the thermocouples, heater supply and especially the beam current lead. It is the beam current lead which made it necessary to electrically isolate the cryomite cylindrical copper block from ground. Secondly, precautions should be taken to insure that the sample holder can rotate through the required number of revolutions for the experiment. Otherwise, the electrical leads may become entangled and, in doing so, become damaged.

After the pumpdown is completed and the experimental chamber has been put onto the diffusion pump, then the trap for the liquid nitrogen shield can be filled. The overall time required to bring the sample holder to equilibrium (77°K) is about one hour. At this point, the cryomite can be turned on, making sure at first that the cryomite temperature controller is either off or set to zero. Figure 13, temperature versus time for the cryomite, shows that it takes between 15 to 20 minutes before the sample holder reaches the minimum value of 40°K.

<u>Notes of Caution</u>: 1) The gate value isolating the experimental chamber from the rest of the beam line should not be opened during low temperature measurements until the cryoshields and target holder have reached the minimum temperature settings. Otherwise, carbon or other contami$\overset{\text{tion}}{\text{nance}}$ build-up will occur on the sample surface. For the present system, if operated as prescribed, it was not possible to detect any build-up of impurities during a 24 hour experimental period regardless of the target temperature.

2) The solid state counter (detector) should not be powered

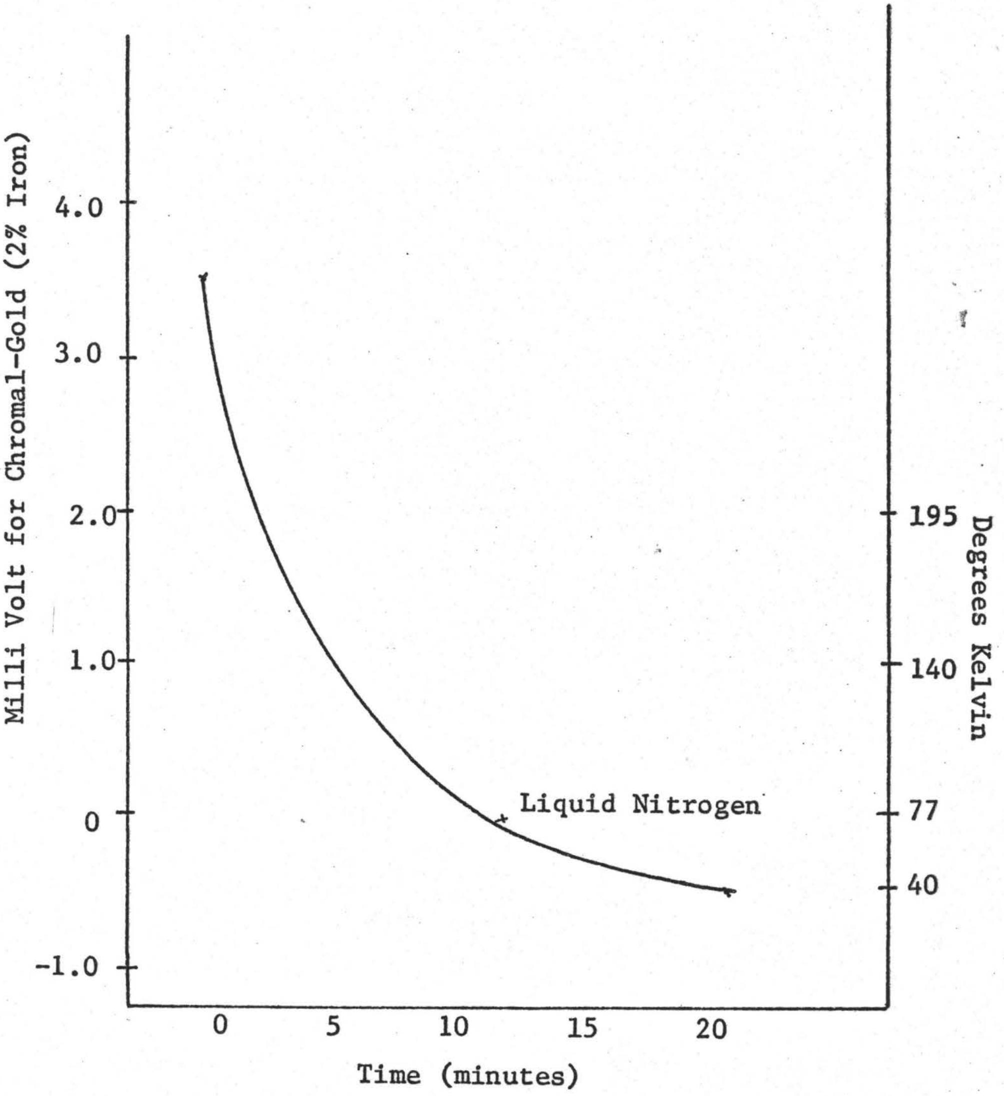

Figure 13: Temperature versus Time to cool target holder.

while the experimental chamber is at atmosphere and should only be turned on after the chamber goes on the diffusion pump. Similarly, the detector, and therefore the liquid nitrogen cryoshield, should not be brought up to ambient temperature too quickly or by using a "hot" air gun. The best possible procedure is to use the air gun to blow room temperature air into the liquid nitrogen filling trap. It will take approximately one to two hours to bring the inside shield and detector up to room temperature, but no damage will be done to the solid state detector.

DISCUSSION

This report is not intended as an operating or repair manual for the 150 kV accelerator and related cryogenic experimental chamber. Rather, its function is to illustrate the main constituents of the overall system, emphasizing the most important items, in order that the system works properly!

It is with deep regret, however, that the writer has not been able to proceed with the intended research for which this system was initially constructed. The problem stems from the Danfysik ion source. As a piece of machinery, it is a white elephant; as a design concept, it appears to be quite good judging from an evaluation of its dimensional parameters and operating characteristics: It operated successfully for about 6 hours. Where it lacks, however, is in the workmanship, the quality of materials used in the construction, and the amount of information supplied by the company for setting up and operating the source.

According to High Voltage Engineering, the North American representative for Danfysik, all ion sources are pretested before they leave Denmark. However, in our first run, the extraction electrodes shorted together under vacuum, damaging the extraction voltage supply. Later, it was discovered that the extraction port had not been machined to tolerance and was sitting at an angle in its positioning flange. Both the extraction electrodes and port had to be re-machined before an ion beam could be extracted from the gun. Before the faults could be found and rectified, the angled ion beam had apparently been hitting the plastic einzel lens electrode, managing to distort the "o"-ring seal.

Separating the extraction electrodes is a 12.5 inch annular-shaped plastic insulator. This insulating piece is also used to keep the alignment between the ion gun assembly and the extraction electrode port, which as illustrated in this report is crucial for obtaining a well-formed (stigmatic) beam. Even though the whole ion gun assembly requires no more than 200 to 230 watts, there is sufficient heat generated to cause the piece of plastic to soften. This softening, not only mis-aligns the ion beam, but has been the cause of vacuum breaks on several occasions.

Without going any further into a long elaboration, the following list describes the corrections now being made, and found necessary before the "Danfysik" ion source can operate successfully:

1) Remaking the annular disc;- material Kel-F thermal plastic; softening temperature 200°C.

2) Install a water-cooled heat exchanger;- deionized water for 150 kV with corona shield in place. This should eliminate any possibility of beam mis-alignment due to overheating.

3) Redesign the einzel lens system;- at present, (i) the lens is not located for proper focusing of the ion beam, (ii) increasing the diameters of the lens mounting insulators to eliminate flashovers between V_2 and V_1. Described in the section of this report on Beam

Transport, Part II, the new location for the einzel has been calculated. The new position will now allow the beam to be focussed over a range of accelerating voltage and independent of the accelerator potential. Previously, it was the accelerator voltage, set at 50 kV, which had been doing the focusing. Consequently, unless a beam with an energy of 50 kV was desired, most of the ion current never reaches the target area.

4) The redesign of the gas flow system; this meant drilling out a section of the boron nitride oven, Figure 3, and installing a piece of the same material that would make a proper fitting between the gas input tube and the ionizing chamber. The redesign of this means that the oven assemblies as supplied by Danfysik are of no value.

5) Redesign the oven assemblies - fortunately, these have not been required for any initial runs, therefore, nothing has been done.

6) Boron nitride (BN) is contaminated by organic compounds; any slight amount of back streaming from an oil diffusion or mechanical pump will leave some trace of oil on the BN insulators. Thus, oil film build-up appears to increase when the ion source is shut down for a few days. The build-up of oil decomposes to form a carbon conducting path between the cathode and anode electrodes, eventually shortening out and causing the ion discharge to extinguish.

7) Stainless steel screws and threads used to support the ion gun assembly either "corrode" or "deform" (the mechanism is not yet fully understood) such that it becomes impossible to disassemble the gun. Correction for this seems to be a thin coating of molybdenum

disulphide (MoS_2) on all stainless steel fasteners used on the gun assembly.

The seven items above are the most pressing problems before the 150 kV ion source is ready for operation. Although the theory appears to be good, the workmanship, materials used, and the cooperation of the manufacturer leaves an awful lot to be desired!

APPENDIX I

Kirstein$^{(9)}$ gives the equation for paraxial ray equations in an axially symmetric electrostatic field only as

$$\frac{d^2r}{dz^2} + \frac{V_o'}{2V_o}\frac{dv}{dz} + \frac{V_o''r}{4V_o} = -\frac{\rho r}{4V_o\varepsilon_o} \quad , \tag{AI-1}$$

where $V_o(z)$ is the potential in the axis and the primes denote derivative with respect to z; r is the radial component $(x^2 + y^2 = r^2)$ of the ray; ρ represents the space-charge density assumed uniform over the beam cross section; and V_o'' relates to the focusing as less action of the structure.

Assuming that the space-charge density is negligible, then the right hand side of Equation (AI-1) is equal to zero. This is then a linear second-order homogeneous differential equation with coefficient depending upon z. Boundary conditions for solutions to this equation are normally set between two planes located a given distance apart along the axis. Therefore, if solutions can be found for the ray path within these boundaries, then any other ray path can be expressed in terms of these solutions.

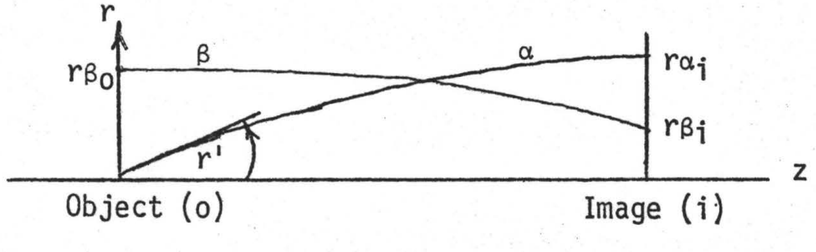

Boundary conditions for these special ray solutions:

$$r\alpha_0 = 0; \quad r\alpha'_0 = 1; \quad r\beta_0 = 1; \quad r\beta'_0 = 0$$

where subscript 0 refers to the object plane and i to the image.

Solution to the paraxial ray equation (AI-1) is given$^{(10)}$ as

$$r_i = r\beta_i r_o + r\alpha_1 r'_o ,$$

$$r'_i = r'\beta_i r_o + r'\alpha_i r'_o. \qquad \text{(AI-2)}$$

Coefficient a_{ij} can be related to the parameter of the special α and β rays by

$$a_{11} = r\beta_i; \quad a_{12} = r\alpha_i; \quad a_{21} = r'\beta_i; \quad a_{22} = r'\alpha_i$$

$$\begin{pmatrix} r_i \\ r'_i \end{pmatrix} = \begin{pmatrix} a_{11} & a_{12} \\ a_{21} & a_{22} \end{pmatrix} \begin{pmatrix} r_o \\ r'_o \end{pmatrix} \qquad \text{(AI-3)}$$

The relationship between the matrix element and the cardinal points (Figure AI-2) are given as$^{(6)}$;

$$M_{16} = \begin{vmatrix} a_{11} & a_{12} \\ a_{21} & a_{22} \end{vmatrix}$$

$$f_i = \frac{-\sqrt{V_i}}{a_{21}} , \quad \text{object - plane focal length} \qquad \text{(AI-4)}$$

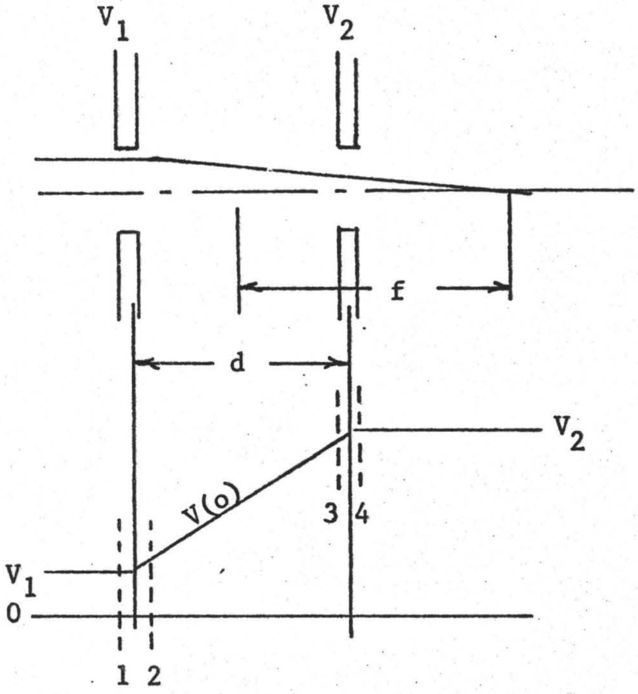

Figure AI-1(a): Double-Aperture Lens

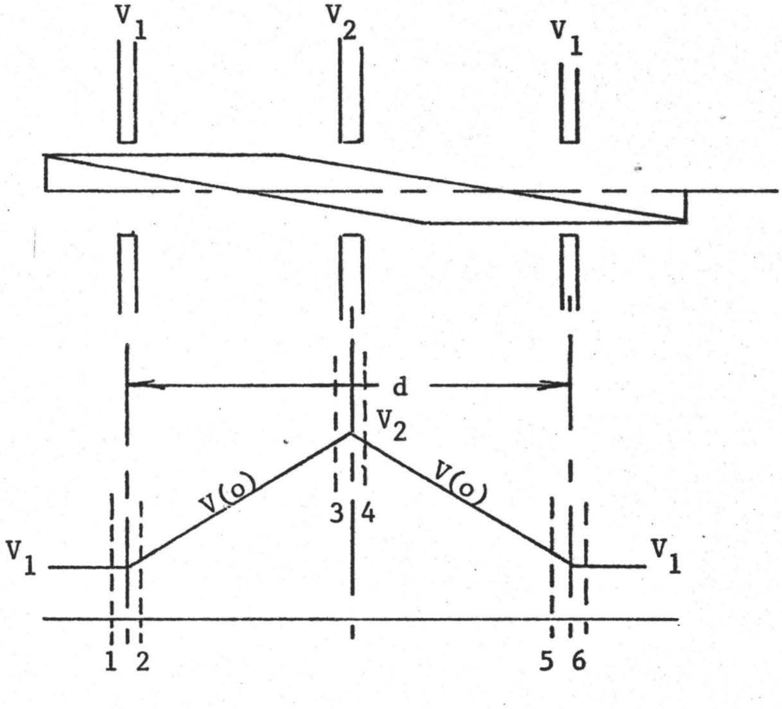

Figure AI-1(b): Einzel Lens

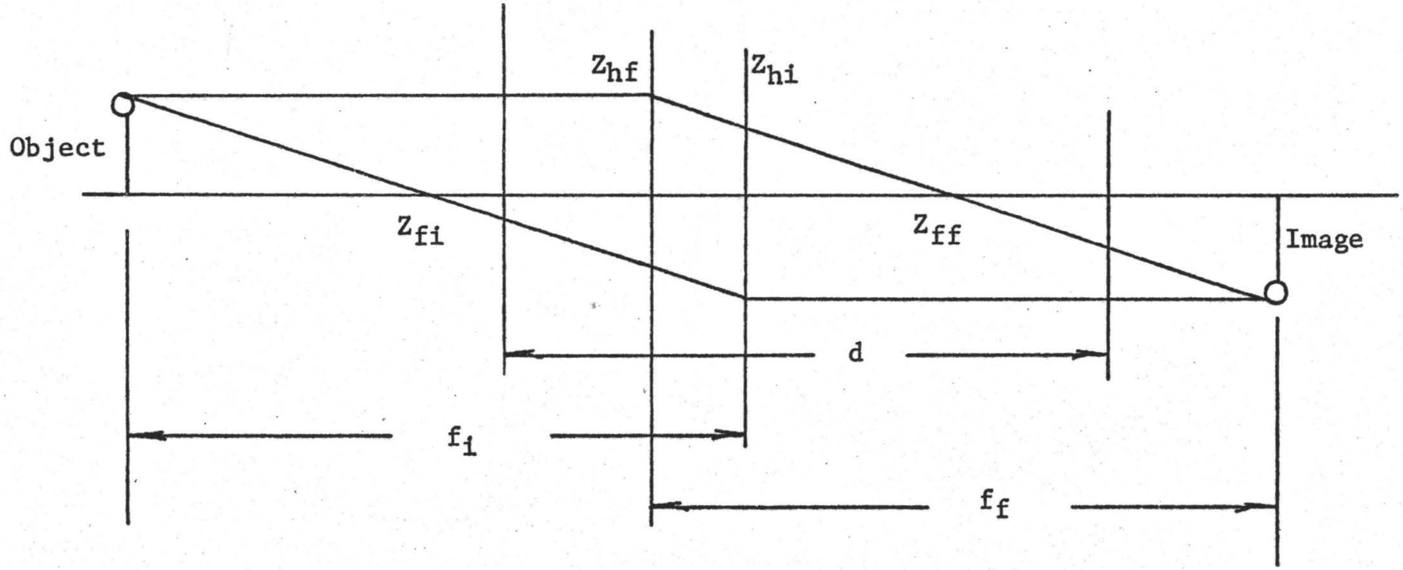

d = length of lens

Figure AI-2: Definition of Cardinal Points.

$$f_f = \frac{\sqrt{V_f}}{a_{21}} \text{ , image - plane focal length} \tag{AI-5}$$

$$z_{fi} = \sqrt{V_i}\,\frac{a_{22}}{a_{21}} \text{ , location of object - plane focal point} \tag{AI-6}$$

$$z_{ff} = d - \sqrt{V_f}\,\frac{a_{11}}{a_{21}} \text{ , location of image - plane focal point} \tag{AI-7}$$

$$z_{ni} = z_{fi} - f_i \text{ , location of object - principal plane} \tag{AI-8}$$

$$z_{hf} = z_{ff} - f_f \text{ , location of image - principal plane} \tag{AI-9}$$

where d is the overall length of the lens assembly.

For stigmatic conditions the relationship between the object (l_o) and the image (l_i) distances are:

$$a_{12} = l_i(1 - \frac{l_o}{f}) + l_o = 0 \tag{AI-10}$$

and the magnification factor is

$$a_{11} = 1 - \frac{l_o}{f} \tag{AI-11}$$

Double-Aperture Lens

The Double-Aperture Lens as derived by Zworykin$^{(5)}$ asserts that the lens beam transfer matrix can be formed by multiplying together the appropriate matrices, for the initial and final breaking points in the electric field together with the uniform field region (refer to

Figure AI-1(a)). The matrix elements referred to are:

$$M_{12} = \begin{vmatrix} 1 & 0 \\ \frac{V_1 - V_2}{4d\sqrt{V_1}} & 1 \end{vmatrix}$$

$$M_{23} = \begin{vmatrix} 1 & \frac{2d}{\sqrt{V_1} + \sqrt{V_2}} \\ 0 & 0 \end{vmatrix}$$

$$M_{34} = \begin{vmatrix} 1 & 0 \\ \frac{V_2 - V_1}{4d\sqrt{V_2}} & 1 \end{vmatrix}$$

Combining these matrices, the transfer matrix is;

$$M_{14} = M_{34} \cdot M_{23} \cdot M_{12}$$

$$M_{14} = \begin{vmatrix} \frac{3\sqrt{V_1} - \sqrt{V_2}}{2\sqrt{V_1}} & \frac{2d}{\sqrt{V_1} + \sqrt{V_2}} \\ \left(\frac{3(V_2 - V_1)}{8d}\right)\left(\frac{\sqrt{V_1} - \sqrt{V_2}}{\sqrt{V_1 V_2}}\right) & \frac{3\sqrt{V_2} - \sqrt{V_1}}{2\sqrt{V_2}} \end{vmatrix} \qquad \text{(AI-12)}$$

An einzel lens can be approximated if we multiply together matrices of the form used for a double-aperture lens. By reversing the notation in the second field region (Figure AI-1(b)), the matrix element becomes

$$M_{16} = (M_{34} \cdot M_{23} \cdot M_{12}) \cdot (M'_{34} \cdot M'_{45} \cdot M'_{56})$$

$$M_{16} = \begin{vmatrix} \dfrac{16\sqrt{V_1V_2}-6V_1-6V_2}{4\sqrt{V_1V_2}} & \dfrac{2d}{\sqrt{V_1}+\sqrt{V_2}}\,\dfrac{3\sqrt{V_2}-\sqrt{V_1}}{\sqrt{V_2}} \\ \dfrac{3}{8}\,\dfrac{(V_1-V_2)}{d}\left(\dfrac{\sqrt{V_2}-\sqrt{V_1}}{\sqrt{V_1V_2}}\right)\left(\dfrac{3\sqrt{V_1}-\sqrt{V_2}}{\sqrt{V_1}}\right. & \dfrac{16\sqrt{V_1V_2}-6V_1-6V_2}{4\sqrt{V_1V_2}} \end{vmatrix} \qquad \text{(AI-13)}$$

APPENDIX II

TABLE OF RECOMMENDED SOURCE FEED COMPOUNDS

Partial Reprint From
"The Technology and Chemistry of Heavy Ion Sources"
by
J.H. Freeman and G. Sidenius

Z	ELEMENT	M AMU	E_i eV	COMPOUND	GAS Com. Sup. Tr.	TEMPERATURES, °C. For Vapor Pressures, torr. 10^{-4}	10^{-3}	10^{-2}	760	Melt.	ION SOURCE TYPES -1- °C-	-2- 100 -	-3- 500 -	-4- 1100- °C	-5- Surf.	REMARKS
1	Hydrogen	1	13.5	H_2	H_2	-268	-267	-266	-253	-259	r	r	r	r	i	Explosive in mixture with air.
2	Helium	4	24.5	He	He	/	/	/	-269	-272	r	r	r	r	i	No problems.
3	Lithium	7	5.4	Li	NG	404	467	537	1317	179	i S.p	p	p	p	r	Require special handling.
				LiCl		458	514	582	1380	614	i	d	r	r	p	Also other halides.
4	Beryllium	9	9.3	Be	NG CCl_4	990	1097	1227	2470	1280	i S.p	i C.p	i C.r	r	i	Toxic, (BeO).
				$BeCl_2$		/	176	209	481	405	i	p	p	p	i	Also $BeBr_2$ & BeI_2.
				BeF_2		/	562	632	1159	803	i	d	r	r	i	More stable temperatur control.
5	Boron	11	8.3	B	NG CCl_4	1707	1867	2027	3600	2300	i S.p	i S.p	i C.r	r	i	
				BCl_3	BCl_3	/	/	/	13	-107	d	p	p	p	i	Hydrolyse very readily.
				BF_3	BF_3	/	/	/	-101	-128	d	p	p	p	i	- " - -"- -" -
6	Carbon	12	11.2	CO	CO	-238	-235	-231	-191	-207	r	r	r	r	i	Toxic,but gives best yield.
				CO_2	CO_2	-177	-167	-158	-78	/	r	r	r	r	i	Most convenient.
				CCl_4	CCl_4	/	/	/	77	-24	p	p	p	p	i	
7	Nitrogen	14	14.5	N_2	N_2	-242	-239	-235	-196	-210	r	r	r	r	i	Dominating molecular beam.
8	Oxygen	16	13.6	O_2	O_2	-236	-233	-230	-183	-218	p	p	p	p	i	Some source and filament corrosion.
				CO	CO	-238	-235	-231	-191	-207	p	p	p	p	i	Toxic.
				CO_2	CO_2	-177	-167	-158	-78	/	r	r	r	r	i	Gives best yield.
9	Fluorine	19	17.3	F_2	F_2	/	/	-231	-188	-220	p	p	p	p	i	Toxic.
				KF		/	596	664	1502	880	i	i	r	r	i	Also many other fluorides.
10	Neon	20	21.5	Ne	Ne	-263	-262	-261	-246	-249	r	r	r	r	i	No problems.
11	Sodium	23	5.1	Na	NG	193	235	289	880	98	i	p	p	p	r	Require special handling.
				NaCl		521	588	658	1467	800	i S.p	d	r	r	p	Also other halides.

Z ELEMENT M AMU	E_i eV	COM- POUND	GAS Com. Sup.	 Tr.	TEMPERATURES, °C. For Vapor Pressures, torr. 10^{-4}	 10^{-3}	 10^{-2}	 760	 Melt	ION SOURCE TYPES -1- °C-	 -2- 100 -	 -3- 500 -	 -4- 1100-°C	 -5- Surf.	REMARKS
12 Magnesium		Mg	NG		327	377	439	1100	651	i S.p	p	r	r	i	
24	7.6	$MgCl_2$			479	532	596	1412	708	i S.p	d	p	p	i	Also $MgBr_2$ and MgI_2.
13 Aluminium		Al	NG	CCl_4	972	1082	1217	2467	660	i S.p	i C.p	p C.r	r	p	
27	6.0	$AlCl_3$			/	/	/	183	190	i	p	p	p	d	Temperature control difficult.
14 Silicon		Si	NG	CCl_4	1337	1472	1632	3140	1410	i S.p	i S.p	i C.p	r	i	Also SiO_2.
28	8.1	$SiCl_4$		$SiCl_4$	/	/	/	58	-70	p	p	r	r	i	Also SiF_4.
		SiS_2			/	/	/	1090	Subl.	i	d	r	p	i	
15 Phosporus		P_4	NG		129	157	185	420	/	d.	p	r	r	i	Careful handling required.
31	10.9	PCl_3		PCl_3	/	/	/	75	-28	p	p	p	p	i	Hydrolyse very readily.
		PH_3		PH_3	/	/	/	-88	/	p	p	p	p	i	Toxic.
16 Sulphur		S	NG		55	80	109	445	115	p	p	r	r	i	Many other sulphur compounds
32	1o.3	SO_2		SO_2	-145	-135	-124	-10	-75	r	r	p	p	i	possible.
17 Chlorine		Cl_2		Cl_2	-164	-155	-145	-35	-103	p	p	p	p	i	Also a wide variety of other
35	13.o	CCl_4		CCl_4	/	/	/	77	-23	r	r	r	r	i	chlorides.
18 Argon		Ar		Ar	-237	-234	-230	-186	-189	r	r	r	r	i	No problems.
40	15.7														
19 Potassium		K	NG		123	161	208	770	64	i	r	r	r	r	Require careful handling.
39	4.5	KCl			516	572	637	1500	776	i S.p	p	p	p	p	Also other halides.
20 Calsium		Ca	Nc		459	522	597	1480	842	i S.p	d	r	r	p	
40	6.1	$CaCl_2$			732	814	902	1600	772	i	i	p	p	p	Also other halides.
		CaO		CCl_4	1727	1875	2050	2850	2580	i	i	i C.r	d C.p	r	Also $CaCO_3$, decomp. to $CaO+CO_2$.
21 Scandium		Sc	NG	CCl_4	11o7	1232	1377	3000	1539	i S.p	i S.p	d C.p	r	d	
45	6.7	$ScCl_3$			662	717	787	/	939	i	d	r	r	d	Also other halides.
		Sc_2O_3		CCl_4	/	/	/	/	/	i	i	i C.r	d C.p	r	Also ScO.

Z ELEMENT M AMU	E_i eV	COM-POUND	GAS Com. Sup. Tr.	TEMPERATURES, °C. For Vapor Pressures, torr.					ION SOURCE TYPES					REMARKS
				10^{-4}	10^{-3}	10^{-2}	760	Melt	-1-	-2-	-3-	-4-	-5-	
									°C-	100 -	500 -	1100 -°C	Surf.	
22 Titanium		Ti	NG CCl_4	1442	1577	1737	3260	1675	i S.p	i S.p	i C.p	r	d	As the lanthanides.
48	6.8	$TiCl_4$	$TiCl_4$	/	/	/	136	-30	d	d	p	p	d	
		TiO_2	CCl_4	1780	1930	2100	2750	1840	i	i	i C.r	d C.p	r	Also Ti_2O_3.
23 Vanadium		V	NG CCl_4	1547	1687	1847	3360	1890	i S.p	i S.p	i C.p	r	d	
51	6.7	VF_3		/	687	765	/	/	i	i	r	p	d	Also other halides.
		VO_2	CCl_4	/	/	/	/	1967	i	i	i C.r	d C.p	r	Also other oxides.
24 Chromium		Cr	NG CCl_4	1157	1267	1397	2650	1890	i S.p	i S.p	d C.p	r	d	
52	6.7	$CrCl_3$		/	509	/	949	1150	i	d	r	p	d	Also other halides.
		Cr_2O_3	CCl_4	/	/	/	/	1990	i	i	i C.r	d C.p	r	Also other oxides.
25 Manganese		Mn	NG CCl_4	747	837	937	2037	1244	i S.p	i S.p	p C.r	r	i	
55	7.4	$MnCl_2$		/	/	/	1231	650	i	i	p	p	i	Also other halides.
		MnO	CCl_4	1349	1485	1628	/	1705	i	i	i C.r	d C.p	i	Also other oxides.
26 Iron		Fe	NG CCl_4	1227	1342	1477	2860	1535	i S.p	i S.p	i C.p	r	i	
56	7.8	$FeCl_2$		/	428	482	1012	677	i	d	r	p	i	Also other halides.
		FeO	CCl_4	1371	1500	1640	/	1420	i	i	i C.r	p C.p	i	Also other oxides.
27 Cobalt		Co	NG CCl_4	1257	1382	1517	2870	1492	i S.p	i S.p	i C.p	r	i	
59	7.8	$CoCl_2$		507	612	672	1053	740	i	i	r	p	i	Also other halides.
		CoO	CCl_4	1297	1410	1550	/	1800	i	i	i C.r	p C.p	i	Also other oxides.
28 Nickel		Ni	NG CCl_4	1262	1382	1527	2890	1453	i S.p	i S.p	i C.p	r	i	
58	7.6	$NiCl_2$		/	491	545	973	1001	i	d	r	p	i	Also other halides.
		NiO	CCl_4	1240	1356	1485	/	1990	i	i	i C.r	p C.p	i	Also Ni_2O_3.
29 Copper		Cu	NG CCl_4	1027	1137	1257	2580	1083	i S.p	i S.p	p C.p	r	i	
63	7.7	Cu_2Cl_2		/	/	/	1366	422	i	i	p	p	i	Also $CuCl_2$, which decomposes to Cu_2Cl_2.
		CuO	CCl_4	/	925	1070	/	1326	i	i	p C.r	p	i	
30 Zinc		Zn	NG	247	292	344	907	417	i S.p	r	r	r	i	No particular problems.
64	9.4	ZnS		779	863	962	1185	subl.	i	i	p	p	i	

Z ELEMENT M AMU	E_i eV	COMPOUND	GAS Com. Sup. Tr.	TEMPERATURES, °C. For Vapor Pressures, torr.					ION SOURCE TYPES °C- 100 - 500 -1100-°C					REMARKS
				10^{-4}	10^{-3}	10^{-2}	760	Melt	-1-	-2-	-3-	-4-	-5- Surf.	
31 Gallium		Ga	NG	907	1007	1132	2400	30	i	i	p	r	r	No particular problems.
69	6.0	GaI_3	GaI_3	/	/	/	345	212	p	p	r	p	d	
		Ga_2O_3	CCl_4	/	/	/	/	1900	i	i	i C.r	d C.p	r	
32 Germanium		Ge	NG CCl_4	1137	1257	1397	2830	937	i S.p	i S.p	i C.p	r	i	
74	8.1	GeI_4	GeI_4	/	41	65	377	146	p	r	r	p	i	Cl_2^+ may cause contamination.
		GeS_2		406	447	494	600	800	i	p	r	p	i	
33 Arsenic		As	NG	204	237	277	700	810	i	p	p	p	i	Toxic.
75	10.5	$AsCl_3$	$AsCl_3$	/	/	/	130	-18	p	r	p	p	i	
		GaAs		/	/	/	/	1238	i S.p	d	r	r	i	Decomposes controllably in oven.
34 Selenium		Se	NG	164	199	243	680	217	i S.p	p	r	r	i	Toxic.
80	9.7	SeO_2		75	98	124	337	345	d	r	r	p	i	
		CdSe		/	588	661	/	1350	i	d	r	r	i	Convenient temperature control.
35 Bromine		Br_2	Br_2	-110	-99	-84	59	-7	r	r	r	r	i	
79	11.8	NaBr		667	791	937	1390	755	i	i	r	r	i	Also other bromides.
36 Krypton		Kr	Kr	-224	-219	-214	-153	-157	r	r	r	r	i	No problems.
84	13.9													
37 Rubidium		Rb	NG	94	129	173	700	39	i S.p	r	r	r	r	
85	4.2	RbCl		487	544	614	1380	715	i	p	r	r	p	Also other halides.
		Rb_2CO_3		/	/	/	740	837	i	i	r	p	r	
38 Strontium		Sr	NG	404	465	537	1370	769	i S.p	r	r	r	r	
88	5.7	$SrCl_2$		716	799	888	2000	873	i	i	p	p	p	Also other halides.
		$SrCO_3$	CCl_4	/	/	/	1340	1497	i	i	i C.p	p C.p	r	
39 Yttrium		Y	NG CCl_4	1332	1467	1632	3300	1495	i S.p	i S.p	i C.p	r	p	As the lanthanides.
89	6.5	YCl_3		/	613	698	/	680	i	i	p	p	d	
		Y_2O_3	CCl_4	2098	2250	2412	/	2410	i	i	i C.r	d C.p	r	

Z ELEMENT M AMU	E_i eV	COMPOUND	GAS Com. Sup.	Tr.	TEMPERATURES, °C. For Vapor Pressures, torr. 10^{-4}	10^{-3}	10^{-2}	760	Melt	ION SOURCE TYPES -1- °C- 100	-2- 100 - 500	-3- 500 -1100	-4- 1100 -°C	-5- Surf.	REMARKS
40 Zirconium		Zr	NG	CCl_4	1987	2177	2397	4500	1852	i S.p	i S.p	i C.p	p	d	As the lanthanides.
90	6.9	$ZrCl_4$			82	103	128	331	437	i	d	p	p	d	
		ZrO_2		CCl_4	2o77	2240	2400	5000	2677	i	i	i C.r	d C.r	p	
41 Niobium		Nb	NG	CCl_4	2277	2447	2657	4400	2468	i S.p	i S.p	i S.p	p	d	As the lanthanides.
93	6.9	Nb_2O_3		CCl_4	/	/	/	/	1780	i	i	i C.r	d C.r	p	
42 Molybdenum		Mo	NG		2117	2307	2527	4620	2610	i S.p	i S.p	i S.p	p	i	
98	7.4	MoO_3		CCl_4	565	605	646	1150	795	i	i	p C.r	p C.r	i	Also MoO_2
43 Technetium		Tc			2o77	2257	2487	4580	2200	i	i	i	p	i	No stable isotopes.
(99)	(7.5)	TcO_x		CCl_4	/	/	/	/	/	i	i	i C.p	d C.p	i	
44 Ruthenium		Ru	NG		1987	2147	2347	4070	2250	i S.p	i S.p	i S.p	r	i	Only very unstable compounds.
1o2	7.7	RuF_5		RuF_5	/	31	50	270	106	i	i	p	p	i	
45 Rhodium		Rh	NG		1707	1255	2037	3700	1960	i S.p	i S.p	i S.p	r	i	Only very unstable compounds.
1o3	7.7														
46 Palladium		Pd	NG		1192	1317	1462	3020	1550	i S.p	i S.p	d S.p	r	i	Only very unstable compounds.
106	8.3														
47 Silver		Ag	NG		823	922	1027	2212	961	i S.p	i S.p	r	r	i	No particular problems.
107	7.5	AgCl			539	607	685	1560	455	i	i	r	p	i	
48 Cadmium		Cd	NG		177	217	265	767	321	i S.p	r	r	r	i	No particular problems.
114	9.0	CdS			/	610	686	1382	1750	i	i	r	r	i	
49 Indium		In	NG	CCl_4	742	837	947	21oo	156	i S.p	i C.p	r	r	r	No particular problems.
115	5.8	$InCl_3$			/	224	256	470	586	i	r	p	p	p	
50 Tin		Sn	NG	CCl_4	997	1104	1247	2630	232	i S.p	i C.p	d C.r	r	i	Also with H_2S as transport gas.
120	7.3	$SnCl_4$		$SnCl_4$	/	/	/	120	-33	d	p	p	p	i	
51 Antimony		Sb	NG		475	475	535	1650	631	i S.p	p	r	r	i	Toxic,no problems.
171	8.5														

Z ELEMENT		COMPOUND	GAS		TEMPERATURES, °C. For Vapor Pressures, torr.					ION SOURCE TYPES					REMARKS
M AMU	E_i eV		Com.	Sup. Tr.	10^{-4}	10^{-3}	10^{-2}	760	Melt	-1- °C-	-2- 100 -	-3- 500 -	-4- 1100 -°C	-5- Surf.	
52 Tellurium		Te	NG		280	323	374	1000	450	i S.p	p	r	r	i	Toxic,no particular problems.
130	9.0														
53 Iodine		I_2	I_2		-47	-30	-11	183	114	r	r	r	r	i	
127	10.6	KI			448	499	564	1323	682	i	d	p	p	i	Numerous other iodides.
		AgI			722	845	995	/	/	i	i	p	p	i	Decomposes controllably.
54 Xenon		Xe	Xe		-205	-199	-191	-107	-112	r	r	r	r	i	No problems.
132	12.1														
55 Cesium		Cs	NG		78	114	155	680	29	p	r	r	r	r	Careful handling.
133	3.9	CsCl			448	505	572	1301	642	i	i	r	r	p	Also other halides.
56 Barium		Ba	NG.		462	527	610	1590	725	i S.p	d S.p	r	r	r	Toxic.
138	5.2	$BaCl_2$			734	813	899	1560	962	i	i	r	p	p	Also other halides.
		BaO		CCl_4	1297	1421	1549	2000	1923	i	i	i C.r	p	r	
57 Lanthanum		La	NG		1422	1562	1727	3330	920	i S.p	i S.p	i S.p	r	p	
139	5.6	$LaCl_3$			/	751	825	/	860	i	i	p	p	d	Even that volatile halides exist for all lanthanide elements are they very hygroscopic and difficult to use. It is recommended to use freshly prepared oxides to obtain max. reactivity with the CCl_4.
		La_2O_3		CCl_4	1816	1966	2176	4200	2315	i	i	i C.r	d C.r	r	
58 Cerium		Ce	NG		1377	1522	1697	3468	795	i S.p	i S.p	i S.p	r	p	
140	6.5	CeO_2		CCl_4	/	/	/	/	2600	i	i	i C.r	d C.r	r	
59 Praseodymium		Pr	NG		1147	1277	1427	3030	935	i S.p	i S.p	i S.p	r	p	
141	5.8	Pr_2O_3		CCl_4	/	/	/	/	/	i	i	i C.r	d C.r	r	
60 Neodynium		Nd	NG		1047	1167	1307	3080	1024	i S.p	i S.p	i S.p	r	p	
142	6.3	Nd_2O_3		CCl_4	/	/	/	/	1900	i	i	i C.r	d C.r	r	
61 Promethium		Pm	NG		/	/	/	2730	1035	i	i	d	r	p	No stable isotopes.
(145)	/	Pm_2O_3		CCl_4	/	/	/	/	/	i	i	i C.r	d C.r	r	
62 Samarium		Sm	NG		580	653	742	1800	1072	i S.p	i S.p	p	r	p	
152	6.6	Sm_2O_3		CCl_4	/	/	/	/	/	i	i	i C.r	p C.r	r	

Z ELEMENT M AMU	E_i eV	COMPOUND	GAS Com. Sup. T.	TEMPERATURES, °C. For Vapor Pressures, torr. 10^{-4}	10^{-3}	10^{-2}	760	Melt.	ION SOURCE TYPES -1- °C- 100	-2- - 500	-3- -1100	-4- -°C	-5- Surf.	REMARKS
63 Europium		Eu	NG	466	532	611	1500	826	i S.p	d S.p	p	r	p	Even that volatile halides exist for all lanthanide elements are they very hygroscopic and difficult to use. It is recommended to use freshly prepared oxides to obtain max. reactivity with the CCl_4.
153	5.6	Eu_2O_3	CCl_4	/	/	/	/	/	i	i	d C.r	p C.r	r	
64 Gadolinium		Gd	NG	1077	1192	1327	2730	1312	i S.p	i S.p	i S.p	r	p	
158	6.7	Gd_2O_3	CCl_4	/	/	/	/	/	i	i	i C.r	d C.r	r	
65 Terbium		Tb	NG	1147	1277	1427	3020	1356	i S.p	i S.p	i S.p	r	p	
159	6.7	Tb_2O_3	CCl_4	/	/	/	/	/	i	i	i C.r	d C.r	r	
66 Dysprosium		Dy	NG	897	997	1117	2420	1407	i S.p	i S.p	d	r	p	
164	6.8	Dy_2O_3	CCl_4	/	/	/	/	2340	i	i	i C.r	d C.r	r	
67 Holmium		Ho	NG	947	1052	1117	2580	1461	i S.p	i S.p	i S.p	r	p	
165	6.0	Ho_2O_3	CCl_4	/	/	/	1500	718	i	i	i C.r	p C.r	r	
68 Erbium		Er	NG	947	1052	1177	2580	1497	i S.p	i S.p	i S.p	r	p	
166	6.1	Er_2O_3	CCl_4	/	/	/	/	/	i	i	i C.r	d C.r	r	
69 Thulium		Tm	NG	680	757	847	1750	1545	i S.p	i S.p	p	r	p	
169	6.2	Tm_2O_3	CCl_4	/	/	/	/	/	i	i	i C.r	d C.r	r	
70 Ytterbium		Yb	NG	417	482	557	1540	824	i S.p	i S.p	p	r	d	
174	7.1	Yb_2O_3	CCl_4	/	/	/	/	/	i	i	i C.r	d C.r	r	
71 Lutetium		Lu	NG	1277	1412	1572	3020	1652	i S.p	i S.p	i S.p	r	p	
175	6.2	Lu_2O_3	CCl_4	/	/	/	/	/	i	i	i C.r	d C.r	r	
72 Hafnium		Hf	NG	1997	2177	2397	4430	1652	i S.p	i S.p	i S.p	p	d	As the lanthanides.
180	6.8	HfO_2	CCl_4	2297	2475	2678	5400	2812	i	i	i C.r	d C.r	r	
73 Tantalum		Ta	NG	2587	2800	3050	5230	3000	i S.p	i S.p	i S.p	i S.p	i	As the lanthanides.
181	7.9	Ta_2O_5	CCl_4	/	/	/	/	1800	i	i	i C.r	d C.r	i	
74 Tungsten		W	NG	2760	2980	3230	5530	3380	i S.p	i S.p	i S.p	i S.p	i	Most compounds unstable.
184	8.1	WO_3	CCl_4	1079	1136	1176	/	1473	i	i	i C.p	p C.p	i	

Z ELEMENT M AMU	E_i eV	COMPOUND	GAS Com. Sup. Tr.	TEMPERATURES, °C. For Vapor Pressures, torr. 10^{-4}	10^{-3}	10^{-2}	760	Melt.	ION SOURCE TYPES -1- °C- 100	-2- - 500	-3- -1100	-4- - °C	-5- Surf.	REMARKS
75 Rhenium 187	 7.9	Re Re_2O_7	$O_2 + CCl_4$ NG	2587 /	2807 133	3067 157	5627 362	3180 subl.	i S.p i	i S.p d	i C.r p	i C.p p	i i	Most compounds very unstable.
76 Osmium 192	 8.7	Os OsO_4	$O_2 + CCl_4$ OsO_4	2487 /	2687 -70	2917 -52	5300 130	3000 40	i S.p i	i S.p d	i C.r p	i C.p p	i i	Toxic. Most compounds very unstable.
77 Iridium 193	 9.1	Ir	NG	2107	2287	2497	4530	2443	i S.p	i S.p	i S.p	r	i	Only very unstable compounds.
78 Platium 195	 8.9	Pt	NG	1747	1907	2097	3827	1769	i S.p	i S.p	i S.p	r	i	Only very unstable compounds.
79 Gold 197	 9.7	Au	NG	1132	1252	1397	2770	1063	i S.p	i S.p	d S.p	r	i	Only very unstable compounds.
80 Mercury 202	 10.4	Hg	NG	-7	16	43	357	-39	r	r	r	r	i	Toxic, no problems.
81 Thallium 205	 6.1	Tl TlF	NG	463 /	530 81	609 106	1457 655	304 327	i S.p d	d r	r p	r p	r p	Toxic, no problems.
82 Lead 208	 7.4	Pb $PbCl_2$	NG	547 327	625 385	715 431	1744 954	327 501	i S.p i	i S.p p	r p	r p	i i	No particular problems.
83 Bismuth 209	 8.0	Bi $BiCl_3$	NG	517 /	567 118	672 145	1570 447	271 231	i S.p i	d S.p p	r p	r p	i i	No particular problems.
84 Polonium (209)	 8.4	Po $PoCl_4$	NG	221 /	264 /	315 /	962 390	254 300	i d	r p	r p	r p	i i	No stable isotopes.
85 Astatine (210)	 9.5	At	NG	43	65	91	330	300	p	r	r	r	i	No stable isotopes.
86 Radon (222)	 10.7	Rn	Rn	/	/	/	-62	-71	r	r	r	r	i	No stable isotopes.

Z ELEMENT M AMU	E_i eV	COM-POUND	GAS Com. Sup. Tr.	TEMPERATURES, °C. For Vapor Pressures, torr. 10^{-4}	10^{-3}	10^{-2}	760	Melt	ION SOURCE TYPES -1- °C-	-2- 100 -	-3- 500 -	-4- 1100 -°C	-5- Surf.	REMARKS
87 Francium (223)	4.0	Fr	NG	61	95	137	680	17	d	r	r	r	r	No stable isotopes.
88 Radium (226)	5.3	Ra	NG	417	482	557	1530	700	i	d	r	r	r	No stable isotopes.
89 Actinium (227)	6.8	Ac	NG	1332	1467	1632	3200	1050	i	i	i	r	d	No stable isotopes.
		$AcCl_3$		/	/	/	960	/	i	p	p	p	d	
		Ac_2O_3	CCl_4	/	/	/	/	/	i	i	i C.r	d C.p	r	As the lanthanides.
90 Thorium 232	7.0	Th	NG	1997	2167	2407	4200	1700	i S.p	i S.p	i S.p	p	d	As the lanthanides.
		$ThCl_4$		/	/	/	/	770	i	i	p	p	i	
		ThO_2	CCl_4	2080	2240	2420	4400	3300	i	i	i C.r	d C.r	r	
91 Protactinium (231)	/	Pa	NG	/	/	/	/	1230	i	i	d	p	(d)	As the lanthanides.
		PaO_2	CCl_4	/	/	/	/	/	i	i	i C.r	d C.r	(r)	No stable isotopes.
92 Uranium 238	6.1	U	NG	1582	1737	1927	3818	1132	i S.p	i S.p	i S.p	r	p	As the lanthanides.
		UCl_4		/	/	/	792	590	i	d	p	p	d	
		UO_2	CCl_4	1747	1892	2060	/	2500	i	i	i C.r	p C.r	r	
93 Neptunium (237)	/	Np	NG	/	/	/	3900	640	i	i	i	r	(p)	No stable isotopes.
		NpO_2	CCl_4	/	/	/	/	/	i	i	i C.r	d C.r	(r)	As the lanthanides.
94 Plutonium (239)	5.1	Pu	NG	1207	1342	1507	3330	641	i	i	i	r	p	No stable isotopes.
		PuO_2	CCl_4	1720	1860	2010	/	/	i	i	i C.r	d C.r	r	As the lanthanides.
95 Americium (241)	/	Am	NG	867	972	1100	2600	830	i	i	p	r	(p)	No stable isotopes.
		AmO_2	CCl_4	/	/	/	/	/	i	i	i C.r	d C.r	(r)	As the lanthanides.
96 Curium (247)	/	Cm	NG	/	/	/	/	1340	i	i	d	r	(p)	No stable isotopes.
		CmO_2	CCl_4	/	/	/	/	/	i	i	i C.r	d C.r	(r)	As the lanthanides.
97 Berkelium (249)	/	Bk	NG	/	/	/	/	/	i	i	d	r	(p)	No stable isotopes.
		BkO_2	CCl_4	/	/	/	/	/	i	i	i C.r	d C.r	(r)	As the lanthanides.

APPENDIX III

OPERATING PROCEDURES FOR THE DANFYSIK 911-A ION SOURCE

The general procedure for running the source is as follows:

1) Select the oven which can give a temperature suitable to heat up the charge material in order to give a vapour pressure approximately 10^{-2} - 10^{-1} torr.
2) Put the charge material in the selected oven and assemble the source.
3) Outgas the source (filament current increasing up to approximately 20 amp DC).
4) Start a discharge on a noble gas, for instance argon IE.

   Anode voltage on 200 V DC.

   Filament 20-24 amp DC.

   Apply argon (corresponding to a vacuum of $\sim 1 - 5 \times 10^{-5}$ in the region just outside the source).
5) Let the source stabilize thermally by running a discharge of approximately 2 amp anode current for a couple of minutes.
6) Adjust the analyzer (the separating magnet) on the desired mass number.
7) If necessary, increase the oven power (starting from zero) to obtain the needed current level.
8) In most cases the argon support gas can gradually be reduced and even completely removed while simultaneously increasing the oven,

anode and filament power in order to maintain a constant discharge current.

9) Normally the most ideal way to run the source is to peak the output with all parameters.

ION SOURCE 911-A

ELEMENT	V_F	I_F	V_A	I_A	V_o	I_o	I_M	P_o	REMARKS
	filament		anode		(oven)	(oven)	(magnet)	Torr	
	VOLT	AMP	VOLT	AMP	VOLT	AMP	AMP		
ARSENIC	4.0	23	45	1.3	5.5 V	25	10A	6×10^{-6}	
IRON	5	28	40	2A	8.5	30	-	2×10^{-5}	
SILVER	3.2	20	70	2.4	6	26	2A	10^{-5}	~75% of total current is single charged
COBALT	4.8	24	40	4.4	12	38	10A	-	Main impurity iron is mass 26-27-28
BERYUIUM	4.3	23	45	2	-	35	10A	-	

APPENDIX IV

GAS FEED SYSTEM WITH SAFETY PROCEDURES FOR HAZARDOUS AND DANGEROUS CHEMICALS(4)

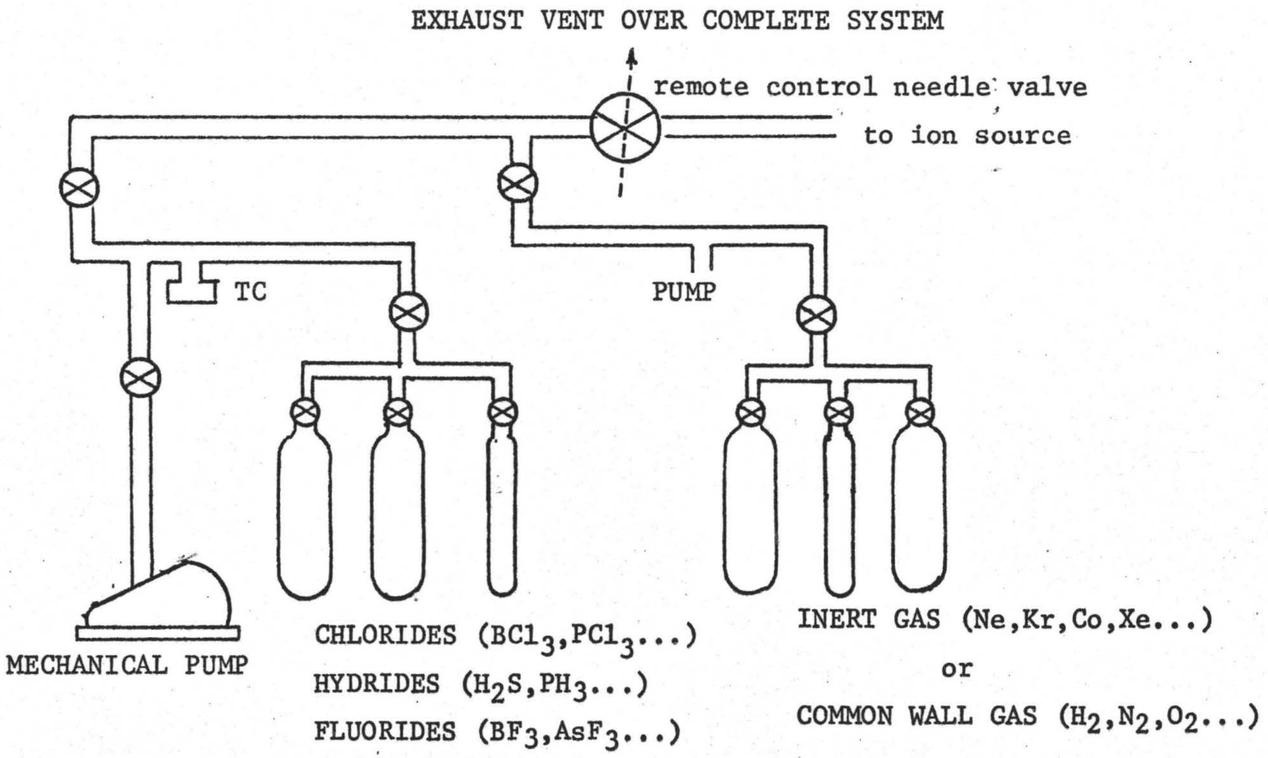

Figure AIV-1: Gas Supply System.

See following pages for Charts of Precautions and Treatments

MATERIAL		DESCRIPTION	HAZARD	
			CLASS	DEGREE
Nitrogen	N_2	colorless, odorless gases	Inhalation D	
Carbon dioxide	CO_2			
Inert gases	He,Ne,A,Kr,Xe			
Oxygen	O_2	colorless, odorless gas	Flammability G	
Hydrogen	H_2	colorless, odorless gas	Flammability D,H Inhalation B	
Chlorine (and HCl vapor)	Cl_2	pale yellow, irritating gas	Inhalation B Contact B	
Fluorine (and HF vapor)	F_2	green-yellow, irritating gas	Inhalation A Contact A Flammability G	
Sulfur	S	yellow solid	Inhalation B (fumes)	
Phosphorus - Red	P	red powder or solid mass	Flammability C Inhalation C	
Phosphorus - White	P	white solid	Flammability F Inhalation B Contact B Water A,B,C	
Zinc	Zn	metal	None	
Cadmium	Cd	metal	Ingestion B (mild)	
Gallium	Ga	metal (liquid)	None	
Indium	In	metal, soft, silver	Ingestion B	
Thallium	Tl	metal	Ingestion B (mild)	
Aluminum	Al	metal	None	
Carbon monoxide	CO	colorless, odorless gas	Flammability D Inhalation B	
Carbon disulfide	CS_2	colorless liquid, putrid odor	Inhalation B Contact D	
Hydrogen sulfide	H_2S	colorless gas, rotten eggs odor	Flammability D Inhalation B/A	
Aluminum chloride	$AlCl_3$	yellow-white crystal	Contact B Inhalation B Water C	
Silicon tetrafluoride	SiF_4	colorless gas	Inhalation B Contact B	
Silicon tetrachloride	$SiCl_4$	colorless, fuming liquid, suffocating odor	Inhalation B Contact B Water B,C	
Diborane	B_2H_6	colorless gas, sickly sweet odor	Flammability D,I Inhalation A Contact B	
Boron trifluoride	BF_3	colorless gas	Inhalation B Contact B	
Boron trichloride	BCl_3	colorless, fuming liquid	Inhalation B Contact B Water C	
Phosphine	PH_3	colorless gas	Flammability D Inhalation A	
Phosphorus pentafluoride	PF_5	colorless gas	Inhalation B Contact B	
Phosphorustrichloride	PCl_3	clear, colorless, fuming liquid	Contact B	
Arsine	AsH_3	colorless gas,garlic odor	Inhalation A	
Arsenic trifluoride	AsF_3	oily liquid	Contact B Inhalation A Ingestion A Water B,C	
Arsenic trichloride	$AsCl_3$	clear-to-pale yellow oily liquid or needle xtal	Contact B Inhalation A Ingestion A Water B,C	
Stibine	SbH_3	colorless gas	Contact B Inhalation B	
Antimony trifluoride	SbF_3	colorless crystal mass	Contact B Inhalation B Water C	
Antimony trichloride	$SbCl_3$	colorless crystal	Contact B Inhalation B Water C	
Hydrogen selenide	H_2Se	colorless gas	Inhalation A	
Hydrogen telluride	H_2Te	colorless gas or yellow needles	Inhalation C	
Lithium, sodium, potassium	Li,Na,K	silvery-white metal	Flammability F Water A	
Rubidium, cesium	Rb,Cs	golden-white liquid or solid	Flammability F Water A	

CLASS OF HAZARD			STATEMENTS OF HAZARD	PRECAUTIONARY MEASURES	INSTRUCTIONS IN CASE OF CONTACT OR EXPOSURE
INGESTION	A	Highly Toxic	MAY BE FATAL IF SWALLOWED	Wash thoroughly after handling	☠ POISON ☠ Call a Physician FIRST AID: If swallowed, induce vomiting by sticking finger down throat or by giving soapy or strong salty water to drink. Repeat until vomit is clear. Never give anything by mouth to an unconscious person.
	B	Toxic	HARMFUL IF SWALLOWED	Wash thoroughly after handling	FIRST AID: If swallowed, induce vomiting by sticking finger down throat or by giving soapy or strong salty water to drink. Repeat until vomit is clear. Call a physician. Never give anything by mouth to an unconscious person.
ABSORPTION	A	Highly Toxic	MAY BE FATAL IF ABSORBED THROUGH SKIN	Do not get in eyes, on skin, on clothing. Wash thoroughly after handling.	☠ POISON ☠ Call a Physician FIRST AID: In case of contact, immediately flush eyes or skin with plenty of water for at least 15 minutes while removing contaminated clothing and shoes. Wash clothing before re-use. (Discard contaminated shoes.)
	B	Toxic	HARMFUL IF ABSORBED THROUGH SKIN	Avoid contact with eyes, skin, and clothing. Wash thoroughly after handling.	FIRST AID: In case of contact, immediately flush eyes or skin with plenty of water for at least 15 minutes while removing contaminated clothing and shoes. Call a physician. Wash clothing before re-use. (Discard contaminated shoes.)
INHALATION	A	Highly Toxic	MAY BE FATAL IF INHALED	Do not breathe (dust, vapor, mist, gas). Keep container closed. Use only with adequate ventilation.	☠ POISON ☠ Call a Physician FIRST AID: If inhaled, remove to fresh air. If not breathing give artificial respiration, preferably mouth-to-mouth. If breathing is difficult, give oxygen.
	B	Toxic	HARMFUL IF INHALED	Avoid breathing (dust, vapor, mist, gas). Keep container closed. Use only with adequate ventilation.	FIRST AID: If inhaled, remove to fresh air. If not breathing give artificial respiration, preferably mouth-to-mouth. If breathing is difficult, give oxygen. Call a physician.
	C	Strong Sensitizer, Lungs	MAY CAUSE ALLERGIC RESPIRATORY REACTION	Avoid breathing (dust, vapor, mist, gas). Keep container closed. Use with adequate ventilation.	Get into fresh air.
	D	Physiologically Inert Vapor or Gas	(VAPOR) (GAS) REDUCES OXYGEN AVAILABLE FOR BREATHING	Keep container closed. Use with adequate ventilation. Do not enter storage areas unless adequately ventilated.	Get into fresh air.

CLASS OF HAZARD			STATEMENTS OF HAZARD	PRECAUTIONARY MEASURES	INSTRUCTIONS IN CASE OF CONTACT OR EXPOSURE
CONTACT	A	Corrosive, Eye	CAUSES (SEVERE) EYE BURNS	Do not get in eyes. Avoid breathing (dust, vapor, mist, gas). Keep container closed. Use with adequate ventilation. Wash thoroughly after handling.	FIRST AID: In case of contact, immediately flush eyes with plenty of water for at least 15 minutes. Call a physician.
	B	Corrosive, Eye and Skin	CAUSES (SEVERE) BURNS	Do not get in eyes, on skin, on clothing. Avoid breathing (dust, vapor, mist, gas). Keep container closed. Use with adequate ventilation. Wash thoroughly after handling.	FIRST AID: In case of contact, immediately flush eyes or skin with plenty of water for at least 15 minutes while removing contaminated clothing and shoes. Call a physician. Wash clothing before re-use. (Discard contaminated shoes.)
	C	Irritant, Eye	CAUSES EYE IRRITATION	Avoid contact with eyes. Wash thoroughly after handling.	FIRST AID: In case of contact, immediately flush eyes with plenty of water for at least 15 minutes. Call a physician.
	D	Irritant, Eye and Skin	CAUSES IRRITATION	Avoid contact with eyes, skin, and clothing. Wash thoroughly after handling.	FIRST AID: In case of contact, immediately flush eyes with plenty of water for at least 15 minutes. Call a physician. Flush skin with water. (Wash clothing before re-use).
	E	Strong Sensitizer, Skin	MAY CAUSE ALLERGIC SKIN REACTION	Avoid prolonged or repeated contact with skin. Wash thoroughly after handling.	FIRST AID: In case of contact, immediately wash skin with soap and plenty of water.
FLAMMABILITY	A	Extremely Flammable Liquid	EXTREMELY FLAMMABLE	Keep away from heat, sparks, and open flame. Keep container closed. Use with adequate ventilation.	
	B	Flammable Liquid	FLAMMABLE	Keep away from heat, sparks, and open flame. Keep container closed. Use with adequate ventilation.	
	C	Flammable Solid	FLAMMABLE	Keep away from heat, sparks, and open flame.	
	D	Flammable Gas	EXTREMELY FLAMMABLE (GAS)(LIQUID AND GAS) UNDER PRESSURE	Keep away from heat, sparks, and open flame. Use with adequate ventilation. Never drop cylinder. Keep cylinder out of sun and away from heat.	
	E	Combustible Liquid	COMBUSTIBLE	Keep away from heat and open flame.	
	F	Pyroforic Substance	EXTREMELY FLAMMABLE. CATCHES FIRE IF EXPOSED TO AIR.	Keep away from heat, sparks, and open flame. Keep container closed.	
	G	Strong Oxidizer	STRONG OXIDIZER. CONTACT WITH OTHER MATERIAL MAY CAUSE FIRE	Keep from contact with clothing and other combustible materials. Do not store near combustible materials. Store in tightly closed container.	Remove and wash contaminated clothing promptly.
	H	Explosive in Air		Keep sparks or flame away.	
	I	Explosive any Conditions		Evacuate	
WATER REACTIVITY	A	Flammable or Explosive	BURNS IN WATER OR EXPLODES	Use no water to fight fire.	
	B	Highly Toxic	FORMS POISONOUS GAS WITH WATER REACTION	See above inhalation A & B	Use no water.
	C	Toxic	FORMS BURNING GAS WITH WATER REACTION	See above contact A,B,C, & D	Use no water.

APPENDIX V

ELECTRICAL DIAGRAMS FOR THE ION SOURCE

1) Ion Source Power Supply System.
2) Ion Source Schematics.
3) Telemetering System.
4) Safety Interlock System.
5) Remote Control Gas Feed System.
6) Remote Control Analyzer Magnet System.

Power Requirements

The magnet coil mounted on the ion source housing must be connected so that the magnetic field on the axis from the filament can be cancelled out.

Filament Supply: P out ∿ 120-130 W (6 V/20 A and 4, 5 V/30 A)

Anode Supply: 250-300 V/0.1 A and 30-50 V/4-5 A

Oven Supply: 9.5 V/30 A (I_{max} ∿ 40 amp.)

Ion Source Trouble-Shooting

If the source will not start on argon, check:

a) Symptom: No pressure rise when the needle valve is opened.

Cause: (i) Gas bottle empty; replace with full bottle.

(ii) Needle valve damaged and/or shaft has no connection to the needle. Repair.

b) Symptom: Filament currents in excess of ∿26-28 amp needed to start the source.

1. Measure the voltage over the filament feed-throughs on the ion source (switch off the extraction supply). If the resistance of the filament is <0.1-0.15Ω at ∿20-25 amp the filament is probably partly shorted. Replace the filament.
2. If there are large amounts of mass 28 and mass 14 (nitrogen), and only little or no mass 40 there probably is a leak in the gas supply system. Use a perspex or trovidur tube ∿0.5 m long (for insulating against voltage extraction) to spray the parts of the gas supply

system with gaseous helium and adjust the separating magnet to mass 4 (in this case the separator part is used as a gas leak detector!). Any leak detected must be sealed.

3. If the main contribution is mass 40, the discharge chamber is probably leaking. Check whether the springs on the gas injector are properly positioned. Check all the insulators for cracks. Check whether the gas injector, or ovens are properly placed.

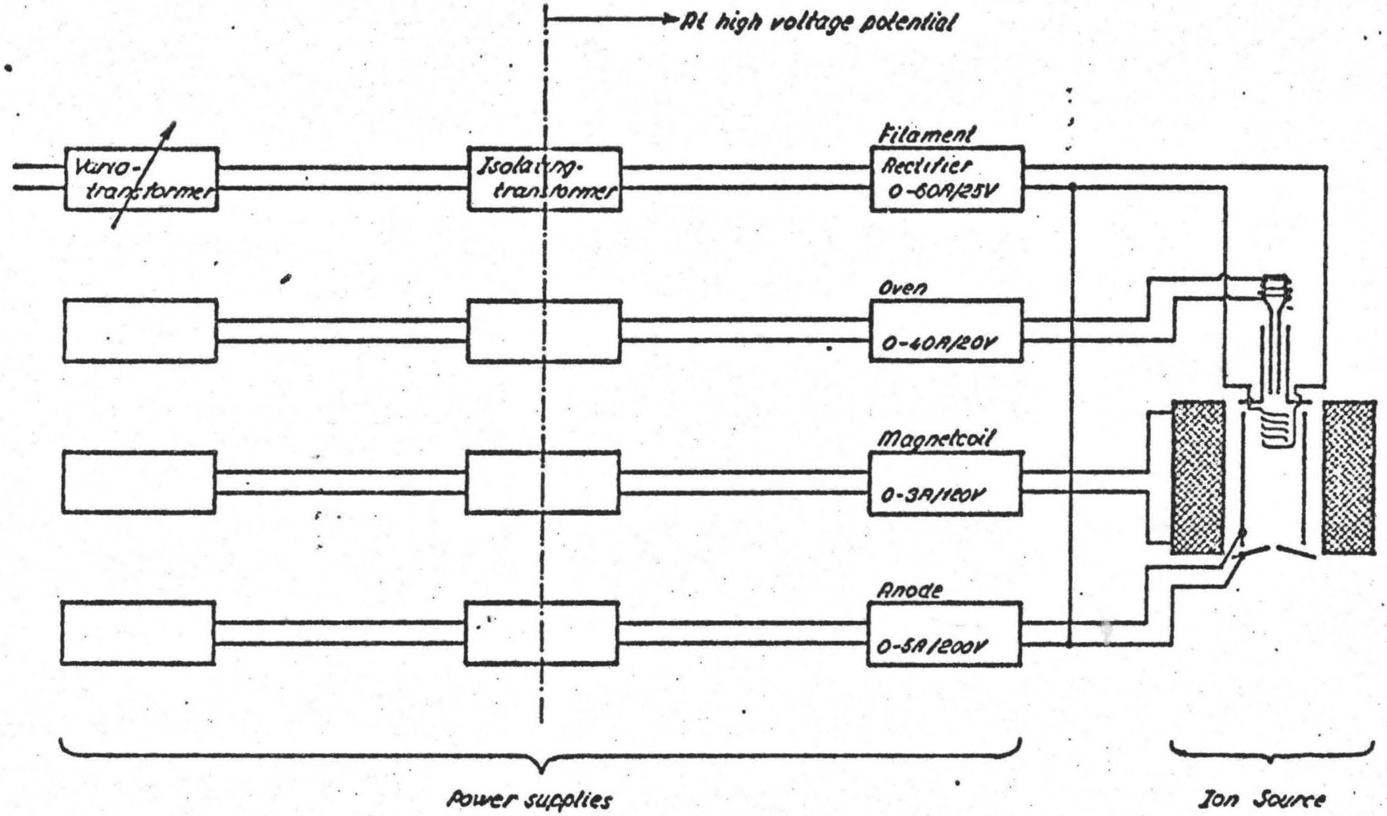

Figure AV-1: Ion Source with Power Supplies.

1'-1 Current output to input, Figure AV-5

2'-2 Voltage output to input, Figure AV-5

A'-A To Ion Source

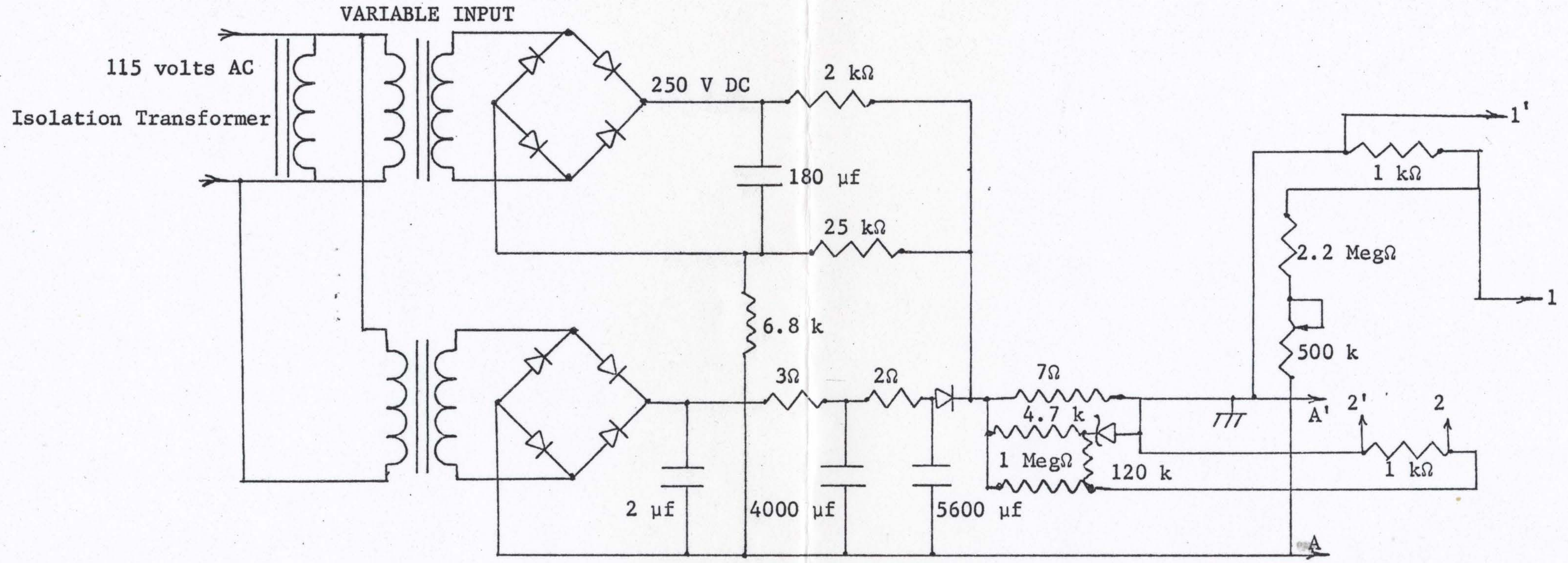

Figure AV-2: Anode Voltage Supply

1'-1 Voltage Output to Input, Figure AV-4

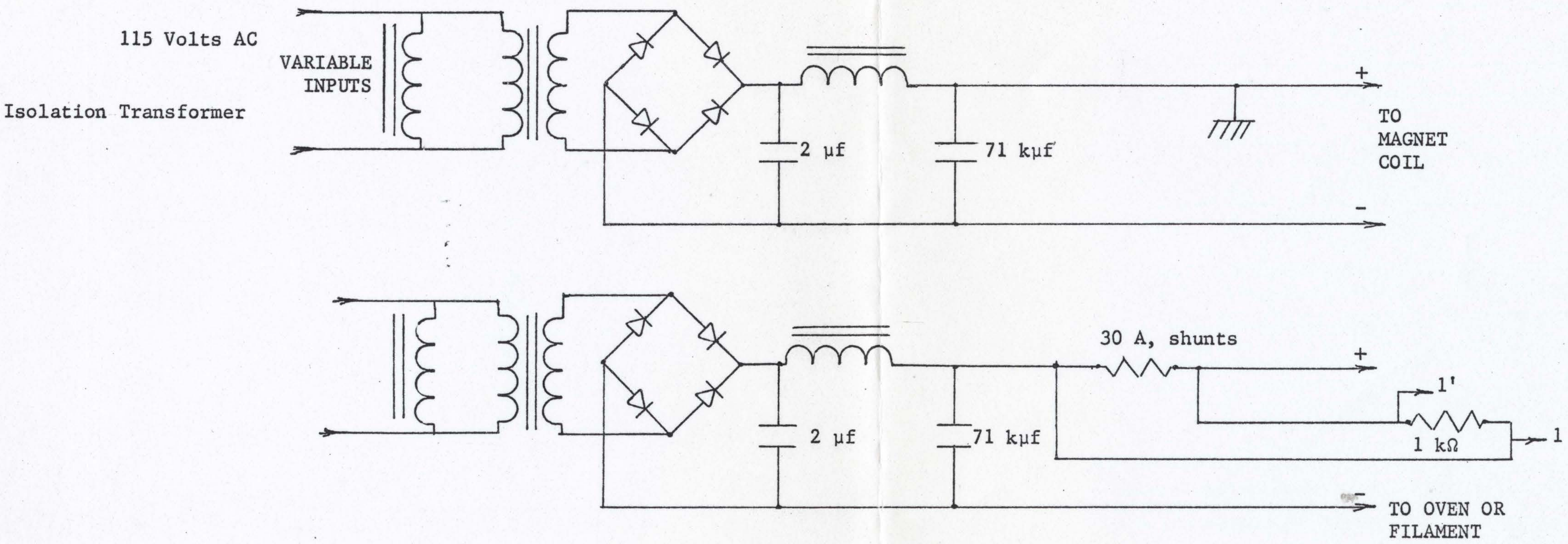

Figure AV-3: Magnet Supply (top diagram).

Filament and Oven Supplies.

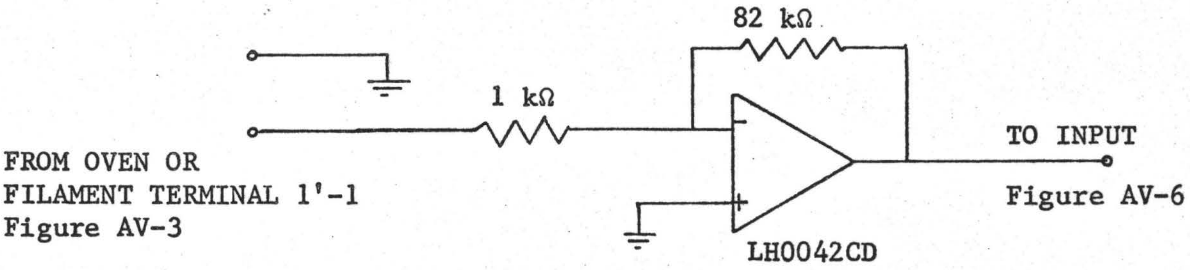

Figure AV-4: Filament and Oven Input Circuits to the Telemetering System.

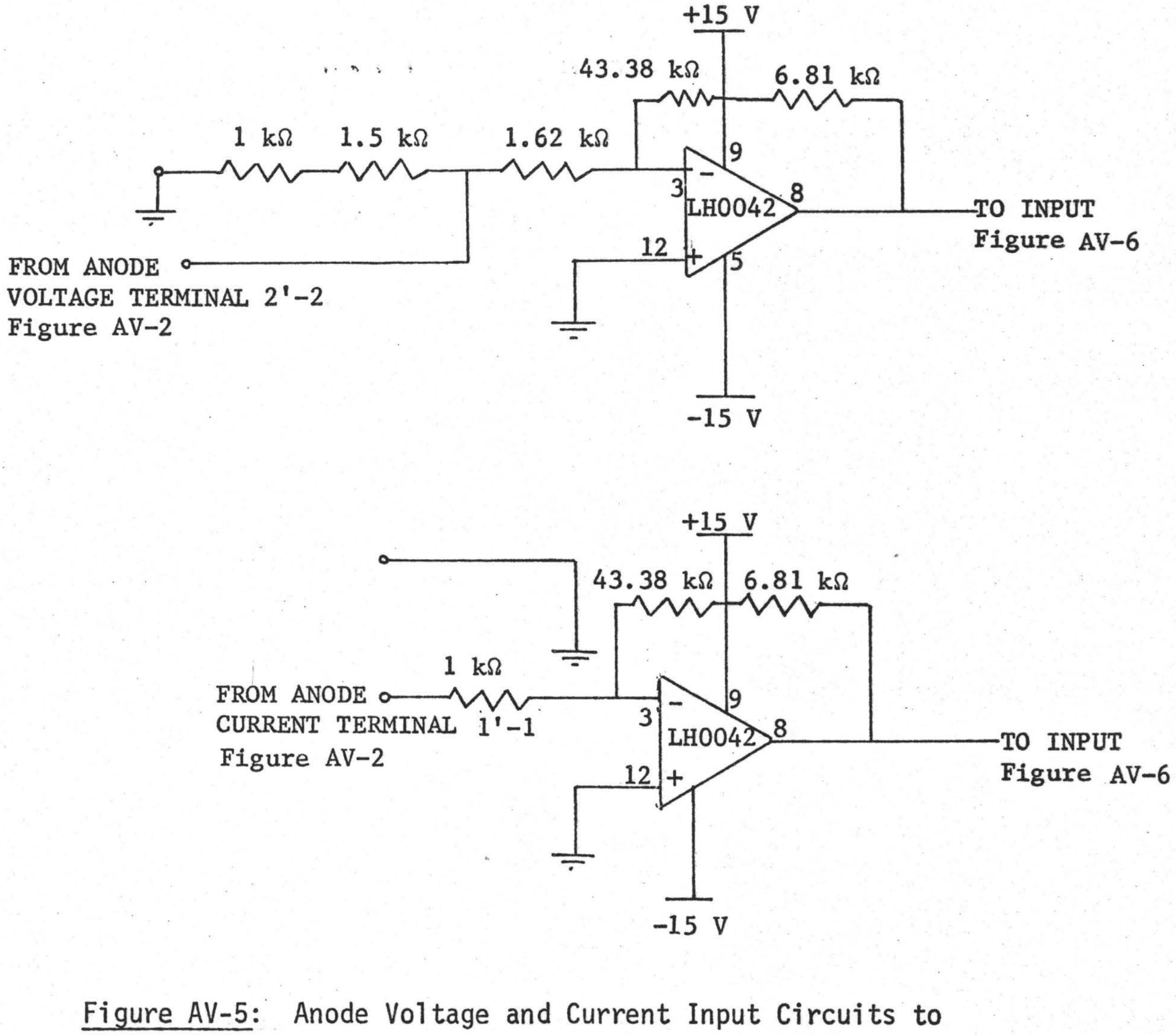

Figure AV-5: Anode Voltage and Current Input Circuits to the Telemetering System.

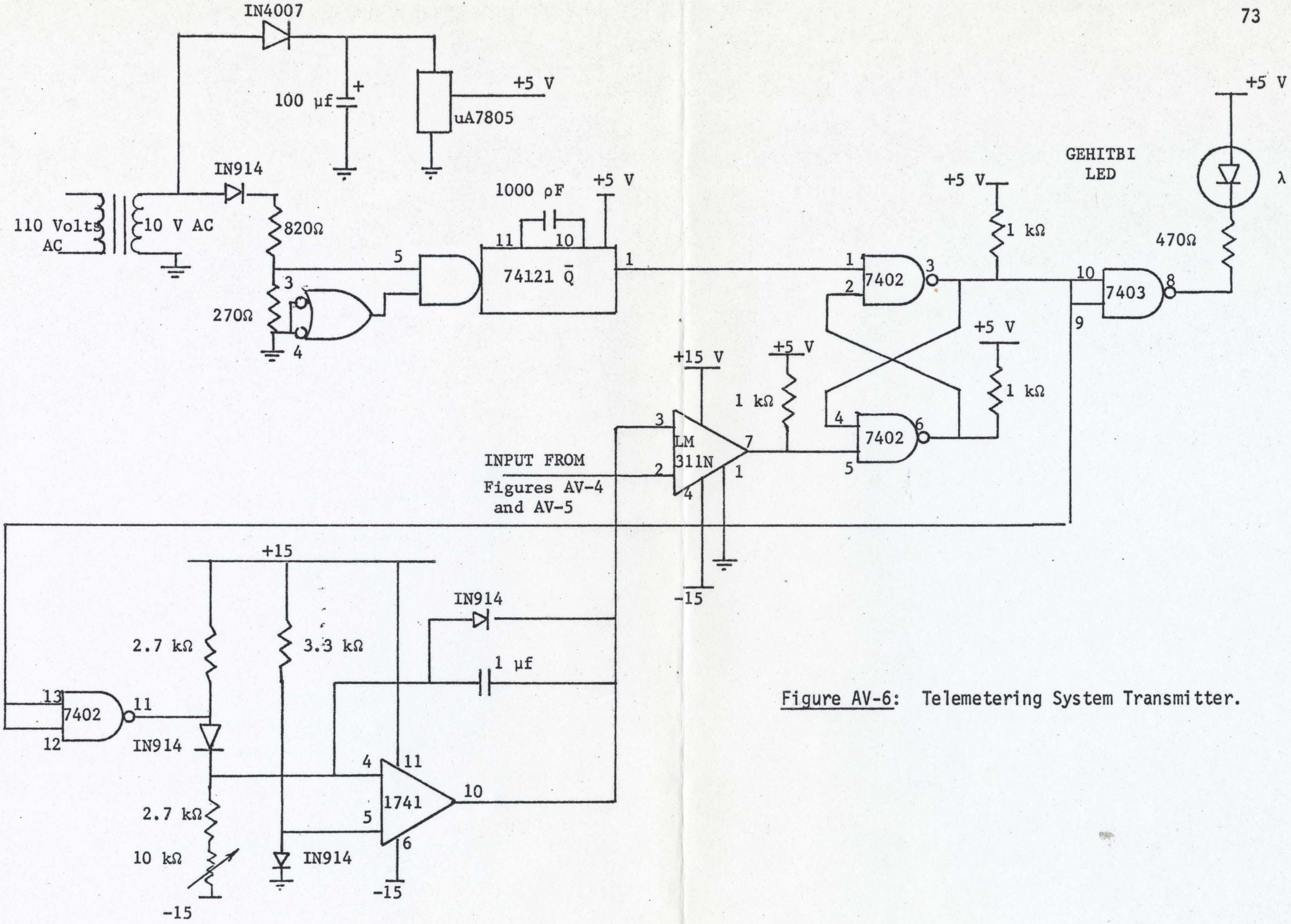

Figure AV-6: Telemetering System Transmitter.

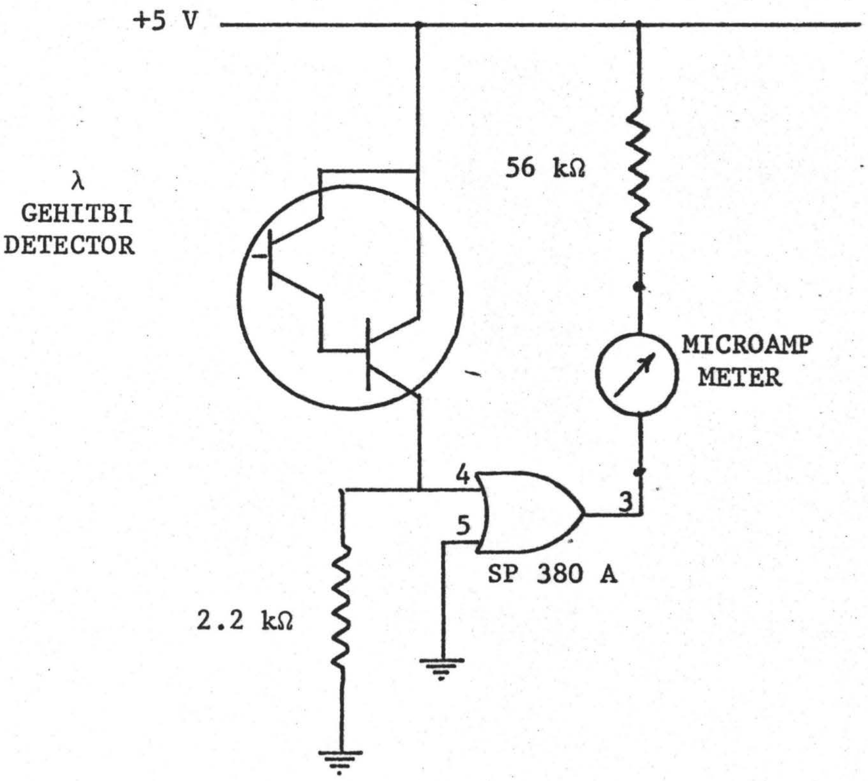

Figure AV-7: Single Channel Receiver for Telemetering System.

A	Isolation Transformer
B	Fence Door
C	Key Switch
D	High Voltage
IS-A	Isolation Area
V_+	15 Volts DC

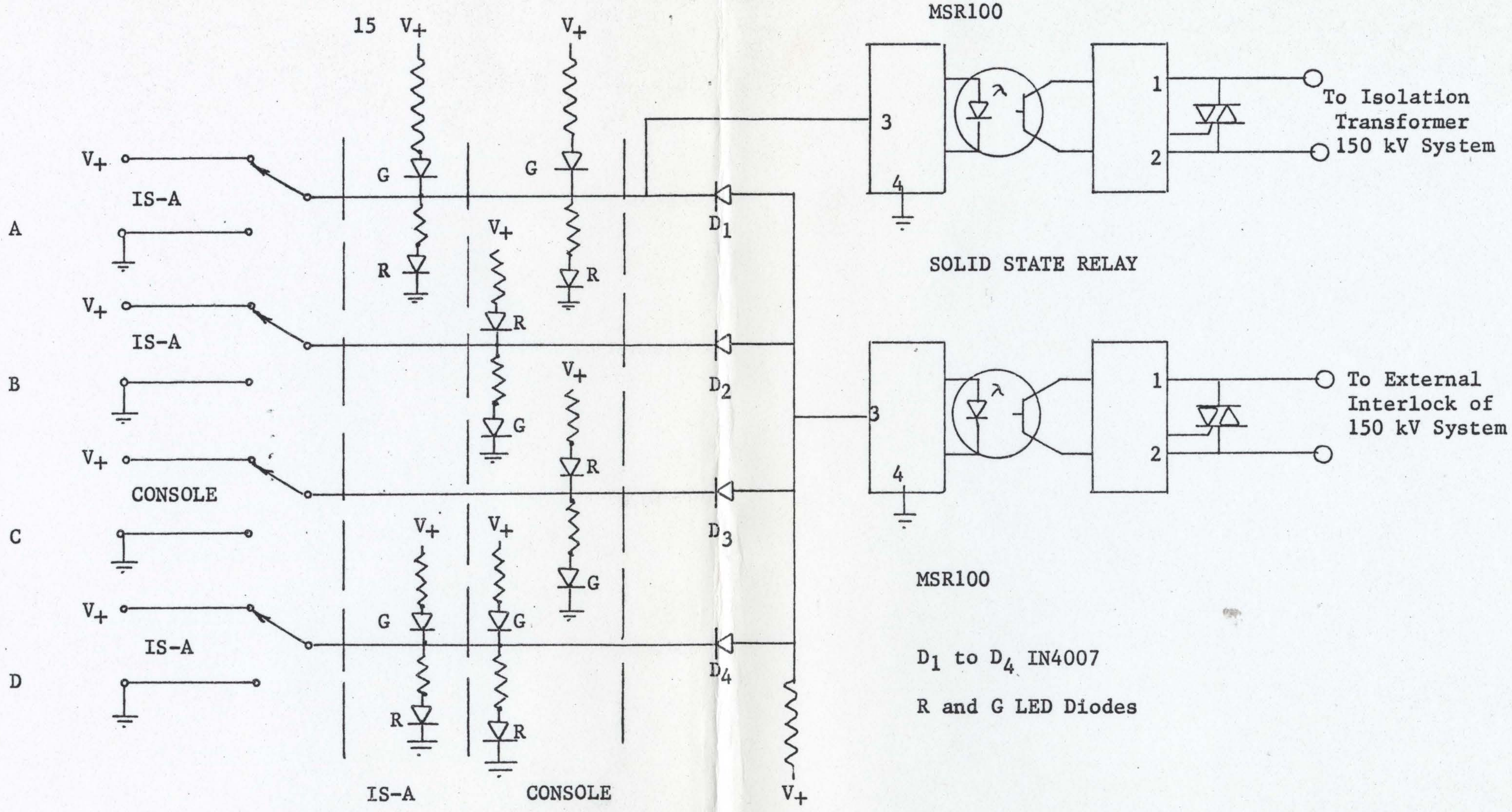

Figure AV-8: 150 kV Safety Interlock.

Note

Electrical diagrams of Figure 5, Remote Control Gas Feed System, and Figure 6, Remote Control Analyzer Magnet System, have been designed but have not undergone a rigorous bench testing procedure. Consequently, the schematics of the finished circuit are not included in this report.

APPENDIX VI

HEAT EXCHANGER FOR ION SOURCE

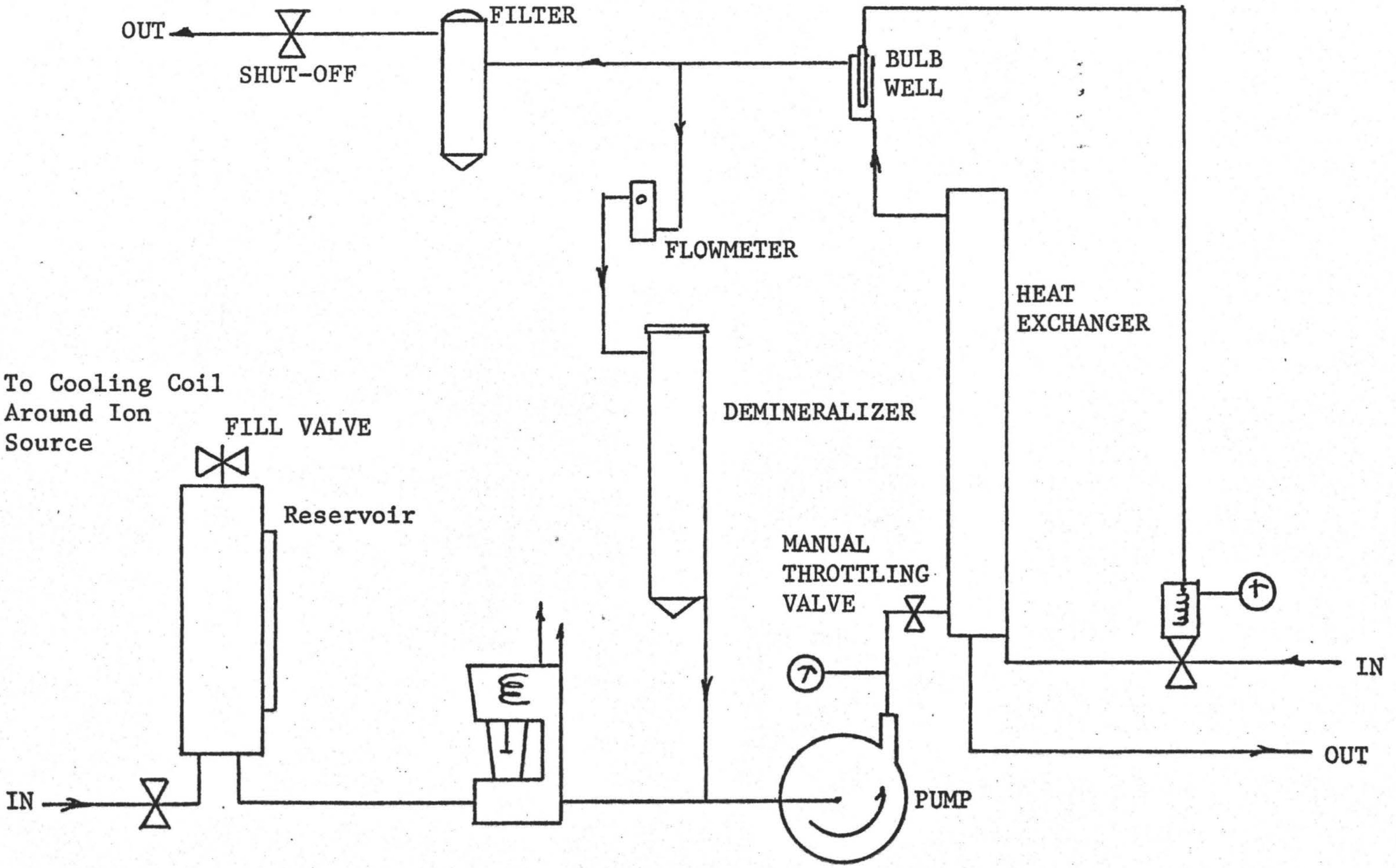

Figure AVI-1: Demineralized Water Supply.

REFERENCES

1. A. von Engel, Ionized Gases, Oxford University Press, Oxford, England (1965).
2. W. Bleakney, Phys. Rev., 35, 139 (1930).
3. J.D. Cobine, Gaseous Conductors: Theory and Engineering Applications, Dover Publications, New York, N.Y. (1965).
4. R.G. Wilson and G.R. Brewer, Ion Beams with Applications to Ion Implantation, Interscience, John Wiley and Sons, New York, N.Y. (1973).
5. V.K. Zworykin et. al., Electron Optics and the Electron Microscope, John Wiley and Sons, New York, N.Y. (1945) p.447.
6. A. Galejs and P.H. Rose, Focusing of Charged Particles, Oxford University Press, Oxford, England (1965).
7. H.A. Enge, Chapter 5.1 in Focusing of Charged Particles, Vol. II, A. Septier, editor, Academic Press, New York, N.Y. (1967).
8. K.G. Steffen, High Energy Beam Optics, Interscience, John Wiley and Sons, New York, N.Y. (1965).
9. P.T. Kirstein, G.S. Kino and W.E. Waters, Space Charge Flow, McGraw-Hill, New York, N.Y. (1967).
10. V.E. Cosslett, Introduction to Electron Optics, Oxford University Press, Oxford, England (1950) p.110.